





Fénisse et al.,

21 **Abstract**

22           Pollen records are one of the most spatially and temporally resolved proxies for  
23 reconstructing past vegetation dynamics, environmental changes and climate variability. Over  
24 the past decade, a large variety of methods based on different ecological or mathematical  
25 concepts has been used to reconstruct paleoclimatic conditions from pollen assemblages.  
26 However, the accuracy of these climate reconstructions strongly depends on the choice of the  
27 modern calibration dataset, the taxonomic resolution, and/or the modelling assumptions. The  
28 lack of a univocal response still limits the application of pollen-based climate reconstructions  
29 to assess key climate changes over multiple time periods especially during the Last Glacial  
30 Maximum (LGM, ~23-19 kyr BP). Here, we present a multi-method approach, including the  
31 Modern Analogue Technique (MAT), the Weighted Averaging Partial Least Squares regression  
32 (WA-PLS) and the probability density function-based Climate REconstruction SoftWare  
33 (CREST), to reconstruct European climates during the LGM. The quality and performance of  
34 our climate reconstructions show strong heterogeneity when based on large calibration  
35 datasets encompassing wide climatic and vegetation gradients, making local sampling for  
36 climate reconstructions difficult. Instead of sampling the global calibration dataset, we test  
37 the effect of the latest biomization and megabiomization methods (local calibrations based  
38 on megabiome procedures) on climate reconstructions by introducing a new biome-based  
39 approach. Unlike previous studies, we use the weighted mean of climate variables from all  
40 megabiome scores rather than only considering the dominant (i.e., highest score) megabiome.  
41 This significantly reduces some of the statistical noise of climate reconstructions, drastically  
42 minimizing threshold and non-linear effects associated with megabiome classification  
43 changes. With these methodological advancements and our multi-method comparison, we  
44 evaluate the uncertainties (RMSEP) of the paleoclimate reconstructions for the LGM in  
45 Europe. Across climate reconstruction methods (MAT, WA-PLS and CREST methods),  
46 European LGM annual temperatures from the biomization method were on average  
47  $6.7 \pm 2.2^\circ\text{C}$  (mean SD) colder than today, consistent with megabiomization results ( $7.4 \pm 2.3^\circ\text{C}$   
48 colder). Winter temperature (mean temperature of the coldest month, MTCO) results exhibit  
49 substantial spatial variability across Europe. Local calibration techniques significantly reduce  
50 uncertainties in LGM MTCO reconstructions, but they remain highly sensitive to the choice of  
51 calibration datasets.

52

53

54

55

56

57



Fénisse et al.,

58 **I. Introduction**

59 Reconstructing past climates is essential for understanding the mechanisms driving  
60 glacial–interglacial variability and for evaluating the reliability of climate model simulations.  
61 Pollen assemblages preserved in marine, lacustrine and peat bog sediments constitute robust  
62 proxies for reconstructing past climatic conditions (e.g., [Chevalier et al., 2020](#)). Pollen-based  
63 paleoclimate reconstructions are available for many regions (e.g., Europe, Eurasia,  
64 Mediterranean areas) and for various time-periods as the Eemian (e.g., [Brewer et al., 2008](#);  
65 [Sinopoli et al., 2018](#)), the Holocene (e.g., [Davis et al., 2003](#); [Peyron et al., 2013](#); [Salonen et al.,](#)  
66 [2019](#); [Herzschuh et al., 2022a](#)) and other past key periods (e.g., [Charton et al., 2025](#); [Zumaque](#)  
67 [et al., 2025](#)). While reconstructions of warm interglacial periods such as the Eemian and the  
68 Holocene generally show good agreement across different methods ([Sinopoli et al., 2018](#);  
69 [Sassoon et al., 2025](#)), this consistency tends to break down for glacial periods ([Guiot et al.,](#)  
70 [1990](#); [Brewer et al., 2008](#); [Charton et al., 2025](#)). In particular, accurately reconstructing  
71 temperature and precipitation during the Last Glacial Maximum (LGM, ~19–23 thousand years  
72 ago; [Hughes et al., 2013](#)) remains a persistent challenge as environmental gradients are strong  
73 and vegetation–climate relationships are complex ([Peyron et al., 1998](#); [Bartlein et al., 2011](#);  
74 [Davis et al., 2024](#)). Over the past decades, a wide range of approaches has been developed  
75 from pollen data to address the issue of glacial climate reconstructions. These include the  
76 Modern Analogue Technique (MAT, [Guiot et al., 1990](#)), transfer functions via the Weighted  
77 Averaging Partial Least Squares regression (WA-PLS, [Ter Braak and Juggins, 1993](#)), the Plant  
78 Functional Type method (PFTs, [Peyron et al., 1998](#)) and the Inverse Modelling approach ([Guiot](#)  
79 [et al., 2000](#); [Wu et al., 2007](#)). The Inverse modelling and the algorithms developed by [Prentice](#)  
80 [et al., \(2022\)](#) and [Cleator et al., \(2020\)](#) take into account the CO<sub>2</sub> effect in the climate  
81 reconstructions: the algorithms explicitly account for the physiological effects of low  
82 atmospheric CO<sub>2</sub> concentrations (pCO<sub>2</sub> ≈ 180 ppm) on LGM vegetation. Despite these  
83 methodological advances, substantial discrepancies remain between the results derived from  
84 these reconstruction methods and those simulated by climate models (e.g., [Jost et al., 2005](#);  
85 [Cleator et al., 2020](#)). Such inconsistencies highlight the complexity of reconstructing reliable  
86 glacial climates, particularly for regions such as Europe and the Mediterranean Basin  
87 ([Zumaque et al., 2025](#); [Charton et al., 2025](#)). Improving the robustness and comparability of  
88 paleoclimate reconstructions for cold periods thus remains a key objective for the  
89 paleoclimate community.

90 Recent studies have emphasized that the choice of reconstruction method can  
91 significantly influence reconstructed climatic parameters ([Dugerdil et al., 2021, 2025](#); [Robles](#)  
92 [et al., 2023](#); [Charton et al., 2025](#)) as the methods and assumptions used are based on different  
93 ecological and mathematical/statistical concepts and algorithms (see [Chevalier et al., 2020](#)  
94 for a review). They assume that proxy–climate relationships remain constant over time and that  
95 pollen variations primarily reflect climate variations. Among all the methods available to  
96 reconstruct past climate changes from pollen data, the MAT and the WA-PLS are the most  
97 commonly used in paleoclimatology (e.g., [Davis et al., 2003, 2024](#); [Birks et al., 2004](#); [Mauri et](#)



Fénisse et al.,

98 *al., 2014, 2015; Liu et al., 2020; Herzschuh et al., 2022a*). Most studies have applied these  
99 approaches individually, with only a few combining MAT and WA-PLS (*Sinopoli et al., 2021;*  
100 *Herzschuh et al., 2022a; Geng et al., 2025*). These studies demonstrated that reconstruction  
101 results can vary substantially between methods, mainly due to variations in modern pollen–  
102 climate calibration datasets, spatial coverage and the ecological tolerances assigned to plant  
103 taxa. They also highlighted the influence of fossil record quality and the reliability of the  
104 quantitative reconstruction methods themselves (e.g., *Brewer et al., 2008; Peyron et al., 2013;*  
105 *Chevalier et al., 2020; Dugerdil et al., 2021, 2025*).

106 To enhance the reliability of paleoclimatic reconstructions, a methodological framework  
107 combining several complementary approaches has been developed over the last decade  
108 (*Peyron et al., 2005, 2011; 2013, Brewer et al., 2008; Salonen et al., 2019*). This multi-method  
109 approach highlights that significant discrepancies can arise depending on the reconstruction  
110 method applied. The reliability of each method is influenced by the composition of the pollen  
111 assemblages, meaning that the most appropriate or robust approach may differ depending on  
112 the taxa present and the specific period being studied. These studies have nevertheless  
113 introduced important methodological advances, representing a significant improvement over  
114 single-method approaches, even though assessing the robustness of the results remains a  
115 complex task. The most robust method can be identified and validated by comparing its results  
116 with independent proxy evidence obtained from the same sediment core, such as chironomid  
117 assemblages or molecular biomarkers (*d'Oliveira et al., 2023; Robles et al., 2023; Martin et al.,*  
118 *2020*). The multi-method approach includes various methods as MAT, WA-PLS, and machine-  
119 learning techniques (e.g., Random Forest, Boosted Regression trees) (e.g., *Salonen et al., 2012,*  
120 *2019; Dugerdil et al., 2021; Robles et al., 2022, 2023; d'Oliveira et al., 2023, 2025, Sassoon et*  
121 *al., 2025; Charton et al., 2025*). Applying this multi-method approach to the quantification of  
122 climatic conditions during glacial periods appears highly promising, yet such applications  
123 remain exceptionally scarce (e.g., *Brewer et al., 2008; Charton et al., 2025*).

124 Statistical methods such as MAT and WA-PLS are based on fixed distance-based vegetation  
125 samples and linear relationships between pollen taxa and climate variables, respectively.  
126 These relationships may oversimplify ecological responses and fail to account for uncertainties  
127 in both modern calibration datasets and fossil assemblages. One promising avenue to better  
128 quantify climatic parameters from pollen data during the LGM is probabilistic approaches like  
129 the Probability Density Functions (PDFs) method (*Kühl et al., 2002, 2010; Trasune et al., 2024;*  
130 *Seirienné and Kisieliené, 2014*). Probabilistic approaches (e.g., *Kühl et al., 2002; Kühl and Litt,*  
131 *2003; Gebhardt et al., 2008*) explicitly model these uncertainties and integrate the full  
132 probability distributions of taxa–climate relationships, thereby capturing the complete range  
133 of climate tolerances of the observed taxa. One version of the PDF-method named CREST  
134 (Climate REconstruction SoftWare, *Chevalier et al., 2014, Chevalier, 2022*) describes the  
135 conditional responses of taxa assemblages to climate variables, by combining generally  
136 unimodal distributions of reconstructed climate spaces from each taxon. The main  
137 innovations of CREST are (i) accounting for taxonomic uncertainties in pollen data, and (ii)



Fénisse et al.,

138 using presence-only data rather than presence/absence data. The multiplication of these PDFs  
139 yields a likelihood distribution, which represents the full range of climatic conditions in which  
140 a given assemblage can occur, derived from the statistical analysis of modern presence-only  
141 data ([Chevalier, 2022](#)).

142 Another promising opportunity to further enhance the reliability of climate  
143 reconstructions for glacial periods is to integrate biomization techniques within each  
144 reconstruction method following [Prentice et al., \(1996\)](#). Applying such biome-based  
145 constraints has been tested with the MAT method and appears to be a particularly promising  
146 ([Guiot et al., 1993](#)) yet still underexplored approach ([Dugerdil et al., 2025](#)). Biomization  
147 techniques have been developed to convert modern and fossil pollen assemblages into  
148 specific vegetation types (i.e., biomes or megabiomes), thereby linking the ecological,  
149 physiological and physiognomic data with both current and past climatic and environmental  
150 conditions ([Prentice et al., 1996](#); [Li et al., 2024](#), [Dugerdil et al., 2025](#)). These techniques have  
151 been widely employed to reconstruct past regional vegetation patterns particularly since the  
152 LGM (e.g., [Peyron et al., 1998](#); [Dallmeyer et al., 2019](#), *biome 6000 project and references*  
153 *therein*; [Li et al., 2024](#)). While such approaches can arguably improve climate interpretations  
154 and facilitate comparisons across spatial and temporal scales, most studies have used them  
155 as a way to drastically restrict the ranges of paleoclimate reconstructions by relying only on  
156 the dominant biome (i.e., the biome with the highest score) (e.g., [Guiot et al., 1993](#); [Tarasov](#)  
157 [et al., 1999, 2013](#); [Davis et al., 2003, 2024](#)). However, transitional states, ecological gradients,  
158 and the variability of biome scores are often overlooked in these studies, potentially  
159 amplifying threshold effects and non-linearities in the reconstructions ([Dallmeyer et al., 2019](#)).  
160 A crucial step toward improving the accuracy of paleoclimate reconstructions is therefore to  
161 better use biome information to inform the modern calibration dataset underpinning the  
162 different reconstruction methods.

163 Across Europe, LGM pollen records generally reveal a high diversity of forests, steppes,  
164 and tundra ([Peyron et al., 1998](#); [Davis et al., 2024](#)), although cold steppe environments were  
165 predominant (e.g., [Binney et al., 2017](#); [Davis et al., 2024](#)), pointing towards more arid climatic  
166 conditions than today. However, because modern cold climates are underrepresented in  
167 Europe, climate reconstructions remain challenging. Although Europe exhibits an exceptional  
168 diversity of continental proxy records, the magnitude and spatial patterns of LGM cooling are  
169 still widely debated. This uncertainty largely arises because different proxies often yield  
170 divergent reconstructions of temperature change (e.g., [Davis et al., 2024](#)), and substantial  
171 disagreements persist between climate model simulations and proxy-based reconstructions  
172 (e.g., [Bartlein et al., 2011](#); [Cleator et al., 2020](#); [Kageyama et al., 2021](#)). Seasonality during the  
173 LGM is primarily documented by pollen data ([Davis et al., 2024](#)) but remains poorly  
174 constrained, despite its potentially uncertain impact on reconstructed LGM cooling signals.  
175 Quantifying European paleoclimates is also particularly important for better constraining the  
176 role of continental thermal amplification in climate dynamics ([Seltzer et al., 2021](#)) and for  
177 evaluating future climate changes using climate models ([Ramstein et al., 2007](#); [Harrison et al.,](#)



Fénisse et al.,

178 [2014](#)) within the framework of the Paleoclimate Modelling Intercomparison Projects (PMIP;  
179 [Joussaume et al., 1999](#); [Braconnot et al., 2012](#)). Although many climate reconstructions have  
180 been carried out for the LGM in Europe ([Peyron et al., 1998](#); [Jost et al., 2005](#); [Wu et al., 2007](#),  
181 [Guiot et al., 2000](#), [Davis et al., 2024](#)), they generally rely on a single reconstruction method  
182 and are based on different datasets, which can contribute to inconsistencies among the  
183 results.

184 In this study, we present a unique methodological framework that combines MAT, WA-  
185 PLS, and CREST to provide robust climate estimates for Europe during the LGM. Our goal is to  
186 significantly improve the accuracy of paleoclimate reconstructions by adapting biomization  
187 techniques - both the classical biomization ([Prentice et al., 1996](#)) and the megabiomization ([Li  
188 et al., 2024](#)) - to our pollen datasets. We use biomization as a constraint to select the most  
189 suitable modern pollen samples, thereby enhancing the calibration step within each  
190 reconstruction method. Using these approaches, we generate specific calibration datasets  
191 that are restricted to single biomes. We also use biomization scores that consider not only  
192 dominant biomes to achieve more robust climate reconstructions but also reconstructions  
193 based on all biome information to account for biomization uncertainties. We test our multi-  
194 method framework on two glacial time periods: (i) to reconstruct climate changes during the  
195 LGM using the well-known pollen record from Lake Bouchet (France), and (ii) to reconstruct  
196 spatial climate patterns across Europe and the Mediterranean region during the LGM.

197

## 198 **II. [Methods](#)**

### 199 **II.1 - [Climate reconstruction methods](#)**

200 We apply three distinct approaches, grounded in different ecological and modelling  
201 assumptions, to the same modern and fossil datasets, to identify and discuss the  
202 methodological biases specific to each reconstruction method.

203

#### 204 **II.1.1 - Assemblages approach: Modern Analogue Technique (MAT)**

205 The Modern Analogue Technique (MAT; [Overpeck et al., 1985](#); [Guiot, 1990](#)) is widely  
206 used to reconstruct past climate variations over time scales ranging from the last million years  
207 to the Holocene, and has been applied in particular to glacial periods ([Guiot et al., 1993](#); [Davis  
208 et al., 2024](#); [Zumaque et al., 2025](#); [Charton et al., 2025](#)). It measures the dissimilarity between  
209 a fossil pollen assemblage and a set of modern assemblages from the modern dataset ([Guiot  
210 et al., 1989, 1990](#)). Climate reconstructions are performed by estimating a dissimilarity  
211 coefficient (hereafter SQChord, for “Squared chord distance”, ([Overpeck et al., 1985](#)) based  
212 on the closest modern analogues, using an optimal number of analogues “k” that minimizes  
213 the RMSEP (i.e., Root Mean Squared Error of Prediction, [Juggins, 2020](#)). This parameter “k” is  
214 specific to each climatic variable and fossil sequence (“k” from 8 to 10). Generally speaking,  
215 the MAT method appears to perform better with pollen taxa that are diverse and poorly  
216 resolved taxonomically like family ([Birks et al., 1005](#), [Willimas and Shuman, 2008](#), [Viau and](#)



Fénisse et al.,

217 [Gajewski, 2009](#)). We used the *rioja* package in R (Analysis of Quaternary Science data, version  
218 1.0-6, R Core Team, <https://cran.r-project.org/web/packages/rioja/index.html>; [Juggins, 2020](#))  
219 to perform MAT reconstructions. Climate reconstruction uncertainties were quantified using  
220 the root mean square error of prediction (RMSEP) derived from leave-one-out cross-  
221 validation.

222

### 223 **II.1.2 - Transfer function: Weighted Partial Least Squares method (WA-PLS)**

224 The Weighted Averaging Partial Least Squares method (WA-PLS; [Ter Braak and Juggins,](#)  
225 [1993](#)) is a transfer function based on climatic optima and tolerances of a pollen taxon defined  
226 by its spatial niches. With this method, the climatic responses of taxa are assumed to be  
227 Gaussian ([Ter Braak and Looman, 1986](#)). This reconstruction method assumes unimodal  
228 (Gaussian) species response. The number of components (i.e., portion of the covariance  
229 between species abundance data and environmental variables) for paleoclimate  
230 reconstructions was selected based on those that produce the lowest root mean square error  
231 (RMSEP), a high prediction linear correlation coefficient ( $R^2$ ), and less biased reconstructions  
232 to minimize mean and maximum bias ([Ter Braak and Juggins, 1993](#)). A minimization of the  
233 number of components (npls; [Ter Braak and Juggins, 1993](#)) is performed to weight and  
234 integrate potential interactions between taxa, in addition to the link that connects them to  
235 the climate. The *rioja* package was also used to carry out WA-PLS reconstructions.  
236 Uncertainties for WA-PLS reconstructions were similarly assessed through RMSEP obtained  
237 via leave-one-out cross-validation.

238

### 239 **II.1.3 - Probability Density approach: Climate REconstruction Software (CREST)**

240 Probabilistic methods provide more accurate and flexible climate reconstructions than  
241 statistical methods, with lower dependence on taxonomic resolution ([Netzel et al., 2025](#)).  
242 CREST describes the conditional responses of taxa assemblages to climate variables by  
243 integrating modern pollen–climate relationships ([Chevalier et al., 2014](#); [Chevalier, 2022](#)). Most  
244 often, when pollen is identified at the genus or family level, the probabilistic method combines  
245 the individual species' parametric PDFs into a single PDF representing the pollen observed in  
246 the fossil sequence. Once estimated for all taxa, the PDFs for the taxa present in a sample are  
247 multiplied together, each weighted according to its observed abundance. CREST is particularly  
248 well suited for regions where pollen data are scarce or geographically unevenly distributed  
249 ([Chevalier, 2019](#); [Chevalier et al., 2020](#)). In detail, this method defines the conditional  
250 response of a plant species to a climate as a parametric PDF. The taxon-climate link is  
251 established by combining these PDFs, weighted by the abundance species that make up the  
252 genera and families of the observed pollen. A composite likelihood distribution is obtained by  
253 multiplying the individual PDFs, providing a complete probabilistic representation of the  
254 climatic conditions compatible with the observed assemblage - thus accounting for the full  
255 ecological range rather than only optimal conditions. This approach allows CREST to quantify



Fénisse et al.,

256 uncertainty explicitly, offering a robust framework for evaluating reconstruction reliability and  
257 comparing it with other statistical methods (MAT or WA-PLS).

258 To date, CREST has proven particularly effective in regions with sparse or poorly sampled  
259 data where other techniques cannot readily be used (*Chevalier et al., 2020*) and has been  
260 widely applied to several tropical ecosystems such as savannas (e.g., *Chevalier and Chase,*  
261 *2015, 2016; Chevalier et al., 2021*). CREST reconstructions were generated using the *CrestR*  
262 package (<https://github.com/mchevalier2/crestr>, *Chevalier, 2022*).

263

### 264 **III. Pollen Datasets**

#### 265 **III.1 - Fossil pollen dataset**

266 43 European fossil pollen samples spanning the LGM 19-23 kyr (cal BP) were selected  
267 (**Table 1**). Locations of pollen records, data sources, archive types, identification number,  
268 taxonomic diversity and resolution of pollen data are summarized in **Table 1**. Most fossil  
269 pollen data used in this study have been recently compiled by *Davis et al. (2024)*. Additional  
270 European fossil records that were not included in *Davis et al. (2024)* are reported in **Table 1**  
271 and in **Appendix 1**. Aquatic and anthropic pollen taxa were excluded from the LGM fossil  
272 pollen assemblages. Pollen assemblages were extracted from databases, such as ACER 1.0  
273 (*Sanchez Goñi et al., 2017*), PANGAEA Database (<https://www.pangaea.de/>), and Neotoma  
274 Paleocology Database (<https://www.neotomadb.org/>; *Williams et al., 2018*). Raw pollen  
275 counts were used when available or digitized from the published diagrams (**Table 1**). Lakes  
276 are the most abundant archive, and peat bogs are second, followed by alluvial and colluvial  
277 sediments (**Fig Appendix 1.a**). One site sequence (Venice) contains only 7 taxa, while others  
278 include up to 70 taxa, with 80% of sequences having more than 10 taxa, reflecting  
279 differences in taxonomic resolution and geographical location (**Fig Appendix 1.b**). While  
280 CREST remains effective with a small number of taxa (~8–10; *Chevalier, 2019*) due to the use  
281 of continuous probability distributions, MAT and WA-PLS generally require  $\geq 10$  taxa to  
282 produce reliable climate reconstructions (*Guiot et al., 1993; Peyron et al., 1998*).

283 Shrub and non-arboreal taxa dominate the LGM pollen assemblages (from 40 to 80%),  
284 except for certain records like Azzano Decimo, Rio Diodis and Pian del Lago, Orgiano records  
285 (northern Italy) for which we observe a prevalence of *Pinus* (>40%; **Fig appendix 1.c**). A table  
286 summarizing each taxon and vegetation types is available in **Appendix 1**. Most of the LGM  
287 samples are dominated by arid-adapted taxa (including *Poaceae*, *Artemisia* and  
288 *Chenopodiaceae/Amaranthaceae*). Steppic taxa such as *Poaceae* and *Artemisia* primarily  
289 dominate lower-latitude areas (<40°N), although, the high pollen productivity and wind  
290 transport of *Artemisia* taxa could somehow overestimate the abundance of steppic biomes  
291 (*Xu et al., 2010*).

292 In contrast to the study of *Davis et al. (2024)*, marine pollen records were excluded here  
293 due to taxonomic, preservation, and chronological biases when compared to terrestrial  
294 records (*Daniau et al., 2019; Xu et al., 2016*). However, the “Les Echets” record was excluded



Fénisse et al.,

295 because of incomplete dating information, such as uncalibrated radiocarbon years and/or  
296 dating uncertainties.

297 The Lake du Bouchet pollen sequence (Eastern France) serves as a reference to study  
298 potential methodological biases in reconstructing LGM climates. Its high temporal resolution,  
299 continuity, and taxonomic richness (56 pollen taxa) make it particularly valuable for assessing  
300 the impact of different reconstruction techniques.

301 From all pollen data, a harmonization table was extracted from *LegacyPollen 2.0* ([Li et al.,](#)  
302 [2024](#); [Herzschuh et al., 2022b](#)) and processed to match the identification of pollen data  
303 between modern and fossil samples.

304

305

306

307

308

309

310

311

312

313

314

315

316

317

318

319

320

321

322

323

324

325

326

327

328

329

330

331

332

333

334

335



SiteName	Latitude (°N)	Longitude (°E)	Elevation (m)	TANN Modern (°C)	PANN Modern (mm)	MTCO Modern (°C)	MTWA Modern (°C)	Archive	Country	Source	Reference	Data Type	Biomes (best) 19-23 kyrs	Megabiomes (best) 19-23 kyrs
Lake Xiniás (1)	39.05	22.27	500	15.0	690.6	3.0	23.6	Lake	Greece	EPD (E#976)	Bottema (1979)	Raw Count	COST	STEP
Cova de les Malladetes (2)	39.06	-0.32	20	17.4	542.2	9.2	23.1	Cave	Spain	Publi.	Dupré Ollivier. (1988)	Digitised	TUND	TEFO
Navarrés (3)	39.10	0.68	225	16.7	546.9	7.3	24.8	Peat Bog	Spain	EPD (E#469)	Carrión & Dupré-Ollivier. (1996)	Raw Count	COST	TEFO
Megali Limni (4)	39.10	26.30	323	15.6	724.1	8.6	25.4	Lake	Greece	Publi.	Margari et al. (2009)	Digitised	COST	TEFO
Ioamina (5)	39.75	20.85	470	14.2	1100.1	1.1	21.5	Peat Bog	Greece	ACER	Tzedakis et al. (2004)	Raw Count	COST	TEFO
Lake Iznik (6)	40.43	29.53	88	13.4	713.0	3.7	23.0	Lake	Turkey	EPD (E#714)	Miebach et al. (2016)	Raw Count	COST	TEFO
Lago Grande di Monticchio (7)	40.94	15.60	1326	11.2	686.9	3.8	24.3	Lake	Italy	EPD (E#932)	Watts et al. (1996)	Raw Count	COST	TEFO
Mire Straldzha Kupena-3 (8)	40.98	24.31	1356	10.1	893.8	4.4	25.0	Lake	Bulgaria	EPD (E#209)	Tonkov et al. (2014)	Digitised	COST	TEFO
Lake Ohrid (9)	41.10	20.63	693	15.3	1019.1	0.3	24.9	Lake	Albania /North Macedonia	Publi.	Sadori et al. (2016)	Digitised	COST	TUND
Torreçilla de Valmadrid (10)	41.45	-0.90	570	14.0	433.5	5.2	23.0	Colluvium	Spain	Publi.	Valero-Garces et al. (2004)	Digitised	WAMX	TUND
Valle di Castiglione (11)	41.89	12.75	44	16.0	974.5	5.8	24.0	Lake	Italy	ACER	Follieri et al. (1989)	Raw Count	TEDE	TEFO
Lake Estanya (12)	42.03	0.53	670	12.6	711.5	2.8	23.4	Lake	Spain	Publi.	Vegas-Villarubia et al. (2013)	Digitised	COST	TUND
Stracciaccapa (13)	42.13	12.32	220	14.5	850.2	5.8	23.3	Lake	Italy	ACER	Giardini. (2007)	Raw Count	COST	TEFO
Banyoles (14)	42.13	2.75	173	14.1	883.3	5.0	23.5	Lake	Spain	EPD (E#931)	Pérez-Obiol & Julia. (1994)	Raw Count	COST	TEFO



33

Lago di Monterosi (15)	42.22	12.43	237	15.0	1084.8	5.5	23.9	Lake	Italy	Publi.	Bonatti, (1970)	Raw Count	<b>COST</b>	<b>TEFO</b>
Lago Vico (16)	42.32	12.17	510	13.4	1086.2	4.6	22.7	Lake	Italy	Publi.	Magri & Sadori, (1999)	Digitised	<b>WAST</b>	<b>TUND</b>
Lagaccione (17)	42.57	11.85	355	14.1	867.9	4.8	22.7	Lake	Italy	ACER	Magri, (1999)	Raw Count	<b>COST</b>	<b>TEFO</b>
Freychinède (18)	42.78	1.43	1350	12.4	626.7	-1.6	20.3	Lake	France	Publi.	Jalut et al., (1992)	Digitised	<b>TUND</b>	<b>TUND</b>
Dzigitia (19)	42.99	41.07	35	11.0	1302.7	2.9	22.2	Peat Bog	Georgia	Publi.	Arslanov et al., (2007)	Digitised	<b>CLMX</b>	<b>TEFO</b>
Lourdes (20)	43.03	-0.08	430	14.0	1619.2	0.9	17.1	Lake	France	Publi.	Reille & Andrieu, (1995)	Digitised	<b>WAST</b>	<b>TUND</b>
Tourbière de l'Estarres (21)	43.09	-0.38	356	12.5	1078.9	3.4	17.3	Peat Bog	France	Publi.	Jalut et al., (1988)	Digitised	<b>COST</b>	<b>TEFO</b>
Pian del Lago (22)	44.32	9.49	833	12.9	1034.3	6.1	21.3	Lake	Italy	Publi.	Guido et al., (2020)	Digitised	<b>COMX</b>	<b>TEFO</b>
Lac du Bouchet B5 (23)	44.92	3.78	1200	12.2	1051.4	-0.4	19.4	Lake	France	Publi.	De Beaulieu et al., (1990)	Digitised	<b>COST</b>	<b>TUND</b>
Lago della Costa (24)	45.27	11.74	7	8.3	1001.7	2.3	23.4	Lake	Italy	Publi.	Paganelli, (1996)	Digitised	<b>COST</b>	<b>BOFO</b>
Orgiano (25)	45.29	11.43	19	12.8	945.6	2.2	23.5	Peat Bog	Italy	Publi.	Miola et al., (2006)	Digitised	<b>COST</b>	<b>TEFO</b>
Venice (26)	45.63	12.65	0	13.0	960.3	3.8	23.3	Peat Bog	Italy	ACER	Pini et al., (2009)	Digitised	<b>COST</b>	<b>TEFO</b>
Azzano Decimo (27)	45.88	12.72	10	13.5	1145.4	2.4	22.7	Alluvial Fan	Italy	ACER	de Beaulieu & Reille, (1984)	Raw Count	<b>COST</b>	<b>TEFO</b>
Rio Doidis (28)	46.12	13.19	152	13.3	1299.7	1.0	21.0	Lake	Italy	Publi.	Monegato et al., (2007)	Digitised	<b>COST</b>	<b>STEP</b>
Lake Sfanta Anna (29)	46.13	25.89	946	12.4	1500.9	-5.3	19.7	Lake	Romania	Publi.	Magyari et al., (2014)	Digitised	<b>COMX</b>	<b>TEFO</b>



	46.20	12.87	220	11.5	751.1	-0.6	19.7	Lake	Italy	Publi.	Monegato et al.. (2007)	Digitised	COST	WTFO
Travesio (30)	46.20	12.87	220	11.5	751.1	-0.6	19.7	Lake	Italy	Publi.	Monegato et al.. (2007)	Digitised	COST	WTFO
Billerio (31)	46.22	13.21	300	12.5	1662.2	-0.1	20.1	Lake	Italy	Publi.	Monegato et al.. (2007)	Digitised	TAIG	TEFO
Orvenco (32)	46.25	13.17	380	12.5	1634.6	-2.0	18.4	Alluvial Fan	Italy	Publi.	Monegato et al.. (2007)	Digitised	COST	STEP
Fehér Lake (33)	46.45	20.65	86	13.4	1277.0	-0.5	22.7	Lake	Hungary	Publi.	Magyari et al.. (2014)	Raw Count	COST	TEFO
Kokad (34)	47.40	21.93	112	11.3	624.0	-1.3	21.8	Peat Bog	Hungary	Publi.	Magyari et al.. (2019)	Raw Count	COST	STEP
La Grande Pile (35)	47.73	6.50	330	10.5	692.1	1.3	19.0	Peat Bog	France	Publi.	de Beaulieu & Reille. (1989) + de Beaulieu (1992) + de Beaulieu & Reille (1992)	Raw Count	COST	TUND
Furamooos (36)	47.99	9.87	200	10.7	1141.5	-1.6	17.0	Lake	France	Publi.	Kern et al.. (2021)	Raw Count	COST	TUND
Bergsee (37)	47.57	7.94	382	8.2	1118.5	-0.3	18.3	Lake	Germany	Publi.	Duprat-Oualid et al.. (2017)	Digitised	COST	TUND
Pilsensee (38)	48.03	11.19	534	9.4	1306.8	-1.8	17.3	Lake	Germany	Publi.	Küster. (1995)	Digitised	COST	TUND
Nagymohos (39)	48.33	20.44	297	9.6	1110.5	-3.0	19.8	Peat Bog	Hungary	Publi.	Magyari et al.. (1999)	Raw Count	COST	TUND
Eifel (40)	50.30	6.51	565	9.5	751.6	-0.1	18.4	Lake	Germany	Publi.	Sirocko et al.. (2016)	Raw Count	COST	TEFO
La Grotte Wailou (41)	50.59	5.54	252	10.9	922.2	1.9	17.3	Cave	Belgium	Publi.	Damblon. (2011)	Digitised	COST	TEFO
Kersdorf-Briesen (42)	52.33	14.27	44	9.2	657.2	-0.3	18.9	Lake	Germany	Publi.	Strahl. (2005)	Digitised	COST	TEFO
Mickunai (43)	54.72	25.53	143	6.3	650.0	-2.8	17.8	Lake	Lithuania	Publi.	Satkunas & Grigiene. (2012)	Digitised	COST	TEFO



Fénisse et al.,

339 **Table 1.** Reference table of fossil pollen data including (i) site locations and archives, (ii)  
340 modern annual and monthly climate data, and (iii) selected biomes and megabiomes derived  
341 from the European Centre for Medium-Range Weather Forecasts Reanalysis v5 (ERA5; from  
342 January 1940) for each site. These values are used to infer climate anomalies during the most  
343 climatically stable interval of the LGM (19–23 kyr). Green and blue lines indicate modified  
344 and additional pollen sites, respectively, relative to [Davis et al. \(2024\)](#). See **Fig.2** for  
345 definitions of biome and megabiome acronyms.

### 347 III.2 - Age models

348 Age models previously based on CLAM v. 1.2 were updated using the Bayesian age-depth  
349 model Bacon (BACON routine in R, [Blaauw et al., 2010](#)). Radiocarbon ages were calibrated  
350 with the INTCAL20 calibration curve ([Reimer et al., 2020](#)). A linear  
351 accumulation/sedimentation rate was assumed over time to extend age models beyond the  
352 youngest and oldest available  $^{14}\text{C}$  age ranges. In addition,  $^{40}\text{Ar}$  age constraints were also  
353 included for the Füramoos fossil site. All ages are reported in calibrated years before 1950 (cal  
354 BP).

### 356 III.3 - Modern pollen and climate datasets

357 Calibrating with modern samples is advantageous because pollen data are highly resolved  
358 spatially, assumed to be largely free of preservation biases, and associated with directly  
359 measured climate variables. A modern dataset covering broad climatic gradients is required  
360 to provide a reliable calibration and ensure robust climate reconstructions (e.g., [Birks, 1995](#);  
361 [Juggins, 2013](#)). The modern pollen training dataset used in this study has been compiled from  
362 the Eurasian Modern Pollen database v2 (EMPD2; <https://empd2.github.io>,  
363 <https://www.pangaea.de/>). It contains a total of 8,746 modern samples mostly across the  
364 Palearctic biogeographic realm, from Asia to Europe. The modern pollen dataset was  
365 harmonized using the same table used for the fossil pollen data (i.e., *LegacyPollen 2.0*).  
366 Modern climate variables associated with these modern pollen samples were extracted  
367 through nearest-neighbor interpolation from ERA5 reanalysis  
368 (<https://rmets.onlinelibrary.wiley.com/doi/10.1002/qj.3803>), at a spatial resolution of 30  
369 seconds (i.e., 1 km<sup>2</sup>), with temporal averages spanning from 1940 to present ([Hersbach et al.,](#)  
370 [2020](#)). We used monthly averages of daily mean data to extract the mean annual and seasonal  
371 climates (i.e., the coldest and warmest climate states of the year). The modern climate  
372 conditions at fossil site locations, extracted from the modern dataset and represented by  
373 colored points in **Appendix 1**, generally show latitudinal dependency, with warmer and drier  
374 climates concentrated at lower latitudes.

375

## 376 IV. Calibration methods

### 377 IV.1 - Local calibration methods from (mega)biomes

#### 378 IV.1.1 - Modern calibration based on (mega)biomes

379 Modern datasets that cover extensive geographic regions (e.g., Europe) span a wide  
380 range of climatic conditions and are thus often challenging for reconstruction methods



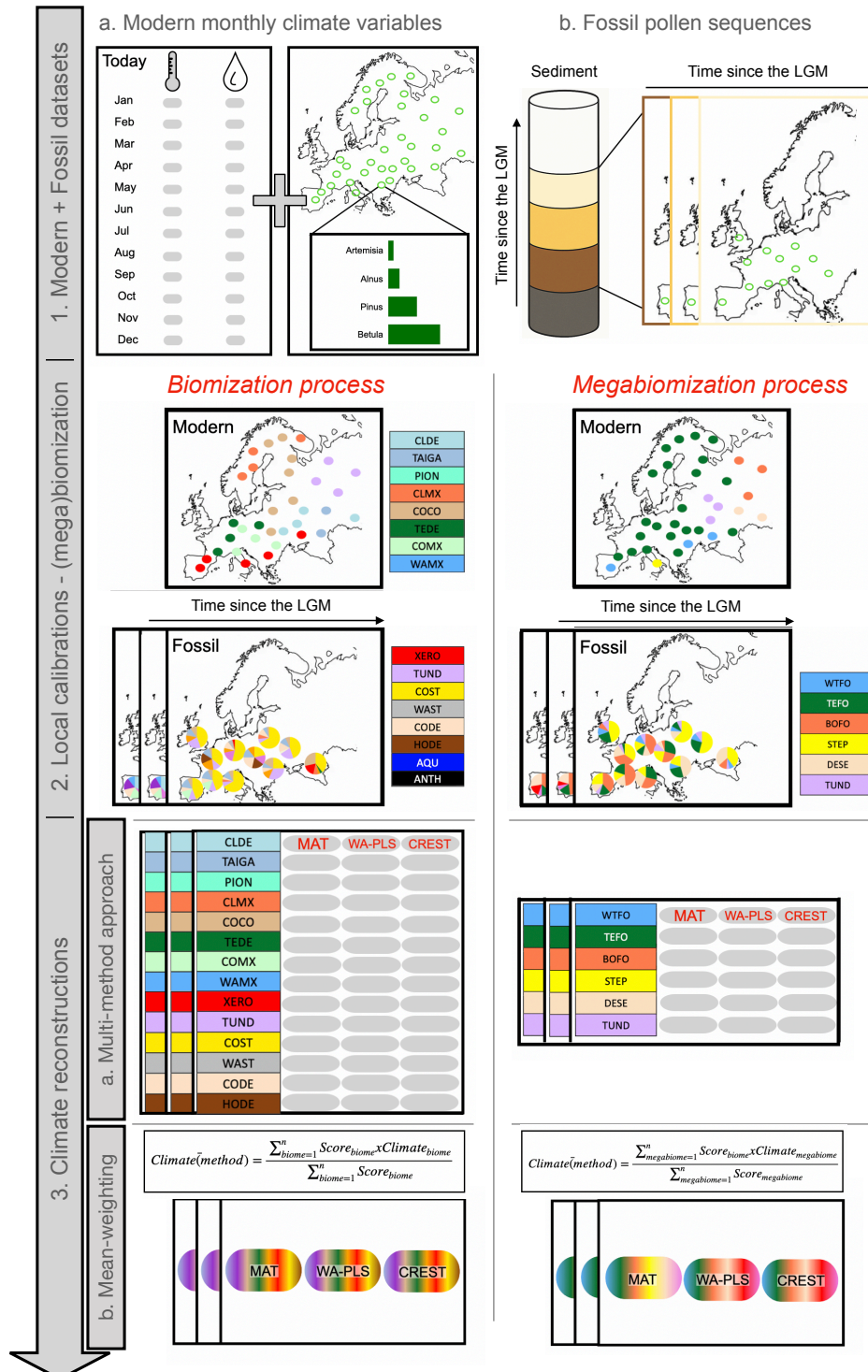
Fénisse et al.,

381 designed to estimate pollen-climate relationships (i.e., WA-PLS and CREST). In Europe, this  
382 difficulty is compounded by the underrepresentation of modern cold climates, limiting their  
383 use for reconstructing past cold conditions. The presence of such heterogeneity can reduce  
384 the ability of these methods to accurately match fossil samples with modern analogues.  
385 Without proper pre-processing of modern analogues, the performance, reliability, and  
386 robustness of reconstruction methods are compromised, potentially leading to less precise  
387 climate estimates (*Cao et al., 2022*).

388 Biomes are large-scale ecological units characterized by dominant vegetation types  
389 and the climatic and environmental conditions that support them (e.g., *Prentice et al., 1992,*  
390 *1996*). They capture broad vegetation patterns and climate-vegetation relationships over  
391 space and time, facilitating comparisons across regions and temporal scales. Biomization  
392 processes prepare the data by classifying the pollen assemblages into PFTs and biomes, which  
393 are then used in reconstruction methods. *Guiot et al. (1993)* suggests using the biome  
394 approach of *Prentice et al. (1992)* to distinguish between steppe and tundra environments,  
395 thereby addressing the lack of good modern analogues.

396 In this study, biome and megabiome classification methods were applied to modern  
397 and fossil (LGM) European pollen assemblages. By processing a large European modern  
398 dataset (see **section III.3**) through the biomization procedure, we minimize the risk of lacking  
399 analogues and integrate spatial heterogeneity of the modern samples to reconstruct  
400 regional vegetation patterns. The methodology for processing pollen data to extract climatic  
401 signals is illustrated in **Fig.1**.

402  
403  
404  
405  
406  
407  
408  
409  
410  
411  
412  
413  
414  
415  
416  
417  
418  
419  
420  
421





Fénisse et al.,

423 **Figure 1.** Schematic representation of the methodological approach developed in the  
424 subsection II of this study. Gray vertical boxes (on the left of this figure) illustrate  
425 methodological steps performed in this study.

426

#### 427 **IV.1.2 - Biomization procedure**

428 Biomization was originally designed to reconstruct past vegetation patterns across specific  
429 regions of the world (e.g., Europe, Africa) for key periods such as the Mid-Holocene or the  
430 LGM ([Prentice et al. 1996](#)). This approach relies on a standardized methodology that uses  
431 modern and/or fossil pollen data ([Prentice and Webb, 1998](#); [Prentice et al., 1996, 2000](#); [Peyron  
432 et al., 1998](#)) and generally follows the sum of square root procedure (square-root  
433 transformation) to assign pollen taxa to biomes ([Prentice et al., 1996](#); [Prentice and Webb,  
434 1998](#)). Here, the taxa list defines PFTs following the European biomization scheme from  
435 [Peyron et al. \(1998\)](#) and [Tarasov et al. \(2000\)](#). A pollen abundance threshold of 0.5% ([Prentice  
436 et al., 1996](#)) - 0.2% for *Corylus* - is subtracted from the initial pollen taxon abundances to  
437 account for pollen transport effects ([Prentice et al., 1998](#)). Counts for *Larix* and *Pinus* were  
438 multiplied by factors of 15 and 0.5, respectively, to account for their specific levels of  
439 production (i.e., underproduction and low preservation) and pollen overproduction,  
440 respectively ([Bigelow et al., 2003](#); [Binney et al., 2017](#)).

441 We assigned 98 pollen taxa to 25 PFTs (**Supp Mat.**, from [Prentice et al., 1996](#)), using the  
442 sum of the square roots of the pollen abundances corrected for thresholds. This approach  
443 allows for floristic and functional heterogeneity within key biomes. Then, biome affinity scores  
444 were calculated by considering the sum of the PFT scores belonging to each biome.  
445 Intermediate biomes ([Tarasov et al., 1998](#)) were used to distinguish warm and cold conditions  
446 from steppe and desert biomes by re-assigning PFT scores based on the dominant biome.  
447 Additionally, PFTs were combined into 16 biomes following [Prentice et al. \(1996\)](#) and using  
448 the standardized biome assignment procedure from [Harrison et al. \(2010\)](#) and [Dallmeyer et  
449 al. \(2019\)](#). The *Taxa-PFT* and *PFT-biome* biomization tables are available in **Supplementary  
450 materials (csv file)** with the following biomes: *cold deciduous forest (CLDE)*, *taiga (TAIG)*,  
451 *pioneer (PION)*, *cold mixed forest (CLMX)*, *cool conifer forest (COCO)*, *temperate deciduous  
452 forest (TEDE)*, *cool/warm mixed forest (COMX/WAMX)*, *xerophytic shrubs (XERO)*, *tundra  
453 (TUND)*, *cool/warm steppes (COST/WAST)*, *cold/hot desert (CODE/HODE)*, *anthropogenic  
454 (ANTH)*, and *aquatic (AQU)* biomes.

455 Biomization studies have considered three main hypotheses regarding the approach to (i)  
456 selecting the pollen-PFT assignment based on vegetation and environmental distributions  
457 from specific regions ([Prentice et al., 1996, 2000](#)), (ii) prioritizing the least PFT-rich biome when  
458 affinity values for multiple biomes are identical ([Harrison et al., 2010](#); [Dallmeyer et al., 2019](#))  
459 and (iii) choosing dominant biomes with the highest affinity score (absolute proportion of a  
460 particular biome) across different regions ([Xu et al., 2013](#)). Generally speaking, biomization  
461 also helps reduce the impact of the non-analogue effect (i.e., when modern samples are



Fénisse et al.,

462 considered too different to the fossil ones to be used for reconstructions) on reconstructed  
463 climates.

464

#### 465 **IV.1.3 – Megabiomization procedure**

466

467 Megabiomes are broad vegetation categories that group multiple biomes into larger  
468 ecological and climatic units (*Dallemeyer et al., 2019*). This classification, used alongside  
469 biomes in this study, relies on a more spatially extensive and global framework, yielding results  
470 that are more directly comparable to global vegetation models. Compared to the biomization  
471 procedure, only the content of the European classifications (linking taxa to PFTs and PFTs to  
472 biomes) is modified, while the methodology for calculating affinity scores remains the same.  
473 This classification aims to (i) define a small set of biomes (i.e., called megabiomes) based on  
474 shared PFTs, and (ii) cover a broader climatic range than individual biomes.

475 In this study, we used the megabiome classifications from *Dallemeyer et al. (2019)* and  
476 *Cao and Tian, (2021)*. The main aim of the PFTs–megabiome assignment is to track key signals  
477 of land-cover changes (e.g., wetland extent, conifer dominance) while minimizing the  
478 influence of the chosen biome classification (*Prentice et al., 1998*). Megabiome assignments  
479 are primarily used in some vegetation models (e.g., BIOME4, *Kaplan, 2003*), particularly when  
480 coupled with climate model simulations (as GCMs, *Haywood et al., 2009*). Affinity scores from  
481 pollen taxa were only calculated for pollen taxa percentages greater than 0.5% in order to  
482 increase signal-over-noise ratios (e.g., *Chen et al., 2010*), following the same scheme as that  
483 of the previously described biomization approach (see **section IV.1.2**). For particular species,  
484 such as *Larix* and *Pinus*, we applied the same pollen production and transport corrections as  
485 described above for the biomization.

486 For Europe, 242 pollen taxa were grouped into PFTs and further assigned to 6  
487 megabiomes (*Dallemeyer et al., 2019*): *temperate forest (TEFO)*, *boreal forest (BOFO)*, *warm-*  
488 *temperate forest (BOFO)*, *tundra and polar desert (TUND)*, *grassland and dry shrubland (STEP)*,  
489 *and desert (DESE)*. We directly used the algorithm implemented in R (*Cao and Tian, 2021*; R  
490 version 4.2.3, <https://www.r-project.org/>). When affinity scores were found equal, the  
491 megabiome with the fewest PFTs was selected. The correspondence of biome and megabiome  
492 tables are reported in **Appendix 2** for typical taxa in **Appendix 3. Table 2** summarizes pollen  
493 taxa to biome and megabiome assignment schemes used in this study.

494

495

496

497

498

499

500



Fénisse et al.,

Biome			
Taxa	PFTs	Biomes	Ref.
98	25	16	<i>Prentice et al., 1998</i>
Megabiome			
Taxa	PFTs	Megabiomes	Ref.
242	41	7	<i>Binney et al., 2017</i> <i>Marinova et al., 2018</i> <i>Cao et al., 2019</i>

501

502 **Table 2.** Summary table of pollen taxa, plant functional types (PFTs), and (mega)biomes used  
503 in the biomisation frameworks, also provided in Supplementary Material 1.

504

505 **IV.2 - A weighted-mean approach to assess (mega)biome scores**

506 One of the most notable issues of the (mega)biomization approaches is the sensitivity  
507 of reconstructed climates to small variations in biome scores (*Cruz-Silva et al., 2022*). The  
508 dominant biome effect (i.e., the biome with the highest affinity score) represents a significant  
509 source of uncertainty and poses major challenges for the reliability of reconstructed climate  
510 variables. This attribution of dominant (mega)biomes ignores potentially important  
511 (mega)biome contributions that are close to the maximum score and result in abrupt  
512 paleoclimate changes that merely reflect competition between (mega)biome scores rather  
513 than any significant bioclimatic shift.

514 To address this issue, we reconstruct fossil climate datasets for each (mega)biome using  
515 the three reconstruction methods (**section II**, MAT, WA-PLS, and CREST), distinguishing the  
516 modern calibration dataset (**section III.3**, EMPD2) by (mega)biome (biome-specific calibration  
517 datasets). We then calculate (mega)biome scores for each fossil sample and combine them  
518 with the climate reconstructions for each (mega)biome using a (mega)biome affinity score-  
519 weighted mean of climate variables (**Fig.1**). Finally, we evaluate the impact of using the  
520 (mega)biome affinity score-weighted mean approach of all fossil (mega)biome scores rather  
521 than relying solely on the dominant biome’s climate signal.

522

523 **V. Results**

524 Vegetation and climate maps presented in this study use the WGS84 projection with  
525 coastal boundaries reflecting present-day conditions (**section III.3**). The LGM ice-sheet mask  
526 was obtained by combining data from *Peltier and Solheim (2004)*, *Ehlers et al. (2011)* and  
527 *Seguinot et al. (2018)*. Climate reconstruction uncertainties of WA-PLS and MAT are provided  
528 as root mean square errors of prediction (RMSEP) derived from leave-one-out cross-  
529 validation.



Fénisse et al.,

530 **V.1 – (Mega)biomization results: (mega)biome score processing**

531 **V.1.1 - Modern (mega)biome distribution maps**

532 The modern distribution of biomes (from EMPD2 pollen dataset) across Eurasia shows  
533 that these are geographically homogeneous (**Fig 2.1.a**), with typical frequencies of biomes  
534 from 5% to 20% (**Fig 2.1.b**), except for cold deciduous forest (CLDE), desert (both cold (HODE)  
535 and hot HODE)) and supplementary biomes (pioneer (PION), anthropogenic (ANTH) and  
536 aquatic (AQU)), which are all minor (<1%) across Europe. Western Europe (e.g., France, Spain,  
537 Italy) exhibits the greatest biome diversity.

538 While cool conifer and cold mixed forests are primarily located in Scandinavia, cool  
539 mixed forests, taiga, and xerophytic woodlands surround the Mediterranean region. The  
540 warm mixed forest biome is dominant in southern Spain, Italy, and parts of the Near and  
541 Middle East. The clustering of different biomes in close geographic regions is attributed to  
542 broad climate patterns, altitude gradients, anthropogenic impacts (e.g., deforestation,  
543 agriculture, climate change), and/or local effects (e.g., proximity to water sources). The lack  
544 of data in Eastern Europe results in an underrepresentation of cold modern climate conditions.

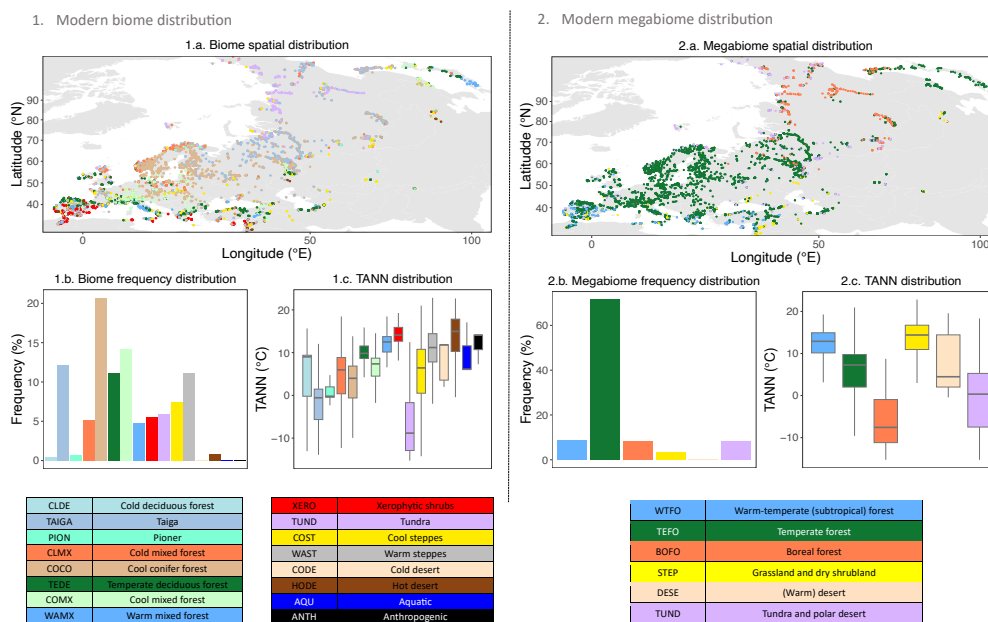
545 Mean annual temperatures (TANN) are spatially variable in Europe and distinguished  
546 by (mega)biomes, reflecting ecological and climatic differences across regions (**Figs 2.1.c and**  
547 **2.2.c**). TANN is generally negative in tundra regions (TUND, medians ~-9°C) and significantly  
548 higher in temperate forests (TEDE), cool mixed forests (COMX), warm mixed forests (WAMX),  
549 warm steppes (WAST), xerophytic woodlands (XERO), and hot deserts (HODE) (**Fig 2.1.b**).  
550 Other biomes, such as cold deciduous forests (CLDE), taiga (TAIG), pioneer (PION), cold mixed  
551 forests (CLMX), cool mixed forests (COMX), and cold steppes (COST), exhibit intermediate  
552 climatic conditions. The overlap of COMX and TEDE biomes in geographic and climatic spaces  
553 is likely due to their physiognomic similarities (*Binney et al., 2017*). As proposed by *Prentice et*  
554 *al. (1998)* and *Tarasov et al. (2000)*, using the same biomization procedure as in this study, we  
555 observe a dominance of tundra and taiga in Russia, where modern conditions are among the  
556 driest in Europe.

557 The modern results derived from the major megabiome analysis (**Fig 2.2.a**) indicate a  
558 strong dominance of the temperate megabiome (TEDE) (~65%, **Fig 2.2.b**) across Europe,  
559 covering much of Western Europe and seemingly obscuring the greater diversity of biomes  
560 observed in **Fig 2.1.a**. While mountain regions exhibit a mix of CLMX, COMX, and COST biomes,  
561 the megabiomization analysis yields a predominance of TEDE, TUND and STEP (**Fig 2.1.b**). The  
562 climate space of the temperate megabiome (TEDE, **Fig 2.2.c**) is more arid (i.e., colder and drier)  
563 than the temperate biome (TEDE, **Fig 2.1.c**). Consequently, steppe megabiomes – including  
564 boreal forest (BOFO), grassland and dry shrubland (STEP), warm desert (DESE), and tundra and  
565 polar desert (TUND) - are sparse, although they share common locations with their modern  
566 biome counterparts (**Fig 2.2.c** and Table in **Appendix 2**).

567  
568  
569  
570



Fénisse et al.,



575 **Figure 2.** European biome (1) and megabiome (2) spatial and modern climate distributions,  
 576 using ECMWF Reanalysis v5 (ERA5; from January 1940,  
 577 <https://www.ecmwf.int/en/forecasts/dataset/ecmwf-reanalysis-v5>) and EMPD2 dataset  
 578 (Eurasian Modern Pollen Database, *Davis et al., 2020*). The biome classification, code and  
 579 output database are available in **Supplementary materials**. The megabiome schema is  
 580 described and in open access in *Li et al., 2024*,  
 581 (<https://doi.pangaea.de/10.1594/PANGAEA.965907>). TANN = Mean Annual Temperature.

### 583 V.1.2 - Fossil (mega)biomes during the LGM

584 LGM biome score results from the 43 selected European fossil sites reveal a clear  
 585 dominance of the cool steppes, called COST (colored outlines around the pie charts from **Fig**  
 586 **3.a**). However, the dominant megabiome reconstructions oppose temperate (TEFO) and  
 587 tundra and polar desert (TUND) megabiomes (**Fig 3.b**), with a few instances of steppic  
 588 conditions around the Mediterranean region. In detail, (mega)biome scores of the LGM  
 589 samples are very close to each other, indicating a strong competition and therefore only a  
 590 weak dominance of any particular (mega)biome. For instance, while the total scores for arid  
 591 megabiomes (i.e., grassland and dry shrubland (STEP) + desert (DESE) + tundra and polar  
 592 desert (TUND)) range between 30% and 60%, these fossil sites remain dominated by the  
 593 temperate megabiome, called TEDE (points with black outlines in **Appendix 4**). Even when one  
 594 megabiome appears dominant during the LGM, several other megabiomes also display  
 595 substantial scores. These results (**Figs 3.a and 3.b**) indicate an absence of a dominant  
 596 vegetation ensemble, while transitional vegetation conditions are also apparent through the  
 597 co-occurrence of multiple (mega)biomes. The selection of the dominant (mega)biome is thus



Fénisse et al.,

598 based on marginal differences between competing scores, which underscores the limitation  
599 of this approach when several (mega)biomes co-exist within the same climatic period. By  
600 accounting for non-dominant (mega)biomes, our (mega)biome affinity score-weighted mean  
601 method based on (mega)biome scores can better capture underlying signals and provide more  
602 nuanced climate reconstructions across Europe.

603 By comparing biome and megabiome dominance scores, the steppic (STEP) and tundra  
604 (TUND) megabiomes - which correspond to the cold and hot steppic biomes (COST and WAST)  
605 and tundra (TUND) in [Appendix 2](#) - are not consistently observed, suggesting that the  
606 (mega)biome definitions (i.e., pollen and PFTs) in these two classification schemes reflect  
607 distinct climatic conditions ([Fig 1](#)). This therefore suggests that the choice of classification  
608 could influence the reconstructed climate conditions. The search for the best analogues across  
609 different climatic spaces grouped by (mega)biome highlights the challenges of distinguishing  
610 local climatic conditions and isolating LGM vegetation analogues for climate reconstructions  
611 at the European scale.

612

613

614

615

616

617

618

619

620

621

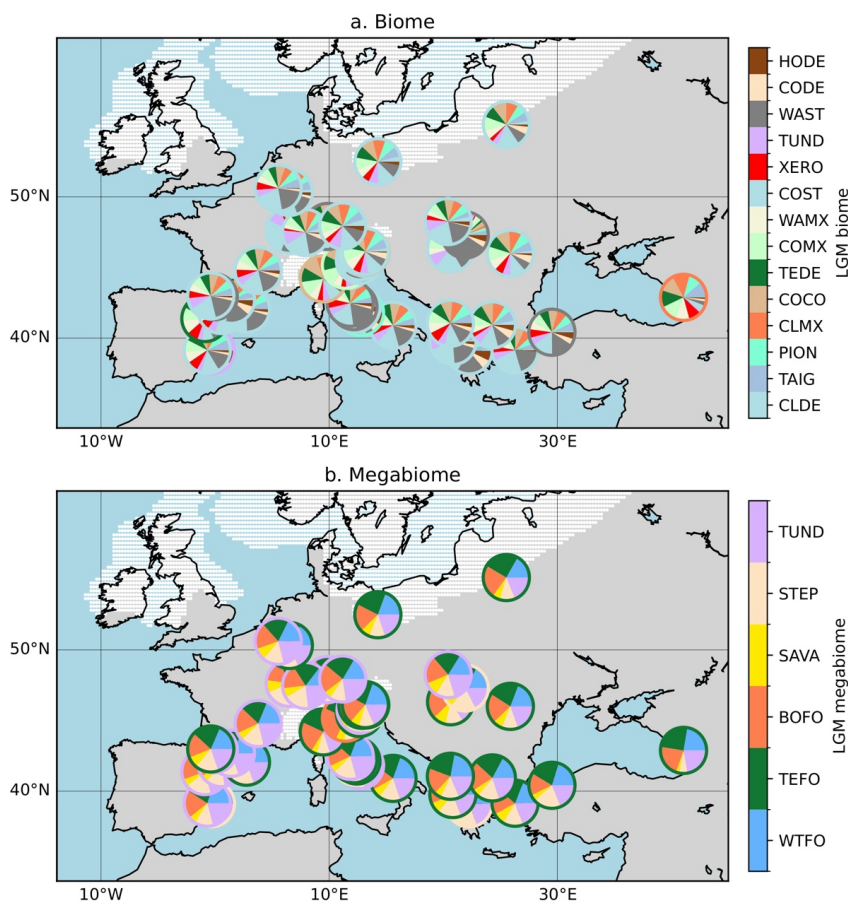
622

623

624

625

626



627 **Figure 3.** Percentage of fossil biomes **(a)** and megabiomes **(b)** in pollen sequences during the  
 628 LGM across Europe. Colored outlines around the pie charts indicate the dominant  
 629 (mega)biomes. The white area represents the ice sheet extent.

630

### 631 V.1.3 - (Mega)biome affinity score-weighted means

632 Mean annual temperature anomalies (i.e.,  $TANN_{reconstructed} - \text{Modern climate}$ ) over the past  
 633 40,000 years, obtained by combining the (mega)biomization and the three different  
 634 reconstruction methods used in this study, are presented for the Lake Bouchet sequence in  
 635 Fig.4. The near-zero climate anomalies observed for the present day at both sites confirm the  
 636 accurate calibration of the reconstruction methods. TANN variations from both methods  
 637 alternate between cold steppe (COST) and warm steppe (WAST) biomes (Fig.3) from 40 kyr to  
 638 10 kyr cal BP, before being mostly driven by temperate (TEDE) biomes from 10 kyr cal BP until  
 639 present. Using the megabiome approach, we observe the same temperate (TEDE) dominance  
 640 between 0 and 10 kyr cal BP, preceded by an alternation between tundra (TUND) and steppe  
 641 (STEP) megabiomes from 40 kyr to 10 kyr cal BP. As shown in Fig.3, the COST biome and the



Fénisse et al.,

642 TUND megabiome mainly dominate at Lake Bouchet during the LGM. The dominant  
643 (mega)biome method produces larger TANN variations due to alternance between these two  
644 co-dominant arid (mega)biomes, which correspond to distinct climatic conditions (Fig 4).

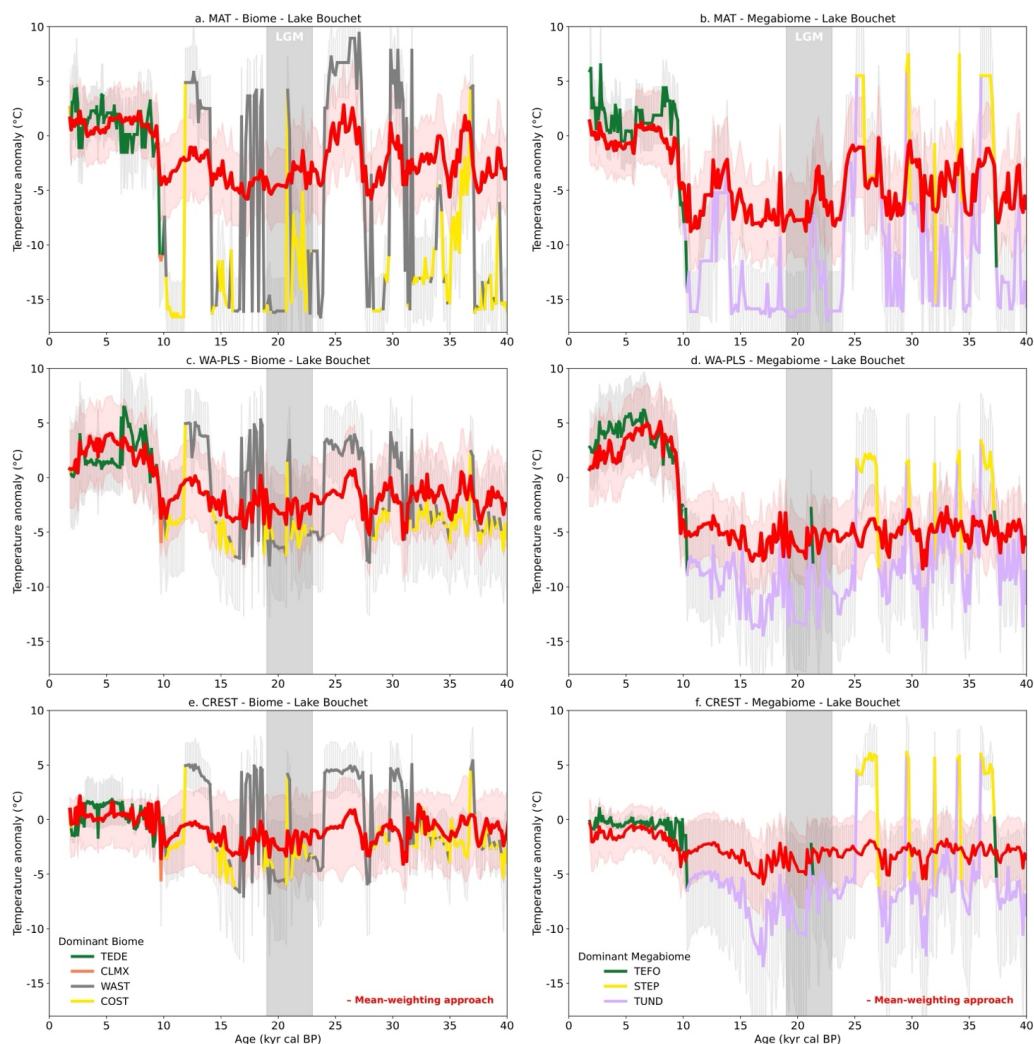
645 While the temporal variations in (mega)biome dominance at Lake Bouchet are  
646 comparable across reconstruction methods, the same (mega)biomes (i.e., based on identical  
647 modern and fossil sub-datasets) produce different TANN reconstructions depending on the  
648 method and calibration procedures (e.g., biomes vs. megabiomes) applied (Fig.4). The MAT  
649 method suggests strong instability in temperature (TANN) variations before 10 kyr cal BP, as  
650 a result of alternating dominant (mega)biomes. However, TANN variations appear  
651 synchronous and of similar amplitude (from -15 to 10°C) between biome and megabiome  
652 results from MAT (Figs 4.a and 4.b). In contrast, TANN variations derived from the WA-PLS  
653 (Figs 4.c and 4.d) and CREST (Figs 4.e and 4.f) methods indicate more stable climatic  
654 conditions that are consistent for a given classification. Nonetheless, TANN variations from  
655 WA-PLS and CREST are generally colder with the megabiome approach than with the biome  
656 approach (Figs 4.e and 4.f). Based on temperate (mega)biomes, TANN variations obtained  
657 with WA-PLS and CREST during the deglaciation gradient (10–0 kyr) show smaller extents of  
658 cooling using the biome rather than the megabiome procedure. While annual climatic  
659 conditions are similar between the megabiome ( $-3\pm 3^{\circ}\text{C}$  and  $-2\pm 1/-5^{\circ}\text{C}$ , from WA-PLS and  
660 CREST methods, respectively) and the biome ( $-2\pm 6^{\circ}\text{C}$  and  $-1\pm 5/-9^{\circ}\text{C}$ , from WA-PLS and CREST  
661 methods, respectively) approach for WA-PLS and CREST during the LGM, the MAT method  
662 shows colder climatic conditions than the two other methods, with consistent values between  
663 the biome and megabiome approaches derived from MAT ( $-4\pm 7^{\circ}\text{C}$  and  $-6\pm 3^{\circ}\text{C}$ , respectively).

664 Due to the strong climatic instability predicted by MAT based on both biome and  
665 megabiome procedures, the (mega)biome affinity score-weighted mean approach appears to  
666 have the greatest impact on MAT-derived reconstructions (Figs 4.a and 4.b). All TANN  
667 variations derived from the biome affinity score-weighted mean approach show climatic  
668 changes that are synchronous with the results from the dominant (mega)biome approach, but  
669 with lower amplitudes. TANN variations from both the dominant and biome affinity score-  
670 weighted mean approaches exhibit LGM coolings, with amplitudes ranging from 2 to 8°C.

671 Most of the observed fluctuations in the modelled dominant vegetation (and therefore  
672 in the reconstructed climates) at Lake Bouchet thus arguably arise from a methodological  
673 limitation related to non-linear threshold effects, (mega)biome score competitions, and a high  
674 sensitivity of the estimation of dominant biomes to minor changes in vegetation assemblages.  
675 TANN reconstructed from biome affinity score-weighted means are less sensitive to this  
676 threshold effect as these transitions become gradual when including all the biome scores. The  
677 combination of these (mega)biome-specific climate reconstructions allows for more reliable  
678 and less noisy reconstructions, still capturing major climatic signals. This approach thus  
679 enhances the accuracy and robustness of pollen-based paleoclimate reconstructions by  
680 explicitly accounting for the uncertainties of (mega)biomization algorithms, representing a  
681 significant methodological advancement.



Fénisse et al.,



682 **Figure 4.** TANN anomaly (LGM – Modern climate, LGM cooling) reconstructed over time at  
 683 Lake Bouchet using three different reconstruction methods for (mega)biome procedures. Bold  
 684 curves show TANN reconstructed and their climatic errors ( $1\sigma$ ) from the dominant  
 685 (mega)biome (colored according to the dominant biome). Bold red curves report the weighted  
 686 mean TANN reconstructed from (mega)biome scores. Confidence in mean-weighting is  
 687 indicated by red areas. The grey area indicates the LGM time interval. The modern climate  
 688 reference is TANN = 8.3°C. All climate data were processed using the current biomization  
 689 assignment scheme in CREST (**Fig.2**).

690  
 691  
 692



Fénisse et al.,

693 **V.2 – Multi-method temperature reconstructions using the (mega)biome affinity score-**  
694 **weighted mean approach during the LGM**

695 **V.2.1 - Cross-validation of the models**

696 To assess the quality, performance and robustness of modeled climates using the three  
697 different methods, we apply a cross validation procedure from modern dominant biome  
698 datasets and show the existence of robust correlations (correlation,  $r$ ) for TANN, Mean  
699 Temperature of the WArmeSt month (MTWA) and Mean Temperature of the COldest month  
700 (MTCO) in [Appendix 5](#). Interestingly, the quality of the correlations of temperature  
701 reconstructions (including the three variables) using MAT and WA-PLS are generally similar  
702 across biomes, except for MAT correlations from the CLDE biome, which remain particularly  
703 low ( $r = 0.39, 0.41, \text{ and } 0.55$  for TANN, MTWA, and MTCO, respectively). The calibration  
704 dataset from the COST biome, which represents the dominant conditions of the LGM, shows  
705 good performances ( $r > 0.65$  and  $\text{RMSEP} < 4.80^\circ\text{C}$ ) for both MAT and WA-PLS. Overall, biomes  
706 richest in PFTs (COCO, COMX, CLMX) show the strongest correlations ( $r > 0.7$ ), consistent with  
707 previous findings by [Ortega-Rosas et al. 2008](#). While megabiomes generally show less  
708 consistent performances than biomes, the DESE megabiome - the least dominant in both  
709 modern and fossil records - performs the worst ( $r < 0.46$ , from 12 modern samples).

710

711 By synthesizing the correlations and errors of the climatic variables across  
712 (mega)biomes ([Appendix 5](#)), we observe that all reconstruction methods reproduce the  
713 general trends of the modern climates reasonably well, with strong correlations ( $r > 0.6$  on  
714 average, [Fig.5](#)). These high correlations are largely independent of the variable considered, as  
715 similar values are obtained for TANN, MTWA, and MTCO, suggesting that the methods capture  
716 the dominant climate gradients rather than being specifically sensitive to a given season.  
717 Among the methods, WAPLS consistently shows weaker correlations than MAT and CREST,  
718 indicating a lower ability to reproduce the modern climatic signals. In contrast, CREST  
719 correlations are less variable and remain tightly grouped (within  $\sim 0.1$ ), which suggests greater  
720 robustness and stability compared to statistical transfer functions. Importantly, the average  
721 correlation values remain stable across calibration datasets, implying that the capacity of  
722 these methods to reproduce modern climate patterns is not significantly affected by the  
723 choice of (mega)biome calibration set.

724 Correlation metrics provide complementary insights into the absolute performance of the  
725 reconstruction methods in the error boxplot of [Fig.5](#). On average, the three methods  
726 reproduce modern climate conditions with a mean error of approximately  $+3^\circ\text{C}$  (RMSEP),  
727 which is generally acceptable for large-scale palaeoclimate reconstructions. However, a clear  
728 seasonal dependency emerges: winter temperatures (MTCO) are associated with larger errors  
729 ( $\text{RMSEP} \leq \pm 4.5^\circ\text{C}$  in RMSEP), particularly when using MAT and CREST. This bias suggests that  
730 these methods struggle to capture the winter climatic conditions, possibly due to limitations  
731 in the underlying calibration data or in the sensitivity of the proxies to winter conditions. In



Fénisse et al.,

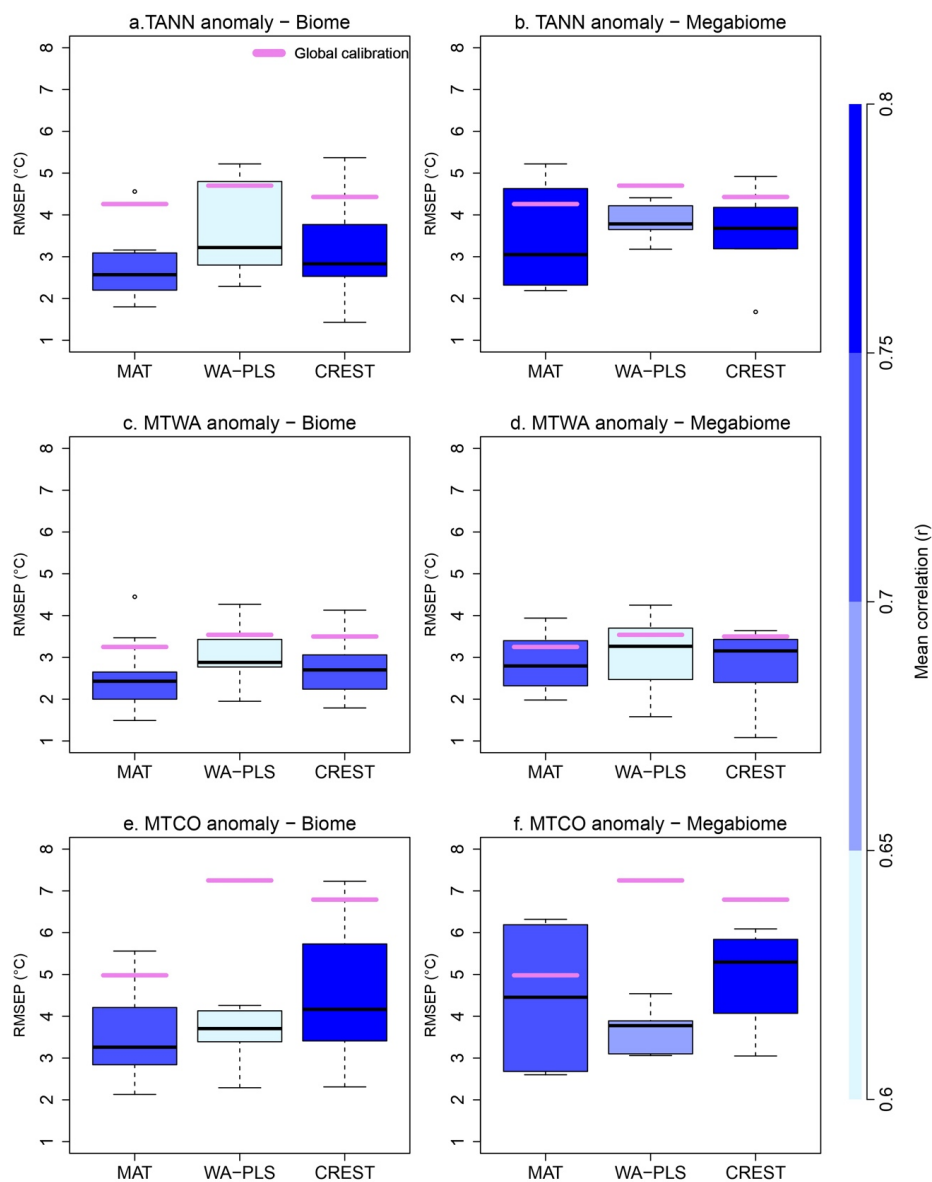
732 contrast, summer (MTWA) and annual mean temperatures (TANN) are more precisely  
733 reconstructed across reconstruction methods, with the small errors around the mean.

734 The errors from global calibrations (in purple in [Fig.5](#)) are systematically higher than those  
735 obtained from (mega)biome calibrations. This observation suggests that calibration  
736 techniques from (mega)biomes increase the uncertainties in climate reconstructions. Error  
737 variability in the (mega)biomization procedure is larger across reconstruction methods than  
738 between the two calibration datasets (biomes). However, the quality and density of the  
739 calibration data, as well as the calibration techniques used, also influence the results and  
740 ultimately contribute to the uncertainties of the climate reconstructions.

741



Fénisse et al.,



742 **Figure 5.** Correlation boxplots of TANN (**a and d**), MTWA (**b and e**) and MTCO (**c and f**) from  
 743 three different reconstruction methods using biomes and megabiomes, in first and second line,  
 744 respectively. Reconstruction methods are indicated on the x-axis. Mean correlations ( $r$ ) are  
 745 reported in the common colorbar. The violet bars represent mean RMSEP values from the  
 746 global calibration procedure. Results are reported **Appendix 5**.

747

748



Fénisse et al.,

749 **V.2.2 – Annual temperature anomalies**

750 LGM climate anomalies based on the (mega)biome affinity score-weighting approach  
751 and the three reconstruction methods are shown in [Fig.6](#) and summarized in [Table 3](#). For the  
752 three different reconstruction methods, results at each core site are presented as anomalies  
753 compared to the modern climate estimated from ERA5-reanalysis ([Hersbach et al., 2020](#);  
754 [Table 2](#)). From both vegetation classification methods, the LGM cooling across all fossil sites  
755 ranges from 1°C to 11°C, in line with LGM conditions significantly different from today. The  
756 mean European LGM cooling using the three reconstruction methods (MAT, WA-PLS, and  
757 CREST) yield  $7.0 \pm 2.3^\circ\text{C}$ ,  $7.1 \pm 2.2^\circ\text{C}$ , and  $5.9 \pm 2.2^\circ\text{C}$  (mean SD,  $1\sigma$ ) from the biomization method  
758 ([Figs 6.a, 6.c and 6.d](#)) and  $8.0 \pm 2.5^\circ\text{C}$ ,  $7.2 \pm 2.4^\circ\text{C}$ , and  $7.0 \pm 2.3^\circ\text{C}$  from the megabiomization  
759 method ([Figs 6.b, 6.d and 6.f](#)), respectively. The largest LGM coolings are observed in  
760 mountain ranges, such as the Alps and the Pyrenees ( $\sim 10^\circ\text{C}$ ), with an agreement across all  
761 methods (standard deviation of  $\sim 1^\circ\text{C}$ , [Appendix 6](#)). The Lake Bouchet (France), Kersdorf-  
762 Briesen (Germany) and Mickunai (Lithuania) fossil sites show the largest disagreement ( $\sim 2^\circ\text{C}$   
763 standard deviation across the three methods). We could not detect any spatial gradient, or  
764 any influence of the proximity of the Fennoscandian ice-sheet from these two sets of  
765 reconstructions (i.e., biomization and megabiomization techniques, [Fig.6](#)).

766  
767  
768  
769  
770  
771  
772  
773  
774  
775  
776  
777  
778  
779  
780  
781  
782  
783  
784  
785



Mean multi-method results

a. Climate anomaly results from biomes

	TANN MAT	TANN WA-PLS	TANN CREST	MTWA MAT	MTWA WA-PLS	MTWA CREST	MTCO MAT	MTCO WA-PLS	MTCO CREST	TANN	MTWA	MTCO
Lake Xinias	-8 ± 3	-8 ± 3	-6 ± 3 / -7	-8 ± 2	-5 ± 2	-5 ± 1 / -9	-5 ± 3	-6 ± 4	-4 ± 3 / -4	-7 ± 2 / -10	-6 ± 3 / -9	-5 ± 2 / -8
Cova de les Malladetes	-8 ± 3	-9 ± 4	-7 ± 1 / -9	-5 ± 3	-4 ± 3	-4 ± 1 / -12	-7 ± 4	-10 ± 6	-7 ± 5 / -7	-8 ± 2 / -11	-4 ± 2 / -10	-8 ± 4 / -12
Navarrés	-10 ± 3	-10 ± 3	-9 ± 2 / -9	-8 ± 3	-7 ± 3	-6 ± 3 / -14	-9 ± 5	-12 ± 5	-9 ± 8 / -11	-9 ± 1 / -12	-7 ± 1 / -12	-10 ± 6 / -14
Megali Limni	-11 ± 3	-12 ± 3	-8 ± 1 / -8	-9 ± 2	-8 ± 2	-8 ± 2 / -15	-17 ± 4	-18 ± 4	-11 ± 11 / -8	-10 ± 2 / -13	-8 ± 2 / -13	-15 ± 11 / -20
Ioannina	-6 ± 1	-7 ± 1	-5 ± 2 / -6	-4 ± 1	-3 ± 1	-2 ± 2 / -6	-2 ± 2	-4 ± 2	-1 ± 1 / -2	-6 ± 2 / -7	-3 ± 0 / -6	-3 ± 1 / -5
Lake Iznik	-6 ± 2	-6 ± 2	-5 ± 2 / -5	-6 ± 2	-4 ± 2	-4 ± 4 / -11	-6 ± 3	-7 ± 4	-5 ± 4 / -7	-5 ± 2 / -8	-5 ± 1 / -9	-6 ± 3 / -9
Lago Grande di Monticchio	-4 ± 1	-4 ± 1	-3 ± 0 / -3	-8 ± 1	-6 ± 1	-6 ± 2 / -9	-6 ± 1	-7 ± 1	-5 ± 5 / -6	-4 ± 1 / -5	-7 ± 4 / -9	-6 ± 5 / -7
Mire Straidzha Kupena-3	-5 ± 2	-5 ± 2	-4 ± 2 / -4	-8 ± 2	-8 ± 2	-8 ± 1 / -14	-13 ± 4	-11 ± 4	-9 ± 9 / -12	-5 ± 2 / -7	-8 ± 3 / -12	-11 ± 8 / -15
Lake Ohrid	-7 ± 2	-7 ± 2	-5 ± 1 / -7	-7 ± 2	-5 ± 2	-5 ± 4 / -12	-2 ± 3	-3 ± 3	0 ± 1 / -1	-7 ± 1 / -9	-6 ± 0 / -10	-2 ± 1 / -5
Torreçilla de Valmadrid	-4 ± 3	-5 ± 3	-5 ± 2 / -7	-5 ± 3	-3 ± 3	-4 ± 7 / -12	-4 ± 3	-7 ± 4	-6 ± 5 / -4	-5 ± 4 / -7	-4 ± 3 / -9	-5 ± 2 / -9
Valle di Castiglione	-6 ± 4	-7 ± 4	-7 ± 3 / -9	-6 ± 3	-5 ± 3	-5 ± 9 / -17	-4 ± 5	-7 ± 5	-7 ± 6 / -10	-7 ± 5 / -10	-5 ± 3 / -13	-6 ± 2 / -11
Lake Estanya	-5 ± 3	-5 ± 3	-3 ± 5 / -6	-6 ± 3	-5 ± 3	-4 ± 8 / -14	-5 ± 5	-6 ± 5	-3 ± 1 / -4	-5 ± 5 / -8	-5 ± 2 / -11	-5 ± 0 / -9
Stracciaccappa	-6 ± 4	-7 ± 4	-6 ± 5 / -6	-4 ± 4	-4 ± 4	-4 ± 11 / -16	-9 ± 6	-10 ± 6	-8 ± 7 / -13	-7 ± 7 / -10	-4 ± 5 / -12	-9 ± 4 / -15
Banyoles	-8 ± 1	-7 ± 1	-6 ± 4 / -6	-5 ± 1	-4 ± 1	-4 ± 1 / -7	-11 ± 1	-10 ± 1	-7 ± 7 / -8	-7 ± 4 / -8	-5 ± 3 / -6	-10 ± 8 / -11
Lago di Monterosi	-10 ± 3	-11 ± 3	-10 ± 2 / -11	-7 ± 2	-7 ± 2	-8 ± 3 / -16	-13 ± 4	-14 ± 4	-11 ± 10 / -17	-10 ± 1 / -13	-7 ± 1 / -12	-12 ± 9 / -17
Lago Vico	-6 ± 2	-6 ± 2	-5 ± 1 / -5	-5 ± 1	-3 ± 1	-4 ± 2 / -8	-8 ± 2	-9 ± 2	-7 ± 7 / -8	-6 ± 1 / -7	-4 ± 0 / -7	-8 ± 6 / -10
Lagaccione	-7 ± 3	-7 ± 3	-6 ± 2 / -6	-5 ± 2	-4 ± 2	-4 ± 2 / -8	-8 ± 4	-10 ± 4	-7 ± 7 / -9	-7 ± 1 / -9	-4 ± 1 / -7	-8 ± 5 / -11



Freychinede	-7 ± 4	-6 ± 5	4 ± 5 / -5	-3 ± 4	-3 ± 4	-3 ± 10 / -13	-8 ± 7	-6 ± 6	-2 ± 2 / -7	-6 ± 6 / -10	-3 ± 5 / -10	-5 ± 0 / -12
Dzigitia	-8 ± 3	-9 ± 3	-6 ± 0 / -7	-6 ± 3	-4 ± 3	-4 ± 6 / -12	-8 ± 4	-10 ± 4	-4 ± 4 / -2	-8 ± 0 / -10	-5 ± 1 / -10	-8 ± 3 / -12
Lourdes	-5 ± 2	-6 ± 2	-5 ± -1 / -5	-1 ± 2	1 ± 1	1 ± 6 / -3	-2 ± 2	-5 ± 3	-4 ± 4 / -5	-5 ± -1 / -7	0 ± 4 / -2	-4 ± -1 / -6
Tourbiere de l'Estarres	-8 ± 3	-7 ± 3	-5 ± 2 / -5	-2 ± 3	0 ± 3	0 ± 10 / -7	-7 ± 4	-7 ± 5	-5 ± -4 / -3	-7 ± 2 / -9	-1 ± 6 / -6	-6 ± -3 / -11
Pian del Lago	-8 ± 2	-8 ± 2	-6 ± -1 / -6	-6 ± 2	-5 ± 2	-5 ± 3 / -11	-12 ± 3	-14 ± 4	-9 ± -9 / -12	-7 ± -1 / -9	-5 ± 0 / -9	-12 ± -8 / -15
Lac du Bouchet B5	-4 ± 1	-2 ± 1	-1 ± 2 / -1	-3 ± 1	-1 ± 1	-1 ± 3 / -5	-7 ± 2	-5 ± 2	-2 ± 2 / -3	-2 ± 1 / -4	-2 ± 1 / -4	-5 ± -2 / -7
Lago della Costa	-11 ± 2	-9 ± 2	-7 ± -2 / -8	-11 ± 2	-7 ± 2	-7 ± 1 / -13	-10 ± 3	-11 ± 3	-7 ± -7 / -11	-9 ± -3 / -11	-8 ± -3 / -13	-9 ± -6 / -13
Orgiano	-12 ± 3	-11 ± 3	-10 ± -5 / -9	-11 ± 3	-8 ± 3	-8 ± 0 / -15	-12 ± 5	-13 ± 5	-9 ± -12 / -5	-11 ± -4 / -14	-9 ± -4 / -14	-11 ± -7 / -16
Venice	-10 ± 3	-10 ± 3	-10 ± -4 / -13	-10 ± 3	-8 ± 3	-8 ± 2 / -16	-10 ± 4	-12 ± 5	-11 ± -9 / -18	-10 ± -3 / -13	-9 ± -3 / -14	-11 ± -7 / -16
Azzano Decimo	-8 ± 3	-9 ± 3	-10 ± -3 / -13	-8 ± 3	-6 ± 2	-7 ± 2 / -13	-6 ± 4	-10 ± 4	-11 ± -9 / -17	-9 ± -1 / -12	-7 ± -1 / -11	-9 ± -5 / -14
Rio Doidis	-4 ± 5	-6 ± 4	-6 ± 3 / -9	-4 ± 4	-3 ± 3	-3 ± 8 / -12	-2 ± 7	-5 ± 6	-6 ± -6 / -13	-5 ± 6 / -9	-3 ± 4 / -9	-5 ± 1 / -11
Lake Sfantia Anna	-9 ± 3	-9 ± 3	-8 ± -3 / -8	-8 ± 2	-5 ± 2	-4 ± 3 / -10	-1 ± 3	-4 ± 4	-1 ± 1 / -5	-9 ± -3 / -11	-6 ± -1 / -10	-2 ± 2 / -6
Travesio	-11 ± 3	-10 ± 3	-8 ± -3 / -7	-8 ± 3	-5 ± 3	-4 ± 4 / -11	-7 ± 4	-8 ± 4	-5 ± -6 / -1	-10 ± -3 / -12	-6 ± 0 / -11	-7 ± -3 / -11
Billerio	-9 ± 3	-9 ± 3	-8 ± -3 / -7	-7 ± 3	-4 ± 3	-4 ± 5 / -11	-5 ± 5	-8 ± 4	-5 ± -7 / -1	-9 ± -2 / -11	-5 ± 0 / -10	-6 ± -2 / -11
Orvenco	-11 ± 3	-10 ± 3	-9 ± -4 / -8	-7 ± 3	-3 ± 3	-3 ± 6 / -10	-4 ± 4	-6 ± 4	-3 ± -5 / 1	-10 ± -3 / -13	-4 ± 2 / -9	-5 ± -1 / -9
Feher Lake	-6 ± 2	-7 ± 2	-6 ± -3 / -7	-7 ± 2	-6 ± 2	-6 ± -1 / -11	-4 ± 3	-7 ± 3	-5 ± -5 / -8	-6 ± -2 / -8	-6 ± -3 / -9	-5 ± -3 / -9
Kokad	-5 ± 6	-6 ± 5	-6 ± 3 / -8	-7 ± 5	-6 ± 4	-6 ± 7 / -15	-2 ± 7	-6 ± 7	-6 ± -5 / -13	-6 ± 6 / -10	-6 ± 2 / -13	-5 ± 2 / -12
La Grande Pile	-6 ± 2	-6 ± 2	-5 ± -1 / -5	-4 ± 1	-3 ± 1	-2 ± 2 / -6	-6 ± 2	-7 ± 2	-5 ± -5 / -7	-5 ± -1 / -7	-3 ± 0 / -6	-6 ± -4 / -8
Furamoso	-4 ± 2	-5 ± 2	-4 ± 1 / -5	-4 ± 1	-2 ± 1	-1 ± 5 / -6	-3 ± 2	-7 ± 2	-4 ± -4 / -8	-4 ± 1 / -6	-2 ± 2 / -6	-5 ± -2 / -8
Bergsee	-5 ± 2	-6 ± 2	-6 ± -1 / -7	-3 ± 2	-4 ± 2	-3 ± 4 / -8	-6 ± 3	-8 ± 4	-6 ± -5 / -10	-6 ± 0 / -8	-3 ± 1 / -7	-6 ± -4 / -10
Pilsensee	-7 ± 3	-7 ± 4	-6 ± -1 / -4	-4 ± 3	-3 ± 3	-2 ± 6 / -9	-5 ± 4	-6 ± 5	-5 ± -6 / 0	-7 ± 0 / -9	-3 ± 2 / -8	-5 ± -1 / -10
Nagymohos	-6 ± 2	-6 ± 2	-5 ± -1 / -6	-5 ± 2	-4 ± 2	-4 ± 1 / -8	-4 ± 3	-5 ± 3	-2 ± -2 / -5	-6 ± -1 / -7	-4 ± -1 / -7	-4 ± -2 / -7
Eifel	-5 ± 1	-7 ± 2	-4 ± 2 / -5	-3 ± 1	-2 ± 1	0 ± 7 / -6	-3 ± 2	-7 ± 2	-4 ± -4 / -8	-5 ± 1 / -7	-2 ± 3 / -5	-5 ± -2 / -8
La Grotte Walou	-5 ± 4	-5 ± 3	-4 ± 4 / -3	-3 ± 3	0 ± 3	1 ± 11 / -7	-3 ± 5	-6 ± 5	-5 ± -4 / -2	-5 ± 4 / -7	-1 ± 6 / -6	-5 ± -1 / -9
Kersdorf-Briesen	-7 ± 3	-6 ± 3	-5 ± 2 / -7	-7 ± 3	-4 ± 3	-3 ± 7 / -11	-7 ± 4	-7 ± 5	-5 ± -4 / -10	-6 ± 2 / -9	-5 ± 2 / -10	-6 ± -2 / -11
Mickunai	-3 ± 4	-1 ± 4	0 ± 8 / -1	-3 ± 4	-2 ± 4	-2 ± 10 / -12	-6 ± 6	-2 ± 6	1 ± 1 / -3	-1 ± 8 / -5	-3 ± 5 / -9	-3 ± 3 / -8
<b>Mean population SD</b>	<b>-7 ± 2</b>	<b>-7 ± 2</b>	<b>-6 ± 2</b>	<b>-6 ± 2</b>	<b>-4 ± 2</b>	<b>-4 ± 2</b>	<b>-7 ± 4</b>	<b>-8 ± 3</b>	<b>-6 ± 3</b>	<b>-7 ± 2</b>	<b>-5 ± 2</b>	<b>-7 ± 3</b>



788

Fénisse et al.,

**b. Climate anomaly results from megabiomes**

**Mean multi-method results**

	TANN MAT	TANN WA-PLS	TANN CREST	MTWA MAT	MTWA WA-PLS	MTWA CREST	MTCO MAT	MTCO WA-PLS	MTCO CREST	TANN	MTWA	MTCO
Lake Xinias	-10 ± 2	-8 ± 2	-8 ± -6 / -9	-8 ± 1	-4 ± 1	-4 ± -2 / -5	-3 ± 2	-8 ± 2	-7 ± -4 / -8	-9 ± -5 / -10	-5 ± -3 / -7	-6 ± -3 / -9
Cova de les Malladetes	-9 ± 4	-8 ± 4	-8 ± -4 / - 11	-8 ± 3	-2 ± 3	-2 ± 2 / -4	-4 ± 6	-10 ± 5	-10 ± -4 / - 14	-8 ± -1 / -12	-4 ± 0 / -8	-8 ± -2 / -14
Navarrés	-12 ± 3	-10 ± 3	-10 ± -6 / - 13	-8 ± 2	-7 ± 2	-6 ± -2 / -8	-11 ± 4	-12 ± 4	-12 ± -6 / - 16	-11 ± -5 / -13	-7 ± -4 / -9	-12 ± -7 / -16
Megali Limni	-13 ± 5	-12 ± 4	-12 ± -6 / - 15	-11 ± 4	-9 ± 3	-9 ± -4 / - 11	-14 ± 6	-17 ± 6	-15 ± -8 / - 19	-12 ± -4 / -16	-10 ± -6 / -13	-15 ± -9 / -21
Ioannina	-8 ± 2	-7 ± 2	-6 ± -4 / -7	-5 ± 1	-3 ± 1	-2 ± 0 / -3	-1 ± 2	-5 ± 2	-3 ± 0 / -5	-7 ± -4 / -9	-3 ± -1 / -5	-3 ± 0 / -6
Lake Iznik	-7 ± 3	-5 ± 3	-5 ± -2 / -7	-7 ± 2	-2 ± 2	-3 ± 1 / -5	-2 ± 4	-7 ± 4	-6 ± -1 / -9	-6 ± 0 / -9	-4 ± -1 / -7	-5 ± 0 / -10
Lago Grande di Monticchio	-6 ± 1	-4 ± 1	-4 ± -2 / -5	-9 ± 1	-6 ± 1	-5 ± -4 / -6	-4 ± 2	-7 ± 2	-6 ± -4 / -8	-4 ± -2 / -6	-7 ± -5 / -8	-6 ± -4 / -8
Mire Straidzha Kupena- 3	-7 ± 3	-7 ± 3	-6 ± -2 / -8	-8 ± 2	-8 ± 3	-6 ± -3 / -8	-10 ± 4	-16 ± 5	-14 ± -7 / - 17	-7 ± 0 / -10	-7 ± -4 / -10	-13 ± -7 / -18
Lake Ohrid	-9 ± 3	-7 ± 3	-7 ± -3 / -9	-8 ± 2	-5 ± 2	-4 ± -1 / -6	0 ± 4	-3 ± 4	-3 ± 3 / -5	-8 ± -2 / -10	-6 ± -3 / -9	-2 ± 3 / -6
Torreçilla de Valmadrid	-6 ± 3	-4 ± 4	-5 ± -1 / -8	-6 ± 3	-2 ± 3	-2 ± 2 / -4	-2 ± 5	-5 ± 5	-8 ± -1 / - 11	-5 ± 2 / -8	-3 ± 1 / -6	-5 ± 1 / -10
Valle di Castiglione	-6 ± 5	-7 ± 5	-8 ± -1 / - 12	-5 ± 4	-4 ± 4	-4 ± 2 / -7	-1 ± 7	-7 ± 8	-10 ± 0 / - 16	-7 ± 3 / -12	-4 ± 1 / -8	-6 ± 3 / -14
Lake Estanya	-7 ± 5	-4 ± 4	-5 ± 0 / -8	-7 ± 3	-4 ± 3	-3 ± 2 / -6	-3 ± 6	-5 ± 6	-7 ± 0 / -10	-5 ± 3 / -10	-5 ± -1 / -8	-5 ± 2 / -11
Stracciaccappa	-8 ± 6	-7 ± 5	-7 ± 0 / -11	-6 ± 4	-3 ± 4	-3 ± 3 / -7	-5 ± 8	-12 ± 8	-11 ± -1 / - 17	-8 ± 3 / -13	-4 ± 1 / -8	-9 ± 0 / -17
Banyoles	-10 ± 1	-7 ± 1	-7 ± -6 / -8	-7 ± 1	-4 ± 1	-4 ± -2 / -4	-8 ± 2	-11 ± 2	-9 ± -7 / - 10	-8 ± -6 / -10	-5 ± -3 / -6	-9 ± -7 / -11
Lago di Monterosi	-12 ± 4	-12 ± 4	-12 ± -6 / - 15	-7 ± 3	-6 ± 3	-7 ± -2 / - 10	-11 ± 5	-17 ± 6	-15 ± -7 / - 20	-12 ± -4 / -16	-7 ± -3 / -10	-15 ± -8 / -21
Lago Vico	-9 ± 2	-6 ± 2	-7 ± -4 / -8	-6 ± 1	-3 ± 2	-3 ± -1 / -4	-7 ± 3	-9 ± 3	-10 ± -6 / - 12	-7 ± -3 / -9	-4 ± -2 / -6	-9 ± -5 / -12

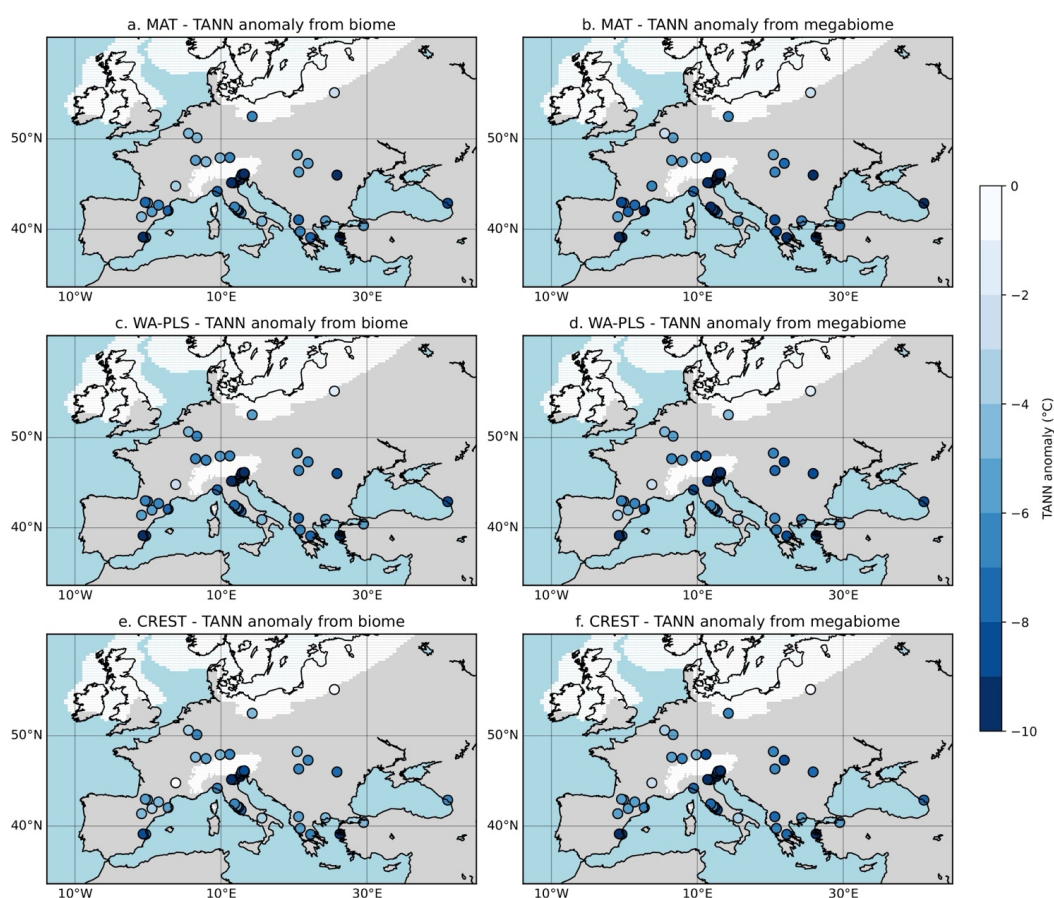


Lagaccione	-9 ± 2	-7 ± 2	-8 ± 5/-9	-6 ± 1	-3 ± 1	-3 ± -1/-4	-7 ± 3	-10 ± 3	-10 ± 7/-12	-8 ± -4/-10	-4 ± -2/-6	-9 ± -6/-12
Freychinède	-7 ± 5	-7 ± 5	-6 ± 1/-10	-3 ± 4	-2 ± 4	-1 ± 5/4	-1 ± 7	-8 ± 8	-6 ± 3/-12	-7 ± 3/-11	2 ± 3/-6	5 ± 3/-13
Dzignata	-11 ± 3	-8 ± 4	-8 ± 3/-10	-6 ± 2	-4 ± 3	-4 ± 0/-6	-10 ± 5	-10 ± 5	-7 ± -1/-10	-9 ± -2/-12	-5 ± -1/-7	-9 ± -3/-14
Lourdes	-7 ± 2	-6 ± 2	-6 ± 3/-7	-1 ± 1	1 ± 2	1 ± 4/0	-1 ± 3	-7 ± 3	-5 ± -1/-7	-6 ± -3/-8	0 ± 2/-2	-4 ± 0/-7
Tourbière de l'Estarrès	-9 ± 4	-6 ± 4	-6 ± -1/-9	-2 ± 3	1 ± 3	1 ± 6/-1	-5 ± 5	-8 ± 5	-6 ± 0/-10	-7 ± 0/-11	0 ± 4/-3	-6 ± 0/-11
Pian del Lago	-8 ± 3	-8 ± 3	-7 ± -3/-9	-5 ± 2	-5 ± 3	-4 ± -1/-6	-10 ± 4	-15 ± 5	-12 ± -7/-15	-8 ± -2/-10	-5 ± -2/-7	-12 ± -7/-16
Lac du Bouchet B5	-6 ± 2	-3 ± 2	-2 ± 0/-3	-5 ± 1	-1 ± 1	-1 ± 1/-2	-5 ± 2	-7 ± 2	-4 ± -2/-6	-4 ± 0/-6	-2 ± 0/-4	-6 ± -3/-8
Lago della Costa	-12 ± 3	-10 ± 3	-9 ± -5/-11	-10 ± 2	-8 ± 3	-6 ± -2/-8	-9 ± 4	-12 ± 5	-10 ± -4/-13	-10 ± -4/-13	-8 ± -4/-11	-10 ± -5/-14
Orgiano	-11 ± 3	-10 ± 4	-10 ± -5/-13	-11 ± 3	-9 ± 3	-7 ± -3/-9	-7 ± 5	-12 ± 6	-11 ± -5/-15	-11 ± -4/-14	-9 ± -5/-12	-10 ± -4/-15
Venice	-11 ± 5	-11 ± 4	-10 ± -5/-14	-9 ± 3	-7 ± 3	-6 ± -1/-9	-11 ± 6	-16 ± 6	-13 ± -5/-18	-11 ± -3/-15	-7 ± -3/-11	-13 ± -6/-19
Azzano Decimo	-10 ± 4	-11 ± 4	-10 ± -5/-14	-8 ± 3	-6 ± 3	-6 ± -2/-9	-5 ± 5	-13 ± 6	-12 ± -4/-17	-10 ± -3/-14	-7 ± -3/-10	-10 ± -3/-17
Rio Doidis	-6 ± 5	-6 ± 4	-6 ± 0/-11	-5 ± 3	-1 ± 3	-2 ± 4/-5	3 ± 7	-8 ± 6	-8 ± 2/-14	-6 ± 3/-11	-2 ± 2/-6	-4 ± 5/-12
Lake Sfanta Anna	-9 ± 3	-8 ± 3	-8 ± -4/-10	-6 ± 2	-4 ± 3	-3 ± 1/-5	0 ± 4	-4 ± 5	-2 ± 3/-5	-8 ± -2/-11	-4 ± -1/-7	-2 ± 3/-6
Travesio	-11 ± 3	-9 ± 4	-8 ± -4/-10	-6 ± 3	-4 ± 3	-3 ± 1/-5	-5 ± 4	-8 ± 6	-6 ± 1/-9	-9 ± -3/-13	-4 ± -1/-7	-6 ± -1/-11
Billerio	-8 ± 3	-8 ± 4	-7 ± -3/-10	-5 ± 3	-3 ± 3	-2 ± 2/-4	-3 ± 5	-8 ± 5	-6 ± 0/-10	-8 ± -1/-11	-4 ± 0/-6	-6 ± 0/-11
Orvenco	-12 ± 4	-10 ± 4	-9 ± -5/-12	-6 ± 3	-3 ± 3	-2 ± 3/-4	-5 ± 5	-7 ± 5	-5 ± 1/-8	-10 ± -4/-14	-4 ± 0/-7	-6 ± 0/-11
Fehler Lake	-6 ± 2	-7 ± 2	-7 ± -4/-8	-7 ± 2	-6 ± 2	-5 ± -3/-7	-2 ± 3	-8 ± 3	-6 ± -2/-8	-7 ± -2/-9	-6 ± -4/-8	-5 ± -1/-9
Kokad	-8 ± 7	-9 ± 5	-9 ± -1/-14	-8 ± 5	-7 ± 4	-6 ± 0/-10	-3 ± 8	-10 ± 8	-9 ± 3/-16	-8 ± 3/-14	-7 ± -2/-11	-7 ± 3/-16
La Grande Pile	-5 ± 2	-6 ± 2	-5 ± -3/-6	-4 ± 1	-3 ± 1	-2 ± 0/-3	0 ± 2	-9 ± 3	-6 ± -3/-8	-6 ± -2/-7	-3 ± -1/-4	-5 ± -1/-9
Furamoos	-5 ± 3	-7 ± 3	-5 ± -1/-7	-2 ± 2	-2 ± 2	-1 ± 2/-2	-3 ± 4	-10 ± 4	-7 ± -2/-10	-6 ± 0/-8	-2 ± 1/-4	-7 ± -1/-12
Bergsee	-5 ± 3	-6 ± 3	-6 ± -2/-9	-1 ± 2	-2 ± 2	-2 ± 1/-4	-3 ± 4	-8 ± 4	-6 ± -1/-9	-6 ± 0/-9	-2 ± 1/-4	-6 ± -1/-10
Pilsensee	-8 ± 3	-7 ± 4	-8 ± -3/-11	-3 ± 3	-2 ± 3	-2 ± 2/-5	-4 ± 5	-8 ± 6	-8 ± -1/-12	-8 ± -1/-11	-3 ± 1/-5	-6 ± 0/-11
Nagymohos	-6 ± 2	-6 ± 2	-6 ± -4/-8	-5 ± 2	-4 ± 2	-3 ± -1/-5	-1 ± 3	-6 ± 3	-4 ± 0/-6	-6 ± -2/-8	-4 ± -2/-6	-4 ± 0/-7
Eifel	-6 ± 3	-6 ± 3	-6 ± -2/-8	-4 ± 2	0 ± 2	0 ± 3/-2	-1 ± 4	-7 ± 4	-7 ± -1/-10	-6 ± 0/-8	-1 ± 2/-4	-5 ± 1/-10
La Grotte Walou	-3 ± 4	-5 ± 4	-3 ± 2/-7	-1 ± 3	0 ± 3	1 ± 6/-1	-1 ± 5	-7 ± 5	-4 ± 3/-7	-4 ± 4/-7	0 ± 4/-3	-4 ± 2/-9
Kersdorf-Bresen	-6 ± 4	-5 ± 4	-6 ± -1/-10	-6 ± 3	-3 ± 4	-4 ± 1/-6	-4 ± 5	-7 ± 6	-6 ± 1/-10	-6 ± 2/-10	-4 ± 0/-8	-6 ± 1/-11
Mickunai	-3 ± 5	-1 ± 5	0 ± 6/-3	-12 ± 4	-2 ± 4	-1 ± 5/-3	-2 ± 7	-3 ± 8	0 ± 7/-4	-1 ± 8/-6	-5 ± 2/-11	-2 ± 6/-8
Mean population SD	-8 ± 3	-7 ± 2	-7 ± 2	-6 ± 3	-4 ± 2	-3 ± 2	-4 ± 4	-8 ± 3	-8 ± 4	-7 ± 2	-4 ± 2	-7 ± 3



Fénisse et al.,

830 **Table 3.** Climate anomaly results (°C) for TANN (mean annual temperature), MTWA (mean  
 831 temperature of the warmest month), and MTCO (mean temperature of the coldest month) from three  
 832 different methods using the biomization (a) and megabiomization (b) procedures across 43 pollen sites.  
 833 In the “Mean multi-method results” column, errors (1σ) represent the combined uncertainty,  
 834 calculated as the square root of the sum of inter-point variance and mean internal errors. In contrast,  
 835 in the row “Mean population SD”, values represent the mean of population standard deviations (SD),  
 836 calculated using population variance (N), without internal error propagation.  
 837  
 838



839  
 840 **Figure 6.** Annual temperature anomaly results (LGM – Modern climate) using the biomization  
 841 (first line; a, b and c) and megabiomization (second line; d, e and f) processes from three  
 842 different methods (MAT, WA-PLS and CREST). Modern climates and LGM climate results are  
 843 reported in Table 3. The white area represents the ice sheet extent.

844  
 845  
 846



Fénisse et al.,

847 **V.2.3 – Seasonal temperature anomalies**

848 The first row of **Fig.7 (Figs 7.a-c)** presents reconstructed LGM summer temperature  
849 (MTWA) anomalies based on the biomization procedure, with values of  $-5.8 \pm 2.4$  °C,  
850  $-4.3 \pm 2.1$  °C, and  $-4.1 \pm 2.3$  °C (mean SD) for MAT, WA-PLS, and CREST, respectively. The  
851 three reconstruction methods yield the most negative MTWA anomalies in southeastern  
852 Europe ( $\sim -5$  °C), whereas values are more homogeneous and closer to zero in northern and  
853 western Europe. MTWA anomalies derived from the megabiomization procedure (**Figs 8.a-c**)  
854 are  $-6.1 \pm 2.7$  °C,  $-3.7 \pm 2.5$  °C, and  $-3.3 \pm 2.4$  °C for the same reconstruction methods,  
855 respectively, yielding similar spatial patterns in MTWA anomalies (**Fig.8**) that from the biome  
856 assignments (**Fig.7**). Interestingly, MAT-based MTWA anomalies from the megabiomization  
857 procedure ( $-6.1 \pm 2.7$  °C) are almost twice as large as those from the WA-PLS and CREST  
858 methods ( $-3.7 \pm 2.5$  °C, and  $-3.3 \pm 2.4$  °C, respectively) for mean values.

859 The winter temperature (MTCO, second row of **Figs 7 and 8**) anomalies are  
860  $-6.5 \pm 3.5$  °C,  $-8.0 \pm 3.2$  °C, and  $-5.6 \pm 3.0$  °C from biomization procedure and  $-4.5 \pm 3.8$  °C,  
861  $-9.0 \pm 3.5$  °C, and  $-7.8 \pm 3.5$  °C from megabiomization procedure, for MAT, WA-PLS, and  
862 CREST, respectively. MAT-based MTCO anomalies (mean value of  $-4.5$  °C) are about half that  
863 of CREST (and to a lesser extent WA-PLS) from the megabiomization procedure.

864

865 Seasonality anomalies (i.e., seasonal amplitudes) can be calculated from the difference  
866 between MTWA and MTCO anomalies at each site, derived from biomization and  
867 megabiomization procedures, as shown in the third row of **Figs 7 and 8** (panels g-i). From the  
868 biomization procedure (**Fig 7.g-i**), seasonality anomalies (LGM – Modern climate) are generally  
869 positive in Western Europe, whereas strongly negative anomalies are mainly observed in  
870 Eastern Europe. Results from the megabiomization procedure show seasonality anomaly  
871 patterns that differ markedly from those obtained with biomization. Megabiomized anomalies  
872 based on WA-PLS and CREST are positive and spatially homogeneous (**Figs 8.h and 8.i**), in  
873 contrast to the predominantly negative seasonality anomalies obtained from MAT (**Fig 8.g**).  
874 These differences arise from higher MTWA anomalies and lower MTCO anomalies obtained  
875 with the MAT method compared to WA-PLS and CREST within the megabiomization  
876 procedure. The discrepancies in seasonality anomalies among the three methods under  
877 megabiomization are therefore larger than those observed in the standard biomization  
878 results.

879

880

881

882

883

884

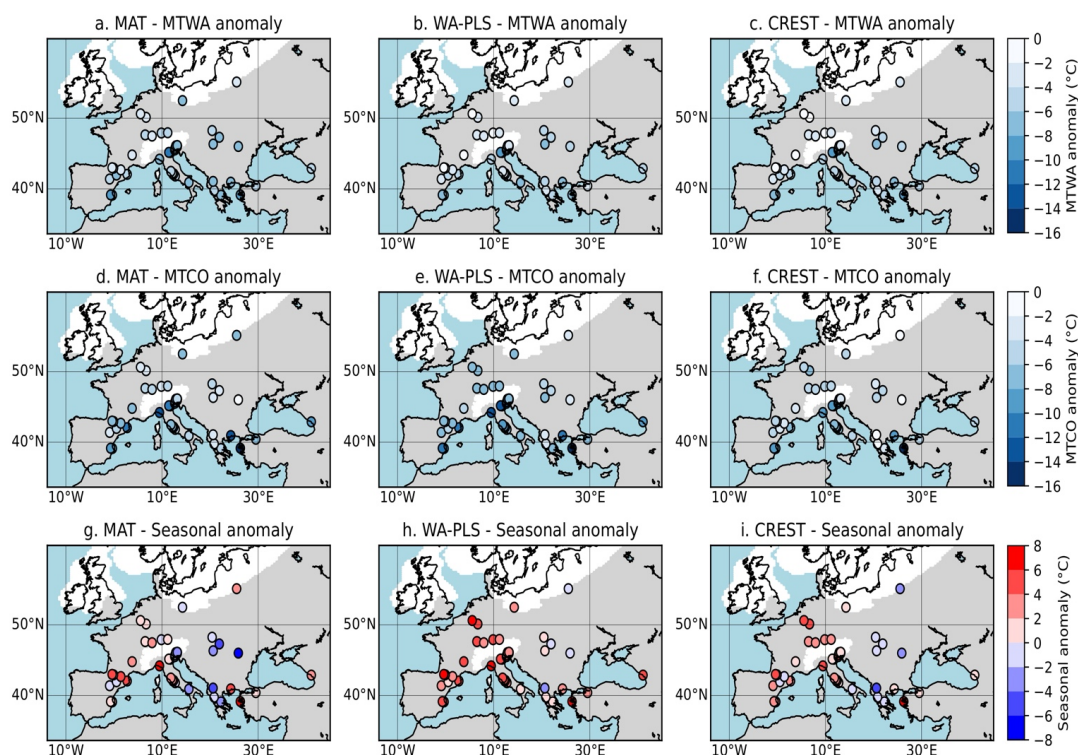
885

886

887



Fénisse et al.,

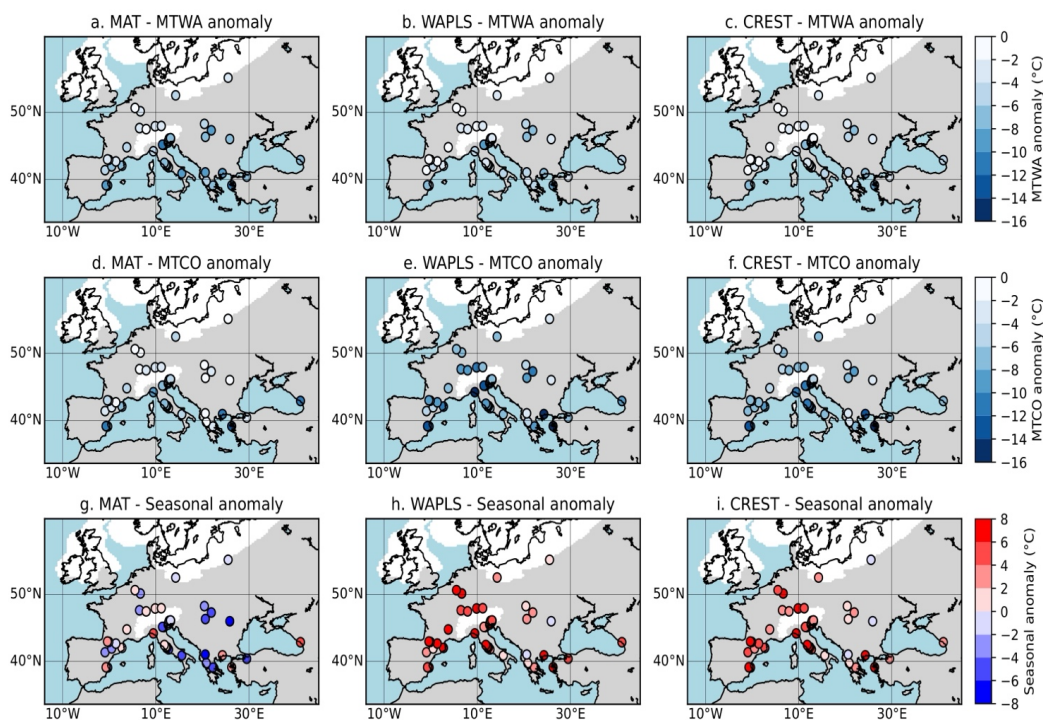


888 **Figure 7.** Monthly (MTWA and MTCO, in **a-c** and **d-f**, respectively) temperature anomaly  
889 (LGM – Modern climate) results, using the biomization process for the three different pollen-  
890 based climate reconstruction methods. From MTWA and MTCO results, seasonal anomalies  
891 are reported on **Figs g-i**. Modern climates and LGM climate results are reported in **Table 3**.  
892 The white area represents the ice sheet extent.

893  
894  
895  
896  
897  
898  
899  
900  
901  
902  
903  
904  
905  
906



Fénisse et al.,



907 **Figure 8.** Monthly (MTWA and MTCO, in **a-c** and **d-f**, respectively) temperature anomaly  
 908 (LGM – Modern climate) results, using the megabiomization process for the three different  
 909 pollen-based climate reconstruction methods. From MTWA and MTCO results, seasonal  
 910 anomalies are reported on **Figs g-i**. Modern climates and LGM climate results are reported in  
 911 **Table 3**. The white area represents the ice sheet extent.

912

913

#### 914 **V.2.4 - Inter-model means from annual and seasonal temperature anomalies**

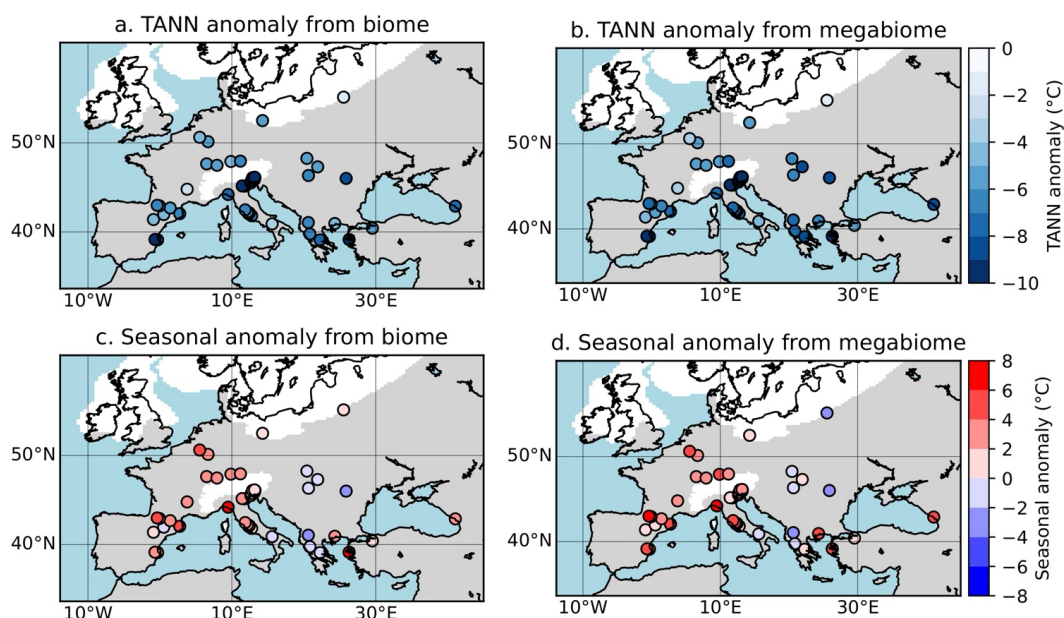
915 We summarize in **Fig.9** the arithmetic means of the LGM cooling and seasonality  
 916 derived from the three approaches, using biomization (**Figs 9.a and 9.c**) and  
 917 megabiomization (**Figs 9.b and 9.d**) procedures. Mean errors from these two climate  
 918 variables are reported in **Appendix 6**.

919 Across Europe, LGM cooling averaged  $6.7 \pm 2.2$  °C and  $7.4 \pm 2.3$  °C (**Table 3**) based on  
 920 biome and megabiome assignments, respectively (**Fig 9.a-b**). These results are generally  
 921 consistent across reconstruction methods, with inter-method standard deviations below  
 922 +2 °C (**Appendix 6**). Inter-model mean MTWA anomalies are similar for both reconstruction  
 923 methods and for biome versus megabiome assignments, with mean multi-method values of  
 924  $-4.7 \pm 2.2$  °C and  $-4.4 \pm 2.3$  °C, respectively. Inter-model mean MTCO anomalies are –  
 925  $6.7 \pm 3.0$  °C for the biomization approach (**Fig 7.d-f**) and  $-7.1 \pm 3.4$  °C for the  
 926 megabiomization approach (**Fig 8.d-f**). Mean seasonal anomalies across methods are



Fénisse et al.,

927  $+2.0 \pm 2.5$  °C and  $+2.7 \pm 2.7$  °C for biome and megabiome assignments, respectively (Fig 9.c-  
 928 d). MAT-based seasonal anomalies are lower ( $-1.7 \pm 3.5$ °C) than those from WA-PLS and  
 929 CREST ( $+5.7 \pm 2.8$  °C and  $+3.0 \pm 1.3$  °C, respectively) using megabiome procedures. In  
 930 contrast, seasonal anomalies are relatively consistent across methods using the biomization  
 931 approach, with inter-method standard deviations of  $\approx 2$ °C (Appendix 6).  
 932



933 **Figure 9.** Mean annual temperature (a and c) and seasonal index (b and d) anomaly results  
 934 (LGM – Modern climate) using averages of biomization and megabiomization results from  
 935 three different pollen-based climate reconstruction methods. Seasonal anomalies = MTWA -  
 936 MTCO anomalies. Standard deviation maps of climate anomalies are reported in Appendix 6.  
 937 The white area represents the ice sheet extent.

938

### 939 V.3 – Methodological implications on paleoclimate reconstructions

#### 940 V.3.1 - Local and global calibration effects on climate reconstructions

941 To isolate and quantify the impact of local calibration (i.e., (mega)biome procedures)  
 942 on global climate reconstructions during the LGM across Europe, Fig 10.a shows TANN  
 943 anomalies calculated as the difference between climates obtained using the (mega)biome  
 944 mean-weighting approaches and those derived from global calibration (i.e., by sampling the  
 945 entire calibration EMPD2 pollen dataset).

946 As the MAT method is inherently based on dissimilarity coefficients (Guiot et al., 1989),  
 947 it is theoretically able to directly identify the dominant analogues with no requirement for  
 948 (mega)biome calibration using all modern pollen spectra. As a result, one expects only a  
 949 minimal (if any) effect of (mega)biomization on TANN reconstructions from the MAT method



Fénisse et al.,

950 (Fig 10.a). Here, only a few fossil sites show a warming effect ( $\sim +5^{\circ}\text{C}$ ) of reconstructed TANN  
951 using local calibrations based on (mega)biomes (Venice, Billerio and Feher) rather than the  
952 global calibration. Then, the MAT method is thus arguably suitable for large-scale spatial  
953 studies using global datasets, to reconstruct annual temperature across Europe. Although the  
954 effects of local versus global calibration TANN anomalies for MAT may depend on the time  
955 period considered and the reconstructed climate variables (Xu et al., 2010), the magnitude of  
956 these effects remain generally close to zero. However, the WA-PLS method produces generally  
957 inconsistent results between local and global calibration results, with a mean TANN anomaly  
958 of  $\sim -4.5^{\circ}\text{C}$ , indicating colder TANN using local rather than global calibrations. Two significantly  
959 negative anomalies ( $\sim -10^{\circ}\text{C}$ ), were also identified using the WA-PLS method (Lake Iznik,  
960 Kersdorf-Briesen). Similarly, the CREST method appears more sensitive to calibration, as  
961 evidenced by predominantly negative TANN anomalies (from  $-1.2^{\circ}\text{C}$  to  $-10.9^{\circ}\text{C}$ , with a mean  
962 of  $-6.5^{\circ}\text{C}$ , Fig 10.a). This underscores the importance of a robust (mega)biomization scheme –  
963 climatic and environmental gradients of the study area – when applying CREST in Europe  
964 during the LGM to ensure that reconstructed TANN remains sufficiently cold and consistent  
965 with other statistical methods (see Figs 6 and 9). The importance of modern regional  
966 calibrations for quantitative climate reconstructions has also been noticed in previous studies  
967 (e.g., Trasune et al., 2024).

968 In Fig 10.b, the application of the (mega)biomization methods to MAT, WA-PLS and  
969 CREST does not significantly impact the reconstructed MTWA ( $\sim 0^{\circ}\text{C}$  on average from the  
970 difference between local and global calibration). In Fig 10.c, the differences in MTCO anomaly  
971 results between local and global calibrations are however more variable than MTWA results,  
972 across fossil sites. In detail, the MAT method generally produces larger MTCO anomalies with  
973 local calibration than with global calibration ( $+4.0^{\circ}\text{C}$  on average), whereas the WA-PLS and  
974 CREST methods tend to yield similarly lower MTCO anomalies ( $-4.5^{\circ}\text{C}$  on average). These  
975 findings highlight an opposite effect of the (mega)biomization procedure from the MAT versus  
976 WA-PLS and CREST methods in reconstructing the MTCO variable.

977 For TANN and MTWA reconstructions, MAT appears to be the most suitable  
978 reconstruction method, for identifying dominant analogues within a global calibration dataset  
979 to infer past climate conditions. However, MTCO outputs are sensitive to the modern  
980 subsamples defined by biome and megabiome classifications (Fig.10), from MAT and CREST  
981 methods.

982

983

984

985

986

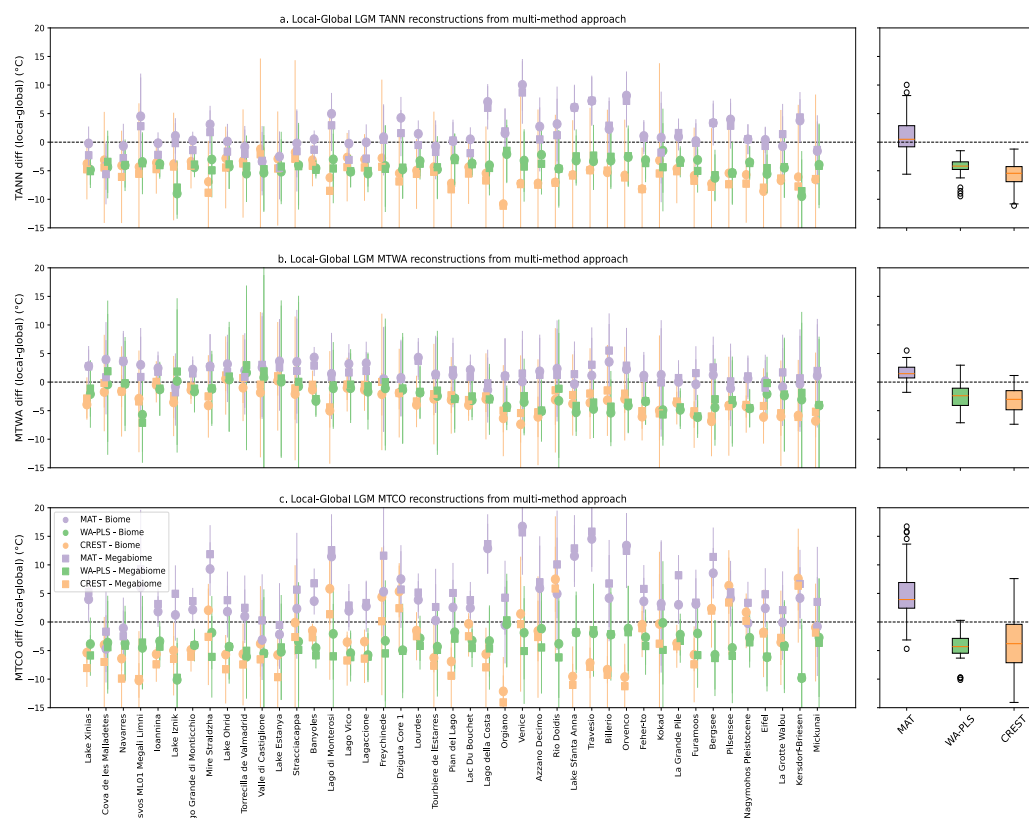
987

988

989



Fénisse et al.,



990  
 991 **Figure 10.** Mean LGM annual temperature **(a)**, MTWA **(b)** and MTCO **(c)** anomalies for each  
 992 fossil site, calculated as the difference between (mega)biomized and not-(mega)biomized  
 993 (global calibration) climate variables for the three methods of pollen-based climate  
 994 reconstruction. The biomization and megabiomization results are shown using circle and  
 995 square symbols, respectively. Site names are arranged (left to right) in ascending order of  
 996 latitude. Results are reported **Table 3**. Errors are  $1\sigma$ . The boxplots on the right represent the  
 997 distributions of the mean local–global differences for each climate variable across  
 998 reconstruction methods (in color).

999  
 1000 **V.3.2 - Biomization vs. Megabiomization effects on climate reconstructions**

1001 Across reconstruction methods, TANN and MTWA results derived from the biomization  
 1002 process are consistent with the megabiomization outputs (i.e., anomalies defined as the  
 1003 difference between the two treatments - are close to 0, **Figs 11.a and 11.b**). This result  
 1004 highlights the minimal impact of distinguishing between cold and hot arid conditions into  
 1005 steppe and desert biomes (not the case for megabiomes) on reconstructed LGM TANN and  
 1006 MTWA in Europe from three different methods.

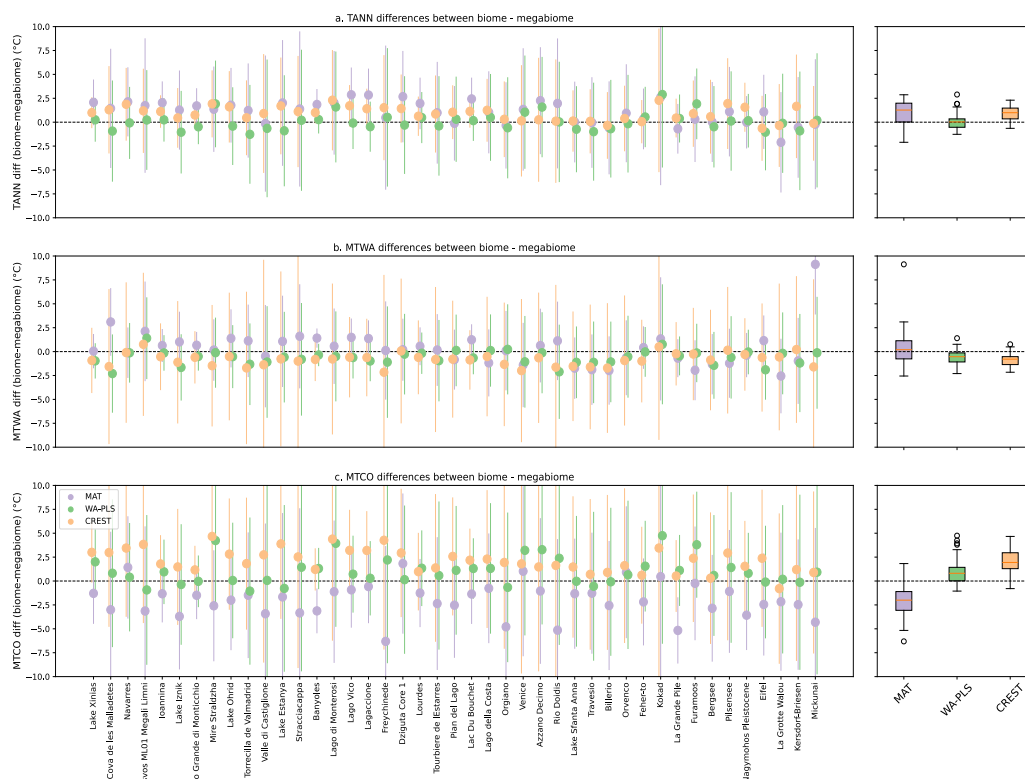
1007 However, MTCO anomaly results from MAT show slightly lower anomalies, by a few  
 1008 degrees ( $-2.5^{\circ}\text{C}$  on average, **Fig 11.c**), when using biomes instead of megabiomes, suggesting



Fénisse et al.,

1009 a further flattening of seasonal amplitude compared to present-day conditions (see Fig 8-9).  
 1010 While the differences in MTCO obtained by WA-PLS between biome and megabiome  
 1011 classifications vary across sites, biome-based MTCO anomaly results from CREST generally  
 1012 show greater anomalies than those obtained using the megabiome procedure (~+2°C on  
 1013 average, Fig 11.c).

1014 In summary, MAT-based biomization increases seasonality at some sites compared to  
 1015 the megabiomization process, which can be explained by MTCO anomalies being lower using  
 1016 biomization compared to megabiomization (-6.5°C vs. -4.5°C on average). CREST methods  
 1017 also show a high sensitivity to local calibrations, with higher MTCO anomalies from biomes  
 1018 compared to megabiomes (-5.7°C vs. -7.8°C on average). MAT and CREST methods exhibit a  
 1019 strong dependence on the calibration dataset for winter temperature reconstructions, which  
 1020 could be attributed to the spatial variability of MTCO anomalies in the modern calibration  
 1021 dataset. Overall, these results highlight the dependence of climate reconstructions on the  
 1022 chosen method, calibration, and climatic variables.  
 1023



1024 **Figure 11.** Mean LGM annual temperature (a), MTWA (b) and MTCO (c) anomalies for each  
 1025 fossil site, calculated as the difference between biomized and megabiomized climate  
 1026 variables for the three methods of pollen-based climate reconstruction. Site names are  
 1027 arranged in ascending order of latitude. Results are reported Table 3. Errors are 1σ. The  
 1028



Fénisse et al.,

1029 *boxplots on the right represent the distributions of the mean biome–megabiome differences*  
1030 *for each climate variable across reconstruction methods (in color).*

1031

## 1032 **VI. Discussion**

### 1033 **VI.1 - Comparing vegetation distributions from the (mega)biome assignments**

1034 The pollen-based modern biome distribution (**Fig.2**) closely resembles European  
1035 results obtained using the same biomization method as *Prentice et al. (1998)*. In particular,  
1036 the diversity of biomes in Spain (TEDE, COMX, XERO, and WAST), as well as the geographic  
1037 extent of temperate forests and xerophytic vegetation, aligns well with previous findings  
1038 (*Hengl et al., 2018*). However, our results indicate a broader modern extent of cold forest  
1039 (CLMX) across the Scandinavian countries, relative to *Prentice et al. (1998)*.

1040 In 2017, *Binney et al.* proposed a BIOME 6000 approach, building upon *Prentice and Webb III*  
1041 *(1998)*, to identify dominant biomes using the biomization procedure of *Bigelow et al. (2003)*,  
1042 super-PFT contributions, and BIOME 4 model biomes (*Kaplan et al., 2003*). Their biome  
1043 distributions similarly reveal patterns for the TEDE, TAIGA, and TUND biomes, although with  
1044 a stronger TUND dominance in Northern Europe compared to our results. Meanwhile, during  
1045 the LGM, *Kaplan et al. (2016)* show that forest-cover reconstructions from vegetation models  
1046 constrained by climate simulations suggest greater forest cover - and consequently less  
1047 extensive steppe conditions - than pollen-based reconstructions indicate.

1048 Furthermore, the “Regional Estimates of Vegetation Abundance from Large Sites” (REVEALS)  
1049 land-cover model, described by *Kern et al. (2024)*, compiles European pollen datasets to  
1050 reconstruct plant-specific parameters over time, including high-frequency events. A  
1051 comparison between outputs from this vegetation model and LGM megabiome results  
1052 indicates an overrepresentation of modeled arboreal vegetation (**Fig. 2**), at the expense of  
1053 grasses and herbs. This discrepancy may reflect an aridification bias in climate reconstructions  
1054 based on the megabiome approach.

1055 Global megabiome reconstructions in this study closely match modeled vegetation  
1056 distributions from *Li et al. (2025)* and align with previous European results using the same  
1057 biomization procedure (*Bigelow et al., 2003*), demonstrating good reproducibility across  
1058 Europe.

1059 Then, the modern (mega)biome distribution is geographically coherent, seemingly  
1060 realistic and compatible with previous studies, thus confirming the robustness of our biome  
1061 outputs for European climate reconstructions.

1062

### 1063 **VI.2 - Comparing climate reconstructions**

1064 As shown in **Figs 6 and 9**, the climate reconstruction methods (MAT, WA-PLS, and  
1065 CREST) using (mega)biomization procedures globally yield similar results, as indicated by the  
1066 high correlation coefficients ( $R^2 \geq 71\%$ , **Figs 12.a-f**) across reconstruction methods. The



Fénisse et al.,

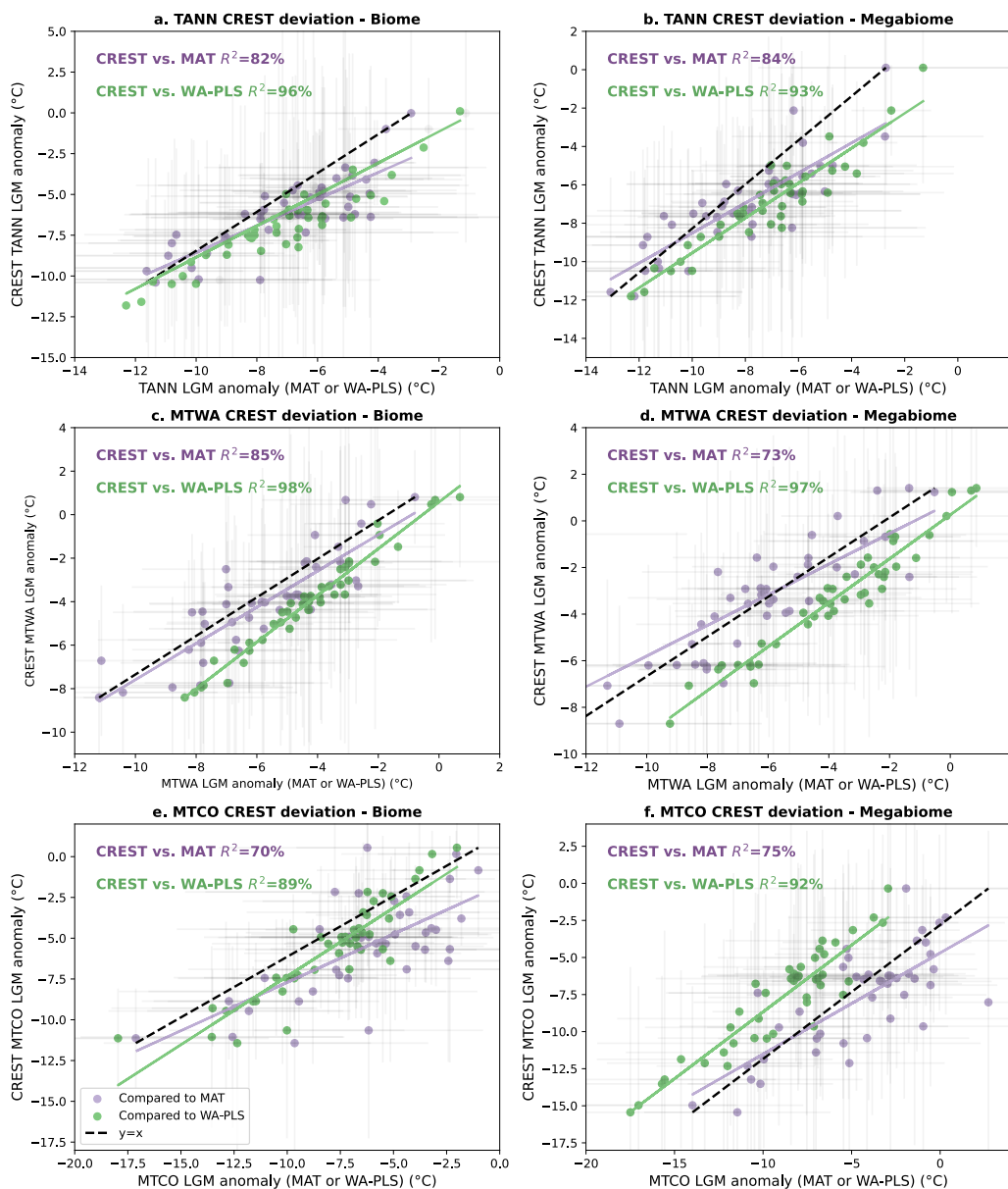
1067 significance of the regressions ( $R^2$ ) is maintained between the biomization and  
1068 megabiomization approaches, although TANN reconstructions derived from CREST are  
1069 somewhat less consistent with MAT under the megabiomization procedure compared to the  
1070 biomization approach ( $R^2=82\%$  and  $84\%$ , from biome and megabiome techniques,  
1071 respectively, [Fig 12.a-b](#)). Moreover, the climates inferred from CREST appear to be more  
1072 closely correlated with WA-PLS than with MAT results, with  $R^2$  values systematically higher for  
1073 “CREST vs. WA-PLS” than for “CREST vs. MAT” in [Fig 12](#).

1074 A key advantage of this multi-method approach is that it isolates the intrinsic  
1075 properties, behaviors, and weaknesses of each method. While MAT is highly dependent on  
1076 the quality of analogues ([Chevalier et al., 2020](#)), it performs well for pollen taxa with low  
1077 taxonomic resolution (at the family and genus level). WA-PLS is also sensitive to the choice of  
1078 modern dataset (e.g., situations with low analogue availability, [Birks and Seppä, 2010](#)), and it  
1079 relies on unimodal vegetation-climate response ([Ter Braak and Juggins, 1993](#)). CREST method  
1080 is less effective for taxa with low taxonomic resolution, accounts for multimodal vegetation  
1081 responses to climate ([Chevalier et al., 2014](#)). However, because TANN, MTWA and MTCO  
1082 exhibit homogeneous patterns across Europe and spatial averages of the three methods yield  
1083 comparable results, we can average outputs (mean SD) from the three reconstruction  
1084 methods to provide spatial mean climate variables during the LGM:  $-6.7\pm 2.1$  °C in TANN  
1085 anomalies,  $-4.8\pm 2.2$  °C in MTWA anomalies, and  $-6.7\pm 3.0$  °C MTCO anomalies from  
1086 biomization procedure, and  $-7.4 \pm 2.3$  °C in TANN anomalies,  $-4.4\pm 2.3$  °C in MTWA anomalies,  
1087 and  $-7.1\pm 3.4$  °C MTCO anomalies from megabiomization procedure across Europe. Thus,  
1088 despite using the same modern and fossil datasets, these methods yield distinct but  
1089 complementary LGM climate reconstructions that can be combined together to provide  
1090 robust estimates for the reconstructed climate variables.

1091  
1092  
1093  
1094  
1095  
1096  
1097  
1098  
1099  
1100  
1101  
1102  
1103  
1104  
1105  
1106  
1107



1108



1109 **Figure 12.** Linear relationship between TANN (a and b), MTWA (c and d) and MTCO (e and f)  
 1110 anomaly results (LGM – Modern climate) from the three pollen-based climate reconstruction  
 1111 methods, using biomization and megabiomization procedures. All  $R^2$  values reported in this  
 1112 study are statistically significant, with  $p$  values  $< 0.01$ . These plots show relationships  
 1113 between CREST results and those from statistical methods (MAT in blue and WA-PLS in  
 1114 green) from the 43 fossil sites. Errors are  $1\sigma$ .



Fénisse et al.,

1115 **VI.3 – Pollen-based reconstruction comparisons from literature**

1116 **VI.3.1 - Local calibration effects from MAT-based climate reconstructions: comparison with**  
1117 *Davis et al. (2024)*

1118 To study the reliability of our LGM climate reconstructions with results published in  
1119 literature, we compare our biomized and megabiomized multi-method results for three  
1120 different climate variables with those of *Davis et al. 2024*. *Davis et al. 2024* also used the  
1121 calibration dataset (EMPD2 dataset) and some input fossil records, common with our study.  
1122 Comparison maps (differences) between the two studies are presented in **Appendix 7** and  
1123 summarized as boxplots in **Fig.13**. We use error metrics to compare the results of the two  
1124 studies and assess the effect of methodological differences on climate reconstructions. Unlike  
1125  $R^2$ , which is insensitive to systematic biases, error metrics (RMSE) express deviations in the  
1126 original units ( $^{\circ}\text{C}$ ), making them more suitable for comparison.

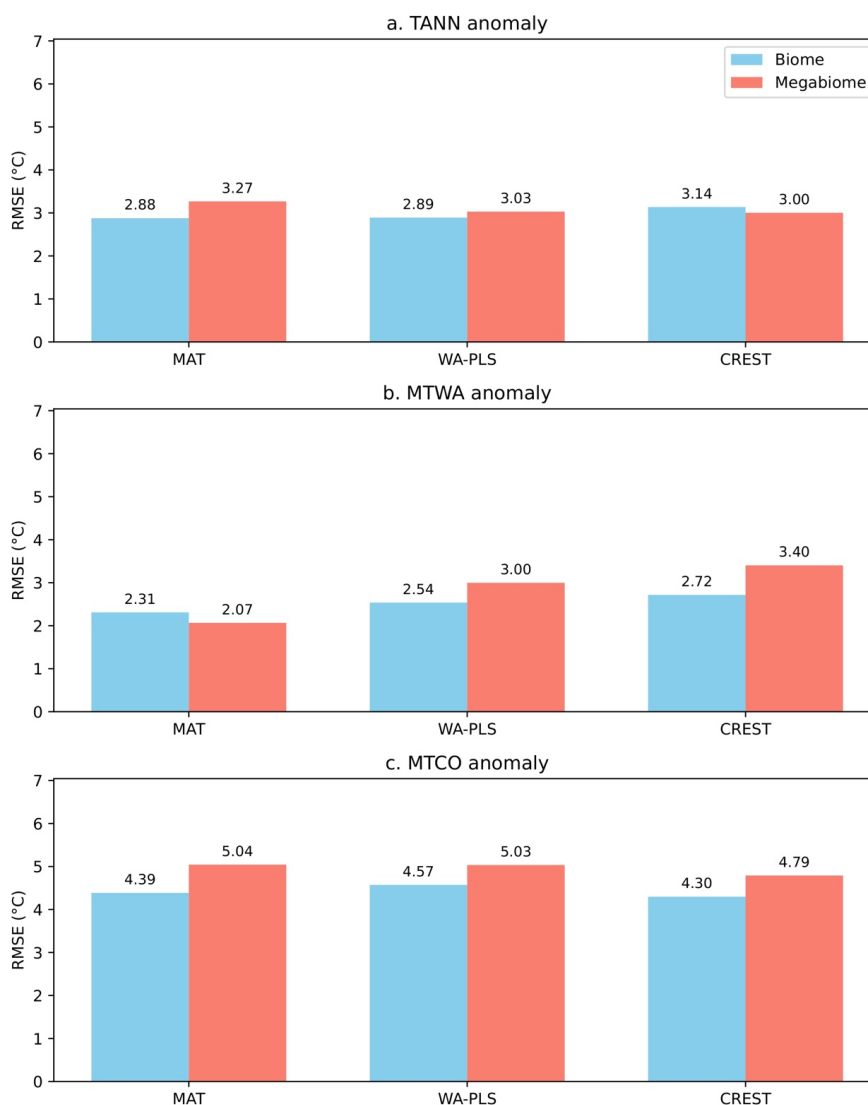
1127 The TANN and MTWA errors (RMSE) between our multi-method reconstructions and  
1128 those of *Davis et al. (2024)* are comparable to the individual reconstruction errors (2–3 $^{\circ}\text{C}$ ; **Figs.**  
1129 **13a–b**), indicating relatively good agreement between the studies regardless of the calibration  
1130 ((mega)biomization) and reconstruction methods. In contrast, MTCO anomalies show larger  
1131 discrepancies between the two studies (4–5 $^{\circ}\text{C}$ ; **Fig. 13c**). MTCO results exhibit poorer  
1132 agreement between the two studies, with RMSE values approximately twice as high as those  
1133 for TANN and MTWA (**Fig. 13c**), particularly for megabiomization (~4.9 $^{\circ}\text{C}$ ) compared to  
1134 biomization (~4.3 $^{\circ}\text{C}$ ). Overall, across these three methods, the results of *Davis et al. (2024)*  
1135 agree more closely with our biomization-based reconstructions than with those based on  
1136 megabiomization, with RMSE differences ranging from 0.5 to 1.5 $^{\circ}\text{C}$ . From **Appendix 7**, our  
1137 study also shows that climatic conditions at sites located closest to the Fennoscandian ice  
1138 sheet are systematically warmer (+5 $^{\circ}\text{C}$  to +10 $^{\circ}\text{C}$ ) in our study compared to *Davis et al. (2024)*.  
1139 Interestingly, our approach leads to substantially higher MTCO anomalies in Northern Europe  
1140 (~+3 $^{\circ}\text{C}$ ) and lower MTCO anomalies in Southern Europe (~–3 $^{\circ}\text{C}$ ).

1141 These results align with those reported in **section V.3**, highlighting the predominant  
1142 influence of the (mega)biome-type assignment scheme (**Figs 10.c** and **11.b**) and  
1143 reconstruction methods on MTCO anomalies, likely due to the high spatial variability of  
1144 modern data within the calibration dataset. MTCO reconstructions show the strongest inter-  
1145 study inconsistencies and are particularly sensitive to methodological choices. The difference  
1146 in modern calibration samples used in *Davis et al. 2024* and in the (mega)biome definitions of  
1147 our study may explain the observed differences in reconstructed temperature, particularly the  
1148 large MTCO discrepancies. These discrepancies demonstrate the strong methodological  
1149 dependence of palaeoclimate reconstructions and the importance of systematic cross-  
1150 validation frameworks.

1151  
1152  
1153  
1154  
1155



Fénisse et al.,



1156 **Figure 13.** RMSE of mean annual (a) and monthly anomalies (b and c) (LGM – Modern  
 1157 climate) between our three reconstruction methods (MAT, WA-PLS, CREST) and results from  
 1158 [Davis et al. \(2024\)](#). Bars represent RMSE for Biome (blue) and Megabiome (orange), with  
 1159 RMSE values reported above each bar to indicate the reconstruction error relative to [Davis et](#)  
 1160 [al. \(2024\)](#).  
 1161

### 1162 VI.3.2 - Systematic climate discrepancies between pollen data and models

1163 The extent of LGM cooling inferred in this study ranges from 0°C to -10°C relative to  
 1164 present ([Fig.6](#)) and appears to fall within the range simulated by climate models (e.g.,  
 1165 [Kageyama et al., 2021](#)). We also provide new constraints on LGM temperature seasonality  
 1166 indicating an amplification near the Atlantic coasts and a relative reduction inland, compared



Fénisse et al.,

1167 to present day. This continental pattern of LGM seasonality is in strong agreement with the  
1168 mean model from PMIP synthesis by *Izumi et al. (2013)*, which shows a gradient from positive  
1169 anomalies in Spain (+10°C) to negative anomalies (−4°C) in Eastern Europe.

1170 However, comparing pollen-based climate reconstructions with climate model outputs  
1171 is complex due to both the heterogeneous spatial coverage of the data, the variability of  
1172 reconstruction methods and the dispersion among climate models (e.g., *Bartlein et al., 2011*;  
1173 *Kageyama et al., 2021*). Moreover, proxies record extreme and local climates, while climate  
1174 models tend to provide spatially-averaged climate conditions. Ongoing improvements in the  
1175 spatial resolution of regional climate models make comparisons with local proxies increasingly  
1176 appropriate, although significant data–model discrepancies remain (*Kageyama et al., 2021*).  
1177 Similarly, expanding the availability of pollen data in Europe would further improve the  
1178 robustness of such comparisons.

1179

## 1180 **VII. Conclusion**

1181

1182 This study presents the first comprehensive comparison of pollen-based climate  
1183 reconstruction methods applied to the LGM in Europe, using a local calibration framework  
1184 integrating both biomization and megabiomization techniques. The approach is applied to a  
1185 compilation of fossil sites spanning the LGM and compared against a comprehensive modern  
1186 calibration dataset (EMPD2). We propose a new conservative method for weighting  
1187 reconstructed climate variables from (mega)biome affinity scores, which corrects for  
1188 threshold effects in (mega)biome shifts and incorporates their continuous variations over  
1189 time. We isolate and quantify the effects of calibration, biome score application methods, and  
1190 reconstruction techniques on the inferred paleoclimates, and synthesize them in the form of  
1191 inter-model means and deviations.

1192 In Europe, the TANN anomalies (mean SD) obtained with biomization are  $-7.0 \pm 2.3^\circ\text{C}$   
1193 (MAT),  $-7.1 \pm 2.2^\circ\text{C}$  (WA-PLS), and  $-5.9 \pm 2.2^\circ\text{C}$  (CREST), whereas those derived from  
1194 megabiomization are  $-8.0 \pm 2.5^\circ\text{C}$  (MAT),  $-7.2 \pm 2.4^\circ\text{C}$  (WA-PLS), and  $-7.0 \pm 2.3^\circ\text{C}$  (CREST). Due to  
1195 these consistent results, we propose LGM climate anomalies (from climate modern) based on  
1196 a mean model integrating the three reconstruction methods:  $-6.7 \pm 2.1^\circ\text{C}$  in TANN anomalies,  
1197  $-4.8 \pm 2.2^\circ\text{C}$  in MTWA anomalies, and  $-6.7 \pm 3.0^\circ\text{C}$  MTCO anomalies from biomization  
1198 procedure, and  $-7.4 \pm 2.3^\circ\text{C}$  in TANN anomalies,  $-4.4 \pm 2.3^\circ\text{C}$  in MTWA anomalies, and  
1199  $-7.1 \pm 3.4^\circ\text{C}$  MTCO anomalies from megabiomization procedure across Europe.

1200 The dependence of reconstruction method outputs on (mega)biome calibrations vary  
1201 depending on both the climate variables and the fossil pollen assemblages (i.e., the sites).  
1202 Local calibration is necessary for WA-PLS and CREST-based reconstructions due to the  
1203 underrepresentation of cold climates in Europe. These results show that, using the biome and  
1204 megabiome calibrations, the CREST (probabilistic) method shows LGM climate results  
1205 generally consistent with those of statistical approaches (MAT and WA-PLS), although the  
1206 consistency of CREST and WA-PLS reconstructions is slightly better than with MAT. Winter  
1207 temperature (MTCO) results exhibit higher sensitivity to reconstruction methods and



Fénisse et al.,

1208 (mega)biomization approaches than TANN and MTWA results. Based on MTCO  
1209 reconstructions, the WA-PLS and CREST method shows an opposite response to local  
1210 calibration compared with MAT, amplifying seasonal anomalies relative to global calibration  
1211 (+4.5°C for CREST and -4°C for MAT on average) while reducing European LGM seasonality by  
1212 the biomization procedure, but less strongly (-2.5°C for CREST and +2°C for MAT on average).

1213

#### 1214 **Scientific contributions - Authorship contribution statement**

1215 Role of each author: Fénisse G. wrote the original draft of the manuscript, which was  
1216 reviewed and edited by all co-authors.

1217

#### 1218 **Acknowledgements**

1219

1220 This study is financially supported by the ANR (ANR-22-CPJ2-0005-24/39 584 01, awarded to  
1221 D.V. Bekaert). Manuel Chevalier was supported by the German Federal Ministry of Education  
1222 and Research (BMBF) as a Research for Sustainability initiative (FONA;  
1223 <https://www.fona.de/en/>) through the PalMod Phase II and Phase III projects (grant no.  
1224 01LP1926D and 01LP2308B).

1225

#### 1226 **Appendix**

1227 Our results including (i) compilation maps from fossil and modern pollen data; (ii)  
1228 observed vs. Predicted relationship; (iii) monthly climate reconstructions since the LGM and  
1229 (iv) standard deviation of four climate variables are available in the online open repository  
1230 ORDAR:

1231 <https://doi.org/10.24396/ORDAR-231>

#### 1232 **Code and data availability**

1233 All support data including (i) the exhaustive modern datasets and fossil pollen  
1234 samples derived from the literature; (ii) our training code of (mega-)biome and three  
1235 reconstruction methods; and (iii) our climate results are available in the online open  
1236 repository ORDAR:

1237 <https://doi.org/10.24396/ORDAR-232>

1238

1239

1240

1241

1242

1243



Fénisse et al.,

1244 **List of Appendix**

- 1245 1. Site location, type of archives (a) and pollen description using taxonomic diversity  
1246 parameters (b) and AP/NAP percentages (c) in 43 pollen LGM records.  
1247 2. Relationship between biome and megabiome  
1248 3. Pollen taxa observed from the fossil pollen cores  
1249 4. Percentage of arid megabiomes (STEP+DESE+TUND) at the LGM in 43 pollen  
1250 sequences. Red contour points referred to the TEDE dominant megabiomes. SAVA  
1251 scores are negligible.  
1252 5. Cross validation procedures between observed and predicted modern climate  
1253 variables of the pollen datasets (EMPD2 dataset).  
1254 6. Standard deviation of annual temperature (a), precipitation (b), MTWA (c) and MTCO  
1255 (d) anomaly results (LGM – Modern climate) using averages of biomization results from  
1256 3 different methods.  
1257 7. Mean annual and monthly map anomalies reconstructed using three methods based  
1258 on biomization and megabiomization, compared with [Davis et al. \(2024\)](#).  
1259

1260 **List of Supplementary material**

- 1261 A. "SyntheseFile" – Compilation of pollen data sequences used in this study  
1262 (*Dataset\_PollenCooling.xlsx*)  
1263 B. "ModernCalibrationDatasets" – Modern calibration dataset including climate  
1264 variables and pollen abundances (*CalibrationDataset\_EMPD2.xlsx*)  
1265 C. "DatasetFass\_Int" – Initial pollen spectra from La Grande Pile (de Beaulieu & Reille,  
1266 1989; de Beaulieu, 1992; de Beaulieu & Reille, 1992) and Lake Bouchet (de Beaulieu  
1267 et al., 1990) (*GPILXX\_age\_model\_pollen\_count.tab* and  
1268 *Lac\_du\_Bouchet\_age\_model\_pollen\_count.tab*, respectively)  
1269 D. "Modele\_Age" – (i) Predicted ages for the sequences from La Grande Pile and Lake  
1270 Bouchet (*ModeleAge\_LGP.txt*; *ModeleAge\_LGP2.txt* and *ModeleAge\_LDB.txt*)  
1271 E. "HarmonizationTable" – (i) Harmonization table (*harmonization\_table.txt*), (ii)  
1272 comparison of taxon names before and after harmonization  
1273 (*HarmonizationTable\_Results.xlsx*)  
1274 F. "Tools\_BiomeScheme" – (i) Taxon-to-PFT biomization matrix (*Taxpftpi\_Class1.csv*),  
1275 and (ii) PFT-to-Biome matrix (*biopftpi\_Class1.csv*)  
1276 G. "Tools\_MegabiomeScheme" – (i) Pollen abundance weighting for PFT score  
1277 calculation (*pollen\_variable.csv*), and (ii) matrix linking Taxa-PFTs and PFTs-  
1278 Megabiomes as described by [Li et al., 2024](#) (*Taxon\_PFT\_Europe.csv* and  
1279 *PFT\_Megabiomes\_Europe.csv*)  
1280 H. "ReconstructionMethods" – R scripts for pollen-based climate reconstructions using  
1281 MAT, with biomization process (*MAT-biomization.R*), WA-PLS (*WA-PLS-*  
1282 *biomization.R*), and CREST (*CREST-biomization.R*)  
1283 I. "TANNGlobaleCalibration\_Results" – TANN results of global calibration  
1284 reconstructions following the three pollen-based reconstruction methods  
1285 (*GlobaleCalibration\_MAT.csv*, *GlobaleCalibration\_WA-PLS.csv*, and  
1286 *GlobaleCalibration\_CREST.csv*)



Fénisse et al.,

1287 J. "ClimateOutput\_LGP&LDB" - Climate series outputs from three different methods  
1288 based on biome and megabiome approaches  
1289 (*Output\_Recon\_MAT\_BiomeWeighted\_LDB.csv*,  
1290 *Output\_Recon\_MAT\_BiomeWeighted\_LGPSynthesis.csv*, *Output\_Recon\_WA-*  
1291 *PLS\_BiomeWeighted\_LDB.csv*, *Output\_Recon\_WA-*  
1292 *PLS\_BiomeWeighted\_LGPSynthesis.csv*,  
1293 *Output\_Recon\_CREST\_BiomeWeighted\_LDB.csv*,  
1294 *Output\_Recon\_CREST\_BiomeWeighted\_LGPSynthesis.csv*)

1295 K. "CV-Results" – R scripts to evaluate pollen-based climate reconstructions using MAT,  
1296 with (mega)biomization process (*CV\_MAT.R*), WA-PLS (*CV\_WAPLS.R*), and CREST  
1297 (*CV\_CREST.R*)  
1298  
1299

1300

1301

1302

1303

1304

1305

1306

1307

1308

1309

1310

1311

1312

1313

1314

1315



## 1316 References

- 1317 Arslanov, K. A., Dolukhanov, P. M., and Gei, N. A.: Climate, Black Sea levels and  
1318 human settlements in Caucasus Littoral 50,000–9000 BP, *Quatern. Int.*, 167–  
1319 168, 121–127, <https://doi.org/10.1016/j.quaint.2007.02.013>, 2007.
- 1320 Bartlein, P.J., Harrison, S.P., Brewer, S., Connor, S., Davis, B.A.S., Gajewski, K., Guiot,  
1321 J., Harrison-Prentice, T.I., Henderson, A., Peyron, O., Prentice, I.C., Scholze,  
1322 M., Seppä, H., Shuman, B., Sugita, S., Thompson, R.S., Vial, A.E., Williams, J.,  
1323 Wu, H.: Pollen-based continental climate reconstructions at 6 and 21 ka: a  
1324 global synthesis. *Clim. Dyn.* 37, 775–802. [https://doi.org/10.1007/s00382-  
1325 010-0904-1](https://doi.org/10.1007/s00382-010-0904-1), 2011.
- 1326 Bigelow, N.H., Brubaker, L.B., Edwards, M.E., Harrison, S.P., Prentice, I.C., Anderson,  
1327 P.M., Andreev, A.A., Bartlein, P.J., Christensen, T.R., Cramer, W., Kaplan, J.O.,  
1328 Lozhkin, A.V., Matveyeva, N.V., Murray, D.F., McGuire, A.D., Razzhivin, V.Y.,  
1329 Ritchie, J.C., Smith, B., Walker, D.A., Gajewski, K., Wolf, V., Holmqvist, B.H.,  
1330 Igarashi, Y., Kremenetskii, K., Paus, A., Pisaric, M.F.J., Volkova, V.S.: Climate  
1331 change and Arctic ecosystems: 1. Vegetation changes north of 55°N between  
1332 the last glacial maximum, mid-Holocene, and present. *J. Geophys. Res.*  
1333 *Atmospheres* 108, 2002JD002558. <https://doi.org/10.1029/2002JD002558>,  
1334 2003.
- 1335 Binney, H., Edwards, M., Macias-Fauria, M., Lozhkin, A., Anderson, P., Kaplan, J.O.,  
1336 Andreev, A., Bezrukova, E., Blyakharchuk, T., Jankovska, V., Khazina, I.,  
1337 Krivonogov, S., Kremenetski, K., Nield, J., Novenko, E., Ryabogina, N.,  
1338 Solovieva, N., Willis, K., Zernitskaya, V.: Vegetation of Eurasia from the last  
1339 glacial maximum to present: Key biogeographic patterns. *Quat. Sci. Rev.* 157,  
1340 80–97. <https://doi.org/10.1016/j.quascirev.2016.11.022>, 2017.
- 1341 Birks, H.J.B.: Quantitative palaeoenvironmental reconstructions. *Stat Model Quat Sci*  
1342 *Data Tech Guid.*, Statistical Modelling of Quaternary Science Data., Technical  
1343 Guide 5, Quaternary Research Association, Cambridge. 271 pp., 1995.
- 1344 Birks, H.J.B., Seppä, H.: Pollen-based reconstructions of late-Quaternary climate in  
1345 Europe – progress, problems, and pitfalls., *Acta Palaeobotanica* 44(2): 317–  
1346 334, 2004
- 1347 Blaauw, M., Wohlfarth, B., Christen, J.A., Ampel, L., Veres, D., Hughen, K.A., Preusser,  
1348 F., Svensson, A.: Were last glacial climate events simultaneous between  
1349 Greenland and France? A quantitative comparison using non-tuned  
1350 chronologies. *J. Quat. Sci.* 25, 387–394. <https://doi.org/10.1002/jqs.1330>,  
1351 2010.
- 1352 Bonatti, E.: Pollen sequence in the lake sediments. In: Hutchinson, G. E. (ed.), *Lanula:*  
1353 *an Account of the History and Development of the Lago di Monterosi, Latium,*  
1354 *Italy.* *T. Am. Philos. Soc.*, 60, 26–31, <https://doi.org/10.2307/1005996>, 1970.
- 1355 Bottema, S.: Pollen analytical investigations in Thessaly (Greece), *Palaeohistoria*, 21,  
1356 19–40, 1979.
- 1357 Braconnot, P., Harrison, S.P., Kageyama, M., Bartlein, P.J., Masson-Delmotte, V., Abe-  
1358 Ouchi, A., Otto-Bliesner, B., Zhao, Y.: Evaluation of climate models using  
1359 palaeoclimatic data. *Nat. Clim. Change* 2, 417–424.  
1360 <https://doi.org/10.1038/nclimate1456>, 2012.



Fénisse et al.,

- 1361 Brewer, S., Guiot, J., Sánchez-Goñi, M.F., Klotz, S.: The climate in Europe during the  
1362 Eemian: a multi-method approach using pollen data. *Quat. Sci. Rev.* 27, 2303–  
1363 2315. <https://doi.org/10.1016/j.quascirev.2008.08.029>, 2008.
- 1364 Cao, X., Herzschuh, U., Telford, R.J., Ni, J.: A modern pollen–climate dataset from  
1365 China and Mongolia: Assessing its potential for climate reconstruction. *Rev.*  
1366 *Palaeobot. Palynol.* 211, 87–96.  
1367 <https://doi.org/10.1016/j.revpalbo.2014.08.007>, 2014.
- 1368 Cao, X., Tian, F.: Pollen-based biome reconstruction in R. Zenodo Code.  
1369 <https://doi.org/10.5281/zenodo.7523423>, 2021.
- 1370 Cao, X., Tian, F., Dallmeyer, A., Herzschuh, U.: Northern Hemisphere biome changes  
1371 (>30°N) since 40 cal ka BP and their driving factors inferred from model-data  
1372 comparisons. *Quat. Sci. Rev.* 220, 291–309.  
1373 <https://doi.org/10.1016/j.quascirev.2019.07.034>, 2019.
- 1374 Cao, X., Tian, F., Herzschuh, U., Ni, J., Xu, Q., Li, W., Zhang, Y., Luo, M., Chen, F.:  
1375 Human activities have reduced plant diversity in eastern China over the last  
1376 two millennia. *Glob. Change Biol.* 28, 4962–4976.  
1377 <https://doi.org/10.1111/gcb.16274>, 2022.
- 1378 Carrión, J. S. and Dupré-Olivier, M.: Late Quaternary vegetational history of Navarrés,  
1379 eastern Spain. A two core approach, *New Phytol.*, 134, 177–191,  
1380 <https://doi.org/10.1111/j.14698137.1996.tb01157.x>, 1996.
- 1381 Charton, L., Combourieu-Nebout, N., Bertini, A., Lebreton, V., Peyron, O., Robles, M.,  
1382 Sassoon, D., Moncel, M.-H. : Vegetation and climate changes during the  
1383 Middle to Upper Palaeolithic transition in the southwestern Mediterranean:  
1384 What happened to the last Neanderthals during Heinrich stadial 4? *Quat. Sci.*  
1385 *Rev.* 359, 109345. <https://doi.org/10.1016/j.quascirev.2025.109345>, 2025.
- 1386 Chevalier, M.: *crestr* : an R package to perform probabilistic climate reconstructions  
1387 from palaeoecological datasets. *Clim. Past* 18, 821–844.  
1388 <https://doi.org/10.5194/cp-18-821-2022>, 2022.
- 1389 Chevalier, M., Davis, B.A.S., Heiri, O., Seppä, H., Chase, B.M., Gajewski, K., Lacourse,  
1390 T., Telford, R.J., Finsinger, W., Guiot, J., Kühl, N., Maezumi, S.Y., Tipton, J.R.,  
1391 Carter, V.A., Brussel, T., Phelps, L.N., Dawson, A., Zanon, M., Vallé, F., Nolan,  
1392 C., Mauri, A., De Vernal, A., Izumi, K., Holmström, L., Marsicek, J., Goring, S.,  
1393 Sommer, P.S., Chaput, M., Kupriyanov, D.: Pollen-based climate  
1394 reconstruction techniques for late Quaternary studies. *Earth-Sci. Rev.* 210,  
1395 103384. <https://doi.org/10.1016/j.earscirev.2020.103384>, 2020.
- 1396 Chevalier, M.: Enabling possibilities to quantify past climate from fossil assemblages  
1397 at a global scale. *Glob. Planet. Change* 175, 27–35.  
1398 <https://doi.org/10.1016/j.gloplacha.2019.01.016>, 2019.
- 1399 Chevalier, M., Chase, B.M.: Determining the drivers of long-term aridity variability: a  
1400 southern African case study. *J. Quat. Sci.* 31, 143–151.  
1401 <https://doi.org/10.1002/jqs.2850>, 2016.
- 1402 Chevalier, M., Chase, B.M.: Southeast African records reveal a coherent shift from  
1403 high- to low-latitude forcing mechanisms along the east African margin across  
1404 last glacial–interglacial transition. *Quat. Sci. Rev.* 125, 117–130.  
1405 <https://doi.org/10.1016/j.quascirev.2015.07.009>, 2015.



Fénisse et al.,

- 1406 Chevalier, M., Chase, B.M., Quick, L.J., Dupont, L.M., Johnson, T.C.: Temperature  
1407 change in subtropical southeastern Africa during the past 790,000 yr. *Geology*  
1408 49, 71–75. <https://doi.org/10.1130/G47841.1>, 2021.
- 1409 Chevalier, M., Cheddadi, R., Chase, B.M.: CREST (Climate REconstruction SofTware): a  
1410 probability density function (PDF)-based quantitative climate reconstruction  
1411 method. *Clim. Past* 10, 2081–2098. <https://doi.org/10.5194/cp-10-2081-2014>,  
1412 2014.
- 1413 Chevalier, M., Davis, B.A.S., Heiri, O., Seppä, H., Chase, B.M., Gajewski, K., Lacourse,  
1414 T., Telford, R.J., Finsinger, W., Guiot, J., Kühl, N., Maezumi, S.Y., Tipton, J.R.,  
1415 Carter, V.A., Brussel, T., Phelps, L.N., Dawson, A., Zanon, M., Vallé, F., Nolan,  
1416 C., Mauri, A., De Vernal, A., Izumi, K., Holmström, L., Marsicek, J., Goring, S.,  
1417 Sommer, P.S., Chaput, M., Kupriyanov, D.: Pollen-based climate  
1418 reconstruction techniques for late Quaternary studies. *Earth-Sci. Rev.* 210,  
1419 103384. <https://doi.org/10.1016/j.earscirev.2020.103384>, 2020.
- 1420 Cleator, S.F., Harrison, S.P., Nichols, N.K., Prentice, I.C., Roulstone, I.: A new  
1421 multivariable benchmark for Last Glacial Maximum climate simulations. *Clim*  
1422 *Past.*, 16, 699–712, <https://doi.org/10.5194/cp-16-699-2020>, 2020
- 1423 Cruz-Silva, E., Harrison, S.P., Marinova, E., Prentice, I.C.: A new method based on  
1424 surface-sample pollen data for reconstructing palaeovegetation patterns. *J.*  
1425 *Biogeogr.* 49, 1381–1396. <https://doi.org/10.1111/jbi.14448>, 2022.
- 1426 Dallmeyer, A., Claussen, M., Brovkin, V.: Harmonising plant functional type  
1427 distributions for evaluating Earth system models. *Clim. Past* 15, 335–366.  
1428 <https://doi.org/10.5194/cp-15-335-2019>, 2019.
- 1429 Damblon, F. : L'enregistrement palynologique de la sequence pléistocène et holocène  
1430 de la grotte Walou, in: *La grotte Walou à Trooz (Belgique)*, edited by: Draily,  
1431 C., Pirson, S., and Toussaint, M., Service public de Wallonie (Etudes et  
1432 Documents, Archéologie, 21), [https://www.academia.edu/23006376/Draily\\_](https://www.academia.edu/23006376/Draily_C_Toussaint_M_and_Pirson_S_Dir_2011_La_grotte_Walou_%E0_Trooz_Belgique_Fouilles_de_1996_%E0_2004_Volume_2_Les_sciences_de_la_vie_et_les_datations_Monographie_Etudes_et_documents_Arch%9ologie_21_Namur_Service_public_de_Wallonie_241_p)  
1433 [C\\_Toussaint\\_M\\_and\\_Pirson\\_S\\_Dir\\_2011\\_La\\_grotte\\_Walou\\_](https://www.academia.edu/23006376/Draily_C_Toussaint_M_and_Pirson_S_Dir_2011_La_grotte_Walou_%E0_Trooz_Belgique_Fouilles_de_1996_%E0_2004_Volume_2_Les_sciences_de_la_vie_et_les_datations_Monographie_Etudes_et_documents_Arch%9ologie_21_Namur_Service_public_de_Wallonie_241_p)  
1434 [%E0\\_Trooz\\_Belgique\\_Fouilles\\_de\\_1996\\_%E0\\_2004\\_Volume\\_](https://www.academia.edu/23006376/Draily_C_Toussaint_M_and_Pirson_S_Dir_2011_La_grotte_Walou_%E0_Trooz_Belgique_Fouilles_de_1996_%E0_2004_Volume_2_Les_sciences_de_la_vie_et_les_datations_Monographie_Etudes_et_documents_Arch%9ologie_21_Namur_Service_public_de_Wallonie_241_p)  
1435 [2\\_Les\\_sciences\\_de\\_la\\_vie\\_et\\_les\\_datations\\_Monographie\\_](https://www.academia.edu/23006376/Draily_C_Toussaint_M_and_Pirson_S_Dir_2011_La_grotte_Walou_%E0_Trooz_Belgique_Fouilles_de_1996_%E0_2004_Volume_2_Les_sciences_de_la_vie_et_les_datations_Monographie_Etudes_et_documents_Arch%9ologie_21_Namur_Service_public_de_Wallonie_241_p)  
1436 [Etudes\\_et\\_documents\\_Arch%9ologie\\_21\\_Namur\\_Service\\_](https://www.academia.edu/23006376/Draily_C_Toussaint_M_and_Pirson_S_Dir_2011_La_grotte_Walou_%E0_Trooz_Belgique_Fouilles_de_1996_%E0_2004_Volume_2_Les_sciences_de_la_vie_et_les_datations_Monographie_Etudes_et_documents_Arch%9ologie_21_Namur_Service_public_de_Wallonie_241_p)  
1437 [public\\_de\\_Wallonie\\_241\\_p](https://www.academia.edu/23006376/Draily_C_Toussaint_M_and_Pirson_S_Dir_2011_La_grotte_Walou_%E0_Trooz_Belgique_Fouilles_de_1996_%E0_2004_Volume_2_Les_sciences_de_la_vie_et_les_datations_Monographie_Etudes_et_documents_Arch%9ologie_21_Namur_Service_public_de_Wallonie_241_p) (last access: 25 July 2024), 84–129, 2011.
- 1438 Daniau, A.-L., Desprat, S., Aleman, J.C., Bremond, L., Davis, B., Fletcher, W., Marlon,  
1439 J.R., Marquer, L., Montade, V., Morales-Molino, C., Naughton, F., Rius, D.,  
1440 Urrego, D.H.: Terrestrial plant microfossils in palaeoenvironmental studies,  
1441 pollen, microcharcoal and phytolith. Towards a comprehensive understanding  
1442 of vegetation, fire and climate changes over the past one million years. *Rev.*  
1443 *Micropaléontologie* 63, 1–35. <https://doi.org/10.1016/j.revmic.2019.02.001>,  
1444 2019.
- 1445 Davis, B.A.S., Brewer, S., Stevenson, A.C., Guiot, J.: The temperature of Europe during  
1446 the Holocene reconstructed from pollen data. *Quat. Sci. Rev.* 22, 1701–1716.  
1447 [https://doi.org/10.1016/S0277-3791\(03\)00173-2](https://doi.org/10.1016/S0277-3791(03)00173-2), 2003.
- 1448 Davis, B.A.S., Chevalier, M., Sommer, P., Carter, V.A., Finsinger, W., Mauri, A., Phelps,  
1449 L.N., Zanon, M., Abegglen, R., Åkesson, C.M., Alba-Sánchez, F., Anderson, R.S.,  
1450 Antipina, T.G., Atanassova, J.R., Beer, R., Belyanina, N.I., Blyakharchuk, T.A.,  
1451 Borisova, O.K., Bozilova, E., Bukreeva, G., Bunting, M.J., Clò, E., Colombaroli,  
1452 D., Combourieu-Nebout, N., Desprat, S., Di Rita, F., Djamali, M., Edwards, K.J.,



Fénisse et al.,

- 1453 Fall, P.L., Feurdean, A., Fletcher, W., Florenzano, A., Furlanetto, G., Gaceur, E.,  
1454 Galimov, A.T., Gałka, M., García-Moreiras, I., Giesecke, T., Grindean, R., Guido,  
1455 M.A., Gvozdeva, I.G., Herzsuh, U., Hjelle, K.L., Ivanov, S., Jahns, S.,  
1456 Jankovska, V., Jiménez-Moreno, G., Karpińska-Kończak, M., Kitaba, I.,  
1457 Kończak, P., Lapteva, E.G., Latałowa, M., Lebreton, V., Leroy, S., Leydet, M.,  
1458 Lopatina, D.A., López-Sáez, J.A., Lotter, A.F., Magri, D., Marinova, E., Matthias,  
1459 I., Mavridou, A., Mercuri, A.M., Mesa-Fernández, J.M., Mikishin, Y.A., Milecka,  
1460 K., Montanari, C., Morales-Molino, C., Mrotzek, A., Muñoz Sobrino, C.,  
1461 Naidina, O.D., Nakagawa, T., Nielsen, A.B., Novenko, E.Y., Panajiotidis, S.,  
1462 Panova, N.K., Papadopoulou, M., Pardoe, H.S., Pędziszewska, A., Petrenko,  
1463 T.I., Ramos-Román, M.J., Ravazzi, C., Rösch, M., Ryabogina, N., Sabariego Ruiz,  
1464 S., Salonen, J.S., Sapelko, T.V., Schofield, J.E., Seppä, H., Shumilovskikh, L.,  
1465 Stivrins, N., Stojakowits, P., Svobodova Svitavská, H., Święta-Musznicka, J.,  
1466 Tantau, I., Tinner, W., Tobolski, K., Tonkov, S., Tsakiridou, M., Valsecchi, V.,  
1467 Zanina, O.G., Zimny, M.: The Eurasian Modern Pollen Database (EMPD),  
1468 Version 2. <https://doi.org/10.5194/essd-2020-14>, 2020.
- 1469 Davis, B.A.S., Fasel, M., Kaplan, J.O., Russo, E., Burke, A.: The climate and vegetation  
1470 of Europe, northern Africa, and the Middle East during the Last Glacial  
1471 Maximum (21 000 yr BP) based on pollen data. *Clim. Past* 20, 1939–1988.  
1472 <https://doi.org/10.5194/cp-20-1939-2024>, 2024.
- 1473 De Beaulieu, J.L.: Pollen profile GPLXX, La Grande Pile, France.  
1474 <https://doi.org/10.1594/PANGAEA.739275>, 2010.
- 1475 De Beaulieu, J.-L., Reille, M.: Long Pleistocene pollen sequences from the Velay  
1476 Plateau (Massif Central, France): I. Ribains maar. *Veg. Hist. Archaeobotany* 1,  
1477 233–242. <https://doi.org/10.1007/BF00189500>, 1992.
- 1478 De Beaulieu, J.D., Reille, M.: A long Upper Pleistocene pollen record from Les Echets,  
1479 near Lyon, France. *Boreas* 13, 111–132. <https://doi.org/10.1111/j.1502-3885.1984.tb00066.x>, 1984.
- 1481 d’Oliveira, L., Dugerdil, L., Ménot, G., Evin, A., Muller, S.D., Ansanay-Alex, S., Azuara,  
1482 J., Bonnet, C., Bremond, L., Shah, M., Peyron, O.: Reconstructing 15 000 years  
1483 of southern France temperatures from coupled pollen and molecular  
1484 (branched glycerol dialkyl glycerol tetraether) markers (Canroute, Massif  
1485 Central). *Clim. Past* 19, 2127–2156. <https://doi.org/10.5194/cp-19-2127-2023>,  
1486 2023.
- 1487 Duprat-Oualid, F., Rius, D., Bégeot, C., Magny, M., Millet, L., Wulf, S., Appelt, O.:  
1488 Vegetation response to abrupt climate changes in Western Europe from 45 to  
1489 14.7k cal a BP: the Bergsee lacustrine record (Black Forest, Germany). *J. Quat.*  
1490 *Sci.* 32, 1008–1021. <https://doi.org/10.1002/jqs.2972>, 2017.
- 1491 Dugerdil, L., Ménot, G., Peyron, O., Jouffroy-Bapicot, I., Ansanay-Alex, S., Antheaume,  
1492 I., Behling, H., Boldgiv, B., Develle, A.-L., Grossi, V., Magail, J., Makou, M.,  
1493 Robles, M., Unkelbach, J., Vannièrre, B., Joannin, S.: Late Holocene Mongolian  
1494 climate and environment reconstructions from brGDGTs, NPPs and pollen  
1495 transfer functions for Lake Ayrag: Paleoclimate implications for Arid Central  
1496 Asia. *Quat. Sci. Rev.* 273, 107235, 2021.  
1497 <https://doi.org/10.1016/j.quascirev.2021.107235>
- 1498 Dugerdil, L., Peyron, O., Violle, C., Joannin, S., Ménot, G., Denelle, P., Bruelheide, H.,  
1499 Chytrý, M., Field, R., Hatim, M.Z., Gholizadeh, H., Dolezal, J., Pillar, V.D.,



Fénisse et al.,

- 1500 Shaltout, K.H., Schrodt, F., Garnier, E.: Functional Signatures of Surface Pollen  
1501 and Vegetation Are Broadly Similar: Good News for Past Reconstructions of  
1502 Vegetation. *J. Biogeogr.* 52, e15100. <https://doi.org/10.1111/jbi.15100>, 2025.
- 1503 Dupre Ollivier, M.: *Palinología y paleoambiente – nuevos datos españoles*  
1504 *referencias*, Universidad de Valencia, 160 pp., ISBN 84-7795-000-8, 1988.
- 1505 Ehlers, J., Giddard, P.L., Hughes, P.D.: *Quaternary Glaciations – Extent and*  
1506 *Chronology A Closer Look*, Elsevier, ISBN 9780444534477. ed.,  
1507 <https://doi.org/10.18814/epiiugs/2008/v31i2/004>, 2011.
- 1508 Follieri, M., Magri, D., and Sadori, L.: Pollen stratigraphical synthesis from Valle di  
1509 Castiglione (Roma), *Quaternary Int.*, 3–4, 81–84,  
1510 [https://doi.org/10.1016/1040-6182\(89\)90076-1](https://doi.org/10.1016/1040-6182(89)90076-1), 1989.
- 1511 Gebhardt, C., Köhl, N., Hense, A., Litt, T.: Reconstruction of Quaternary temperature  
1512 fields by dynamically consistent smoothing. *Clim. Dyn.* 30, 421–437.  
1513 <https://doi.org/10.1007/s00382-007-0299-9>, 2008.
- 1514 Geng, J., Wu, H., Zhang, W., Li, Q., Yu, Y., 2025. Evolution of global vegetation  
1515 patterns since the last glacial maximum. *Quat. Int.* 729, 109780.  
1516 <https://doi.org/10.1016/j.quaint.2025.109780>
- 1517 Giardini, M.: Late Quaternary vegetation history at Stracciacappa (Rome, central  
1518 Italy), *Veg. Hist. Archaeobot.*, 16, 301–316, [https://doi.org/10.1007/s00334-](https://doi.org/10.1007/s00334-006-0037-y)  
1519 [006-0037-y](https://doi.org/10.1007/s00334-006-0037-y), 2007.
- 1520 Guiot, J., Pons, A., De Beaulieu, J.L., Reille, M.: A 140,000-year continental climate  
1521 reconstruction from two European pollen records. *Nature* 338, 309–313.  
1522 <https://doi.org/10.1038/338309a0>, 1989.
- 1523 Guiot, J.: Methodology of the last climatic cycle reconstruction in France from pollen  
1524 data. *Palaeogeogr. Palaeoclimatol. Palaeoecol.* 80, 49–69.  
1525 [https://doi.org/10.1016/0031-0182\(90\)90033-4](https://doi.org/10.1016/0031-0182(90)90033-4), 1990.
- 1526 Guiot, J., Reille, M., De Beaulieu, J.L., Pons, A.: Calibration of the climatic signal in a  
1527 new pollen sequence from La Grande Pile. *Clim. Dyn.* 6, 259–264.  
1528 <https://doi.org/10.1007/BF00193539>, 1992.
- 1529 Guiot, J., Torre, F., Jolly, D., Peyron, O., Boreux, J.J., Cheddadi, R.: Inverse vegetation  
1530 modeling by Monte Carlo sampling to reconstruct palaeoclimates under  
1531 changed precipitation seasonality and CO<sub>2</sub> conditions: application to glacial  
1532 climate in Mediterranean region. *Ecol. Model.* 127, 119–140.  
1533 [https://doi.org/10.1016/S0304-3800\(99\)00219-7](https://doi.org/10.1016/S0304-3800(99)00219-7), 2000.
- 1534 Harrison, S.P., Bartlein, P.J., Brewer, S., Prentice, I.C., Boyd, M., Hessler, I., Holmgren,  
1535 K., Izumi, K., Willis, K.: Climate model benchmarking with glacial and mid-  
1536 Holocene climates. *Clim. Dyn.* 43, 671–688. [https://doi.org/10.1007/s00382-](https://doi.org/10.1007/s00382-013-1922-6)  
1537 [013-1922-6](https://doi.org/10.1007/s00382-013-1922-6), 2014.
- 1538 Harrison, S.P., Prentice, I.C., Barboni, D., Kohfeld, K.E., Ni, J., Sutra, J.-P.:  
1539 Ecophysiological and bioclimatic foundations for a global plant functional  
1540 classification. *J. Veg. Sci.* 21, 300–317. [https://doi.org/10.1111/j.1654-](https://doi.org/10.1111/j.1654-1103.2009.01144.x)  
1541 [1103.2009.01144.x](https://doi.org/10.1111/j.1654-1103.2009.01144.x), 2010.
- 1542 Haywood, A.M., Dowsett, H.J., Valdes, P.J., Lunt, D.J., Francis, J.E., Sellwood, B.W.:  
1543 Introduction. Pliocene climate, processes and problems. *Philos. Trans. R. Soc.*  
1544 *Math. Phys. Eng. Sci.* 367, 3–17. <https://doi.org/10.1098/rsta.2008.0205>,  
1545 2009.



Fénisse et al.,

- 1546 Hengl, T., Walsh, M.G., Sanderman, J., Wheeler, I., Harrison, S.P., Prentice, I.C.: Global  
1547 mapping of potential natural vegetation: an assessment of machine learning  
1548 algorithms for estimating land potential. *PeerJ* 6, e5457.  
1549 <https://doi.org/10.7717/peerj.5457>, 2018.
- 1550 Hersbach, H., Bell, B., Berrisford, P., Hirahara, S., Horányi, A., Muñoz-Sabater, J.,  
1551 Nicolas, J., Peubey, C., Radu, R., Schepers, D., Simmons, A., Soci, C., Abdalla,  
1552 S., Abellan, X., Balsamo, G., Bechtold, P., Biavati, G., Bidlot, J., Bonavita, M.,  
1553 De Chiara, G., Dahlgren, P., Dee, D., Diamantakis, M., Dragani, R., Flemming,  
1554 J., Forbes, R., Fuentes, M., Geer, A., Haimberger, L., Healy, S., Hogan, R.J.,  
1555 Hólm, E., Janisková, M., Keeley, S., Laloyaux, P., Lopez, P., Lupu, C., Radnoti,  
1556 G., De Rosnay, P., Rozum, I., Vamborg, F., Villaume, S., Thépaut, J.: The ERA5  
1557 global reanalysis. *Q. J. R. Meteorol. Soc.* 146, 1999–2049.  
1558 <https://doi.org/10.1002/qj.3803>, 2020.
- 1559 Herschuh, U., Böhmer, T., Chevalier, M., Dallmeyer, A., Li, C., Cao, X., Hébert, R.,  
1560 Peyron, O., Nazarova, L., Novenko, E.Y., Park, J., Rudaya, N.A., Schlütz, F.,  
1561 Shumilovskikh, L.S., Tarasov, P.E., Wang, Y., Wen, R., Xu, Q., Zheng, Z.:  
1562 Regional pollen-based Holocene temperature and precipitation patterns  
1563 depart from the Northern Hemisphere mean trends.  
1564 <https://doi.org/10.5194/egusphere-2022-127>, 2022a.
- 1565 Herschuh, U., Böhmer, T., Li, C., Chevalier, M., Hébert, R., Cao, X., Bigelow, N.H.,  
1566 Nazarova, L., Novenko, E.Y., Peyron, O., Rudaya, N.A., Schlütz, F.,  
1567 Shumilovskikh, L.S.: 1 LegacyClimate 1.0: A dataset of pollen-based climate 2  
1568 reconstructions from 2594 Northern Hemisphere sites covering the 3 last 30  
1569 ka and beyond., *Earth Syst. Sci. Data*, 15, 2235–2258,  
1570 <https://doi.org/10.5194/essd-15-2235-2023>, 2022b.
- 1571 Hughes, P.D., Gibbard, P.L., Ehlers, J.: Timing of glaciation during the last glacial cycle:  
1572 evaluating the concept of a global ‘Last Glacial Maximum’ (LGM). *Earth-Sci.*  
1573 *Rev.* 125, 171–198. <https://doi.org/10.1016/j.earscirev.2013.07.003>, 2013.
- 1574 Izumi, K., Bartlein, P.J., Harrison, S.P.: Consistent large-scale temperature responses  
1575 in warm and cold climates. *Geophys. Res. Lett.* 40, 1817–1823.  
1576 <https://doi.org/10.1002/grl.50350>, 2013.
- 1577 Jalut, G., Marti, J. M., Fontugne, M., Delibrias, G., Vilaplana, J. M., and Julia, R.: Glacial  
1578 to interglacial vegetation changes in the northern and southern Pyrénées:  
1579 Deglaciation, vegetation cover and chronology, *Quaternary Sci. Rev.*, 11, 449–  
1580 480, [https://doi.org/10.1016/0277-3791\(92\)90027-6](https://doi.org/10.1016/0277-3791(92)90027-6), 1992.
- 1581 Jost, A., Lunt, D., Kageyama, M., Abe-Ouchi, A., Peyron, O., Valdes, P.J., Ramstein, G.:  
1582 High-resolution simulations of the last glacial maximum climate over Europe:  
1583 a solution to discrepancies with continental palaeoclimatic reconstructions?  
1584 *Clim. Dyn.* 24, 577–590. <https://doi.org/10.1007/s00382-005-0009-4>, 2005.
- 1585 Juggins, S.: Quantitative reconstructions in palaeolimnology: new paradigm or sick  
1586 science? *Quat. Sci. Rev.* 64, 20–32.  
1587 <https://doi.org/10.1016/j.quascirev.2012.12.014>, 2013.
- 1588 Joussaume, S., Taylor, K.E., Braconnot, P., Mitchell, J.F.B., Kutzbach, J.E., Harrison,  
1589 S.P., Prentice, I.C., Broccoli, A.J., Abe-Ouchi, A., Bartlein, P.J., Bonfils, C., Dong,  
1590 B., Guiot, J., Herterich, K., Hewitt, C.D., Jolly, D., Kim, J.W., Kislov, A., Kitoh, A.,  
1591 Loutre, M.F., Masson, V., McAvaney, B., McFarlane, N., De Noblet, N., Peltier,  
1592 W.R., Peterschmitt, J.Y., Pollard, D., Rind, D., Royer, J.F., Schlesinger, M.E.,



Fénisse et al.,

- 1593 Syktus, J., Thompson, S., Valdes, P., Vettoretti, G., Webb, R.S., Wyputta, U.:  
1594 Monsoon changes for 6000 years ago: Results of 18 simulations from the  
1595 Paleoclimate Modeling Intercomparison Project (PMIP). *Geophys. Res. Lett.*  
1596 26, 859–862. <https://doi.org/10.1029/1999GL900126>, 1999.
- 1597 Juggins, S.: Rioja: Analysis of Quaternary Science Data. [https://doi.org/https://cran.r-](https://doi.org/https://cran.r-project.org/package=rioja)  
1598 [project.org/package=rioja](http://www.staff.ncl.ac.uk/stephen.juggins/), <http://www.staff.ncl.ac.uk/stephen.juggins/>, 2020.
- 1599 Kageyama, M., Harrison, S.P., Kapsch, M.-L., Lofverstrom, M., Lora, J.M.,  
1600 Mikolajewicz, U., Sherriff-Tadano, S., Vadsaria, T., Abe-Ouchi, A., Bouttes, N.,  
1601 Chandan, D., Gregoire, L.J., Ivanovic, R.F., Izumi, K., LeGrande, A.N., Lhardy, F.,  
1602 Lohmann, G., Morozova, P.A., Ohgaito, R., Paul, A., Peltier, W.R., Poulsen, C.J.,  
1603 Quiquet, A., Roche, D.M., Shi, X., Tierney, J.E., Valdes, P.J., Volodin, E., Zhu, J.:  
1604 The PMIP4 Last Glacial Maximum experiments: preliminary results and  
1605 comparison with the PMIP3 simulations. *Clim. Past* 17, 1065–1089.  
1606 <https://doi.org/10.5194/cp-17-1065-2021>, 2021.
- 1607 Kaplan, J.O., Pfeiffer, M., Kolen, J.C.A., Davis, B.A.S.: Large Scale Anthropogenic  
1608 Reduction of Forest Cover in Last Glacial Maximum Europe. *PLOS ONE* 11,  
1609 e0166726. <https://doi.org/10.1371/journal.pone.0166726>, 2016.
- 1610 Kaplan, J.O., Bigelow, N.H., Prentice, I.C., Harrison, S.P., Bartlein, P.J., Christensen,  
1611 T.R., Cramer, W., Matveyeva, N.V., McGuire, A.D., Murray, D.F., Razzhivin,  
1612 V.Y., Smith, B., Walker, D.A., Anderson, P.M., Andreev, A.A., Brubaker, L.B.,  
1613 Edwards, M.E., Lozhkin, A.V.: Climate change and Arctic ecosystems: 2.  
1614 Modeling, paleodata-model comparisons, and future projections. *J. Geophys.*  
1615 *Res. Atmospheres* 108, 2002JD002559.  
1616 <https://doi.org/10.1029/2002JD002559>, 2003.
- 1617 Kern, O.A., Maier, A., Vercauteren, N.: Landscape reconstructions for Europe during  
1618 the late Last Glacial (60–20 ka BP): A pollen-based REVEALS approach.  
1619 <https://doi.org/10.5194/essd-2024-306>, 2024.
- 1620 Kern, O.A., Koutsodendris, A., Pross, J.: Palynological data for the Late Glacial and  
1621 Holocene (14.5–0 ka BP) from Füramoos, Southern Germany. *Data Brief* 39,  
1622 107650. <https://doi.org/10.1016/j.dib.2021.107650>, 2021.
- 1623 Kühl, N., Gebhardt, C., Litt, T., Hense, A.: Probability Density Functions as Botanical-  
1624 Climatological Transfer Functions for Climate Reconstruction. *Quat. Res.* 58,  
1625 381–392. <https://doi.org/10.1006/qres.2002.2380>, 2002.
- 1626 Kühl, N., Moschen, R., Wagner, S., Brewer, S., Peyron, O.: A multiproxy record of late  
1627 Holocene natural and anthropogenic environmental change from the  
1628 Sphagnum peat bog Dürres Maar, Germany: implications for quantitative  
1629 climate reconstructions based on pollen. *J. Quat. Sci.* 25, 675–688.  
1630 <https://doi.org/10.1002/jqs.1342>, 2010.
- 1631 Kühl, N., Litt, T.: Quantitative time series reconstruction of Eemian temperature at  
1632 three European sites using pollen data. *Veg. Hist. Archaeobotany* 12, 205–  
1633 214. <https://doi.org/10.1007/s00334-003-0019-2>, 2003.
- 1634 Küster, H.: Postglaziale Vegetationsgeschichte Südbayerns, *Geobotanische Studien*  
1635 *zur Prähistorischen Landschaftskunde*, Akademie Verlag, Berlin, ISBN 978-3-  
1636 05-501592-2, 1995.
- 1637 Li, C., Dallmeyer, A., Ni, J., Chevalier, M., Willeit, M., Andreev, A.A., Cao, X., Schild, L.,  
1638 Heim, B., Herzschuh, U.: Global biome changes over the last 21,000 years



Fénisse et al.,

- 1639                   inferred from model-data comparisons. <https://doi.org/10.5194/egusphere-2024-1862>, 2024.
- 1640
- 1641   Liu, M., Prentice, I.C., Ter Braak, C.J.F., Harrison, S.P.: An improved statistical
- 1642                   approach for reconstructing past climates from biotic assemblages. *Proc. R.*
- 1643                   *Soc. Math. Phys. Eng. Sci.* 476, 20200346.
- 1644                   <https://doi.org/10.1098/rspa.2020.0346>, 2020.
- 1645   Valero-Garcés, B. L., González-Sampériz, P., Navas, A., Machin, J., Delgado-Huertas,
- 1646                   A., Pena-Monné, J. L., Sancho-Marcén, C., Stevenson, T., and Davis, B.:
- 1647                   Paleohydrological fluctuations and steppe vegetation during the last glacial
- 1648                   maximum in the central Ebro valley (NE Spain), *Quatern. Int.*, 122, 43–55,
- 1649                   <https://doi.org/10.1016/j.quaint.2004.01.030>, 2004.
- 1650   Magyari, E. K., Pál, I., Vincze, I., Veres, D., Jakab, G., Braun, M., Szalai, Z., Szabó, Z.,
- 1651                   and Korponai, J.: Warm Younger Dryas summers and early late glacial spread
- 1652                   of temperate deciduous trees in the Pannonian Basin during the last glacial
- 1653                   termination (20–9 kyr cal BP), *Quat. Sci. Rev.*, 225, 105980,
- 1654                   <https://doi.org/10.1016/j.quascirev.2019.105980>, 2019.
- 1655   Magyari, E. K., Kuneš, P., Jakab, G., Sümegi, P., Pelánková, B., Schäbitz, F., Braun, M.,
- 1656                   and Chytrý, M.: Late Pleniglacial vegetation in eastern-central Europe: Are
- 1657                   there modern analogues in Siberia?, *Quaternary Sci. Rev.*, 95, 60–79,
- 1658                   <https://doi.org/10.1016/j.quascirev.2014.04.020>, 2014.
- 1659   Magyari, E., Jakab, G., Rudner, E., and Sümegi, P.: Palynological and plant macrofossil
- 1660                   data on Late Pleistocene short-term climatic oscillations in NE-Hungary, *Acta*
- 1661                   *Palaeobot. Suppl.*, 2, 491–502, 1999.
- 1662   Magri, D. and Sadori, L.: Late Pleistocene and Holocene pollen stratigraphy at Lago di
- 1663                   Vico, central Italy, *Veg. Hist. Archaeobot.*, 8, 247–260,
- 1664                   <https://doi.org/10.1007/BF01291777>, 1979.
- 1665   Margari, V., Gibbard, P. L., Bryant, C. L., and Tzedakis, P. C.: Character of vegetational
- 1666                   and environmental changes in southern Europe during the last glacial period;
- 1667                   evidence from Lesbos Island, Greece, *Quaternary Sci. Rev.*, 28, 1317–1339,
- 1668                   <https://doi.org/10.1016/j.quascirev.2009.01.008>, 2009.
- 1669   Marinova, E., Harrison, S. P., Bragg, F., Connor, S., de Laet, V., Leroy, S. A. G., Mudie,
- 1670                   P., Atanassova, J., Bozilova, E., Caner, H., Cordova, C., Djamali, M., Filipova-
- 1671                   Marinova, M., Gerasimenko, N., Jahns, S., Kouli, K., Kotthoff, U., Kvavadze, E.,
- 1672                   Lazarova, M., Novenko, E., Ramezani, E., Röpke, A., Shumilovskikh, L., Tanțău,
- 1673                   I., and Tonkov, S.: Pollen-derived biomes in the Eastern Mediterranean–Black
- 1674                   Sea–Caspian–Corridor, *J. Biogeogr.*, 45, 484–499,
- 1675                   <https://doi.org/10.1111/jbi.13128>, 2019.
- 1676   Martin, C., Ménot, G., Thouveny, N., Peyron, O., Andrieu-Ponel, V., Montade, V.,
- 1677                   Davitian, N., Reille, M., Bard, E.: Early Holocene Thermal Maximum recorded
- 1678                   by branched tetraethers and pollen in Western Europe (Massif Central,
- 1679                   France). *Quat. Sci. Rev.* 228, 106109.
- 1680                   <https://doi.org/10.1016/j.quascirev.2019.106109>, 2020.
- 1681   Mauri, A., Davis, B.A.S., Collins, P.M., Kaplan, J.O.: The climate of Europe during the
- 1682                   Holocene: a gridded pollen-based reconstruction and its multi-proxy
- 1683                   evaluation. *Quat. Sci. Rev.* 112, 109–127.
- 1684                   <https://doi.org/10.1016/j.quascirev.2015.01.013>, 2015.



Fénisse et al.,

- 1685 Mauri, A., Davis, B.A.S., Collins, P.M., Kaplan, J.O.: The influence of atmospheric  
1686 circulation on the mid-Holocene climate of Europe: a data–model  
1687 comparison. *Clim. Past* 10, 1925–1938. [https://doi.org/10.5194/cp-10-1925-](https://doi.org/10.5194/cp-10-1925-2014)  
1688 [2014](https://doi.org/10.5194/cp-10-1925-2014), 2014.
- 1689 Miebach, A., Niestrath, P., Roeser, P., and Litt, T.: Impacts of climate and humans on  
1690 the vegetation in northwestern Turkey: palynological insights from Lake Iznik  
1691 since the Last Glacial, *Clim. Past*, 12, 575–593, [https://doi.org/10.5194/cp-](https://doi.org/10.5194/cp-12575-2016)  
1692 [12575-2016](https://doi.org/10.5194/cp-12575-2016), 2016.
- 1693 Miola, A., Bondesan, A., Corain, L., Favaretto, S., Mozzi, P., Piovan, S., and Sostizzo, I.:  
1694 Wetlands in the Venetian Po Plain (northeastern Italy) during the Last Glacial  
1695 Maximum: Interplay between vegetation, hydrology and sedimentary  
1696 environment, *Rev. Palaeobot. Palynol.*, 141, 53–81,  
1697 <https://doi.org/10.1016/j.revpalbo.2006.03.016>, 2006.
- 1698 Monegato, G., Ravazzi, C., Donegana, M., Pini, R., Calderoni, G., and Wick, L.:  
1699 Evidence of a two-fold glacial advance during the last glacial maximum in the  
1700 Tagliamento end moraine system (eastern Alps), *Quatern. Res.*, 68, 284–302,  
1701 <https://doi.org/10.1016/j.yqres.2007.07.002>, 2007.
- 1702 Netzel, T., Miebach, A., Litt, T., Hense, A.: New probabilistic methods for quantitative  
1703 climate reconstructions applied to palynological data from Lake Kinneret.  
1704 *Clim. Past* 21, 357–380. <https://doi.org/10.5194/cp-21-357-2025>, 2025.
- 1705 Ortega-Rosas, C.I., Guiot, J., Peñalba, M.C., Ortiz-Acosta, M.E.: biomisation and  
1706 quantitative climate reconstruction techniques in northwestern Mexico—  
1707 With an application to four Holocene pollen sequences. *Glob. Planet. Change*  
1708 61, 242–266. <https://doi.org/10.1016/j.gloplacha.2007.10.006>, 2008.
- 1709 Overpeck, J.T., Webb, T., Prentice, I.C.: Quantitative Interpretation of Fossil Pollen  
1710 Spectra: Dissimilarity Coefficients and the Method of Modern Analogs. *Quat.*  
1711 *Res.* 23, 87–108. [https://doi.org/10.1016/0033-5894\(85\)90074-2](https://doi.org/10.1016/0033-5894(85)90074-2), 1985.
- 1712 Paganelli, A.: Evolution of vegetation and climate in the Veneto-Po Plain during the  
1713 Late-Glacial and Early Holocene using pollenstratigraphical data, *Alp.*  
1714 *Mediterr. Quat.*, 9, 581–589, 1996.
- 1715 Peltier, W.R., Solheim, L.P.: The climate of the Earth at Last Glacial Maximum:  
1716 statistical equilibrium state and a mode of internal variability. *Quat. Sci. Rev.*  
1717 23, 335–357. <https://doi.org/10.1016/j.quascirev.2003.07.003>, 2004.
- 1718 Pérez-Obiol, R. P. and Julia, R.: Climatic change on the Iberian Peninsula recorded in a  
1719 30,000-year pollen record from Lake Banyoles, *Quaternary Res.*, 41, 91–98,  
1720 1994.
- 1721 Peyron, O., Magny, M., Goring, S., Joannin, S., De Beaulieu, J.-L., Brugiapaglia, E.,  
1722 Sadori, L., Garfi, G., Kouli, K., Ioakim, C., Combourieu-Nebout, N.: Contrasting  
1723 patterns of climatic changes during the Holocene across the Italian Peninsula  
1724 reconstructed from pollen data. *Clim. Past* 9, 1233–1252.  
1725 <https://doi.org/10.5194/cp-9-1233-2013>, 2013.
- 1726 Peyron, O., Bégeot, C., Brewer, S., Heiri, O., Magny, M., Millet, L., Ruffaldi, P., Van  
1727 Campo, E., Yu, G.: Late-Glacial climatic changes in Eastern France (Lake  
1728 Lautrey) from pollen, lake-levels, and chironomids. *Quat. Res.* 64, 197–211.  
1729 <https://doi.org/10.1016/j.yqres.2005.01.006>, 2005.
- 1730 Peyron, O., Guiot, J., Cheddadi, R., Tarasov, P., Reille, M., De Beaulieu, J.-L., Bottema,  
1731 S., Andrieu, V.: Climatic Reconstruction in Europe for 18,000 YR B.P. from



Fénisse et al.,

- 1732 Pollen Data. *Quat. Res.* 49, 183–196. <https://doi.org/10.1006/qres.1997.1961>,  
1733 1998.
- 1734 Pini, R., Ravazzi, C., and Donegana, D.: Pollen stratigraphy, vegetation and climate  
1735 history of the last 215 ka in the Azzano Decimo core (plain of Friuli, north-  
1736 eastern Italy), *Quaternary Sci. Rev.*, 28, 1268–1290,  
1737 <https://doi.org/10.1016/j.quascirev.2008.12.017>, 2009.
- 1738 Prentice, I.C., Villegas-Diaz, R., Harrison, S.P.: Accounting for atmospheric carbon  
1739 dioxide variations in pollen-based reconstruction of past hydroclimates. *Glob.*  
1740 *Planet. Change* 211, 103790.  
1741 <https://doi.org/10.1016/j.gloplacha.2022.103790>, 2022.
- 1742 Prentice, I.C., Harrison, S.P., Jolly, D.: The climate and biomes of Europe at 6000 yr  
1743 bp: comparison of model simulations and pollen-based reconstructions.  
1744 *Quaternary Science Reviews*, 1998, 17 (6-7), pp.659-668.  
1745 [https://doi.org/10.1016/S0277-3791\(98\)00016-X](https://doi.org/10.1016/S0277-3791(98)00016-X), 1998.
- 1746 Prentice, I.C., Webb III, T.: BIOME 6000: reconstructing global mid-Holocene  
1747 vegetation patterns from palaeoecological records. *J. Biogeogr.* 25, 997–1005.  
1748 <https://doi.org/10.1046/j.1365-2699.1998.00235.x>, 1998.
- 1749 Prentice, I.C., Guiot, J., Huntley, B., Jolly, D., Cheddadi, R.: Reconstructing biomes  
1750 from palaeoecological data: a general method and its application to European  
1751 pollen data at 0 and 6 ka. *Clim. Dyn.* 12, 185–194, 1996.
- 1752 Prentice, I.C., Cramer, W., Harrison, S.P., Leemans, R., Monserud, R.A., Solomon,  
1753 A.M.: Special Paper: A Global Biome Model Based on Plant Physiology and  
1754 Dominance, Soil Properties and Climate. *J. Biogeogr.* 19, 117.  
1755 <https://doi.org/10.2307/2845499>, 1992.
- 1756 Ramstein, G., Kageyama, M., Guiot, J., Wu, H., Hély, C., Krinner, G., and Brewer, S.:  
1757 How cold was Europe at the Last Glacial Maximum? A synthesis of the  
1758 progress achieved since the first PMIP model-data comparison, *Clim. Past*, 3,  
1759 331–339, <https://doi.org/10.5194/cp-3-331-2007>, 2007.
- 1760 Reille, M. and Andrieu, V.: The late Pleistocene and Holocene in the Lourdes Basin,  
1761 Western Pyrénées, France: new pollen analytical and chronological data, *Veg.*  
1762 *Hist. Archaeobot.*, 4, 1–21, <https://doi.org/10.1007/BF00198611>, 1995.
- 1763 Reimer, P.J., Austin, W.E.N., Bard, E., Bayliss, A., Blackwell, P.G., Bronk Ramsey, C.,  
1764 Butzin, M., Cheng, H., Edwards, R.L., Friedrich, M., Grootes, P.M., Guilderson,  
1765 T.P., Hajdas, I., Heaton, T.J., Hogg, A.G., Hughen, K.A., Kromer, B., Manning,  
1766 S.W., Muscheler, R., Palmer, J.G., Pearson, C., Van Der Plicht, J., Reimer, R.W.,  
1767 Richards, D.A., Scott, E.M., Southon, J.R., Turney, C.S.M., Wacker, L., Adolphi,  
1768 F., Büntgen, U., Capano, M., Fahrni, S.M., Fogtmann-Schulz, A., Friedrich, R.,  
1769 Köhler, P., Kudsk, S., Miyake, F., Olsen, J., Reinig, F., Sakamoto, M., Sookdeo,  
1770 A., Talamo, S.: The IntCal20 Northern Hemisphere Radiocarbon Age  
1771 Calibration Curve (0–55 cal kBP). *Radiocarbon* 62, 725–757.  
1772 <https://doi.org/10.1017/RDC.2020.41>, 2020.
- 1773 Robles, M., Peyron, O., Ménot, G., Brugiapaglia, E., Wulf, S., Appelt, O., Blache, M.,  
1774 Vannièrè, B., Dugerdil, L., Paura, B., Ansanay-Alex, S., Cromartie, A., Charlet,  
1775 L., Guédron, S., De Beaulieu, J.-L., Joannin, S.: Climate changes during the Late  
1776 Glacial in southern Europe: new insights based on pollen and brGDGTs of Lake  
1777 Matese in Italy. *Clim. Past* 19, 493–515. [https://doi.org/10.5194/cp-19-493-](https://doi.org/10.5194/cp-19-493-2023)  
1778 [2023](https://doi.org/10.5194/cp-19-493-2023), 2023.



Fénisse et al.,

- 1779 Sadori, L., Koutsodendris, A., Panagiotopoulos, K., Masi, A., Bertini, A., Combourieu-  
1780 Nebout, N., Francke, A., Kouli, K., Joannin, S., Mercuri, A.M., Peyron, O., Torri,  
1781 P., Wagner, B., Zanchetta, G., Sinopoli, G., Donders, T.H.: Pollen-based  
1782 paleoenvironmental and paleoclimatic change at Lake Ohrid (south-eastern  
1783 Europe) during the past 500 ka. *Biogeosciences* 13, 1423–1437.  
1784 <https://doi.org/10.5194/bg-13-1423-2016>, 2016.
- 1785 Salonen, J.S., Korpela, M., Williams, J.W., Luoto, M.: Machine-learning based  
1786 reconstructions of primary and secondary climate variables from North  
1787 American and European fossil pollen data. *Sci. Rep.* 9, 15805.  
1788 <https://doi.org/10.1038/s41598-019-52293-4>, 2019.
- 1789 Sánchez Goñi, M.F., Desprat, S., Daniau, A.-L., Bassinot, F.C., Polanco-Martínez, J.M.,  
1790 Harrison, S.P., Allen, J.R.M., Anderson, R.S., Behling, H., Bonnefille, R.,  
1791 Burjachs, F., Carrión, J.S., Cheddadi, R., Clark, J.S., Combourieu-Nebout, N.,  
1792 Mustaphi, Colin.J.C., Debusk, G.H., Dupont, L.M., Finch, J.M., Fletcher, W.J.,  
1793 Giardini, M., González, C., Gosling, W.D., Grigg, L.D., Grimm, E.C., Hayashi, R.,  
1794 Helmens, K., Heusser, L.E., Hill, T., Hope, G., Huntley, B., Igarashi, Y., Irino, T.,  
1795 Jacobs, B., Jiménez-Moreno, G., Kawai, S., Kershaw, A.P., Kumon, F., Lawson,  
1796 I.T., Ledru, M.-P., Lézine, A.-M., Liew, P.M., Magri, D., Marchant, R., Margari,  
1797 V., Mayle, F.E., McKenzie, G.M., Moss, P., Müller, S., Müller, U.C., Naughton,  
1798 F., Newnham, R.M., Oba, T., Pérez-Obiol, R., Pini, R., Ravazzi, C., Roucoux,  
1799 K.H., Rucina, S.M., Scott, L., Takahara, H., Tzedakis, P.C., Urrego, D.H., Van  
1800 Geel, B., Valencia, B.G., Vandergoes, M.J., Vincens, A., Whitlock, C.L., Willard,  
1801 D.A., Yamamoto, M.: The ACER pollen and charcoal database: a global  
1802 resource to document vegetation and fire response to abrupt climate changes  
1803 during the last glacial period. *Earth Syst. Sci. Data* 9, 679–695.  
1804 <https://doi.org/10.5194/essd-9-679-2017>, 2017.
- 1805 Sassoone, D., Combourieu-Nebout, N., Peyron, O., Bertini, A., Toti, F., Lebreton, V.,  
1806 Moncel, M.-H.: Pollen-based climatic reconstructions for the interglacial  
1807 analogues of MIS 1 (MIS 19, 11, and 5) in the southwestern Mediterranean:  
1808 insights from ODP Site 976. *Clim. Past* 21, 489–515.  
1809 <https://doi.org/10.5194/cp-21-489-2025>, 2025.
- 1810 Satkunas, J. and Grigienė, A.: Eemian-Weichselian palaeoenvironmental record from  
1811 the Mickūnai glacial depression (Eastern Lithuania), *Geologija*, 54, 35–51,  
1812 <https://doi.org/10.6001/geologija.v54i2.2482>, 2012.
- 1813 Seguinot, J., Ivy-Ochs, S., Jouvet, G., Huss, M., Funk, M., Preusser, F.: Modelling last  
1814 glacial cycle ice dynamics in the Alps. *The Cryosphere* 12, 3265–3285.  
1815 <https://doi.org/10.5194/tc-12-3265-2018>, 2018.
- 1816 Šeirienė, V., Kūhl, N., Kisieliene, D.: Quantitative reconstruction of climate variability  
1817 during the Eemian (Merkinė) and Weichselian (Nemunas) in Lithuania. *Quat.*  
1818 *Res.* 82, 229–235. <https://doi.org/10.1016/j.yqres.2014.04.004>, 2014.
- 1819 Seltzer, A.M., Blard, P.-H., Sherwood, S.C., Kageyama, M.: Terrestrial amplification of  
1820 past, present, and future climate change. *Sci. Adv.* 9, eadf8119.  
1821 <https://doi.org/10.1126/sciadv.adf8119>, 2023.
- 1822 Sinopoli, G., Masi, A., Regattieri, E., Wagner, B., Francke, A., Peyron, O., Sadori, L.:  
1823 Palynology of the Last Interglacial Complex at Lake Ohrid:  
1824 palaeoenvironmental and palaeoclimatic inferences. *Quat. Sci. Rev.* 180, 177–  
1825 192. <https://doi.org/10.1016/j.quascirev.2017.11.013>, 2018.



Fénisse et al.,

- 1826 Sirocko, Frank; Knapp, Hannes; Dreher, Frank; Förster, Michael W; Albert, Johannes;  
1827 Brunck, Heiko; Veres, Daniel; Dietrich, Stephan; Zech, Michael; Hambach,  
1828 Ulrich; Röhner, Marieke; Rudert, Saskia; Schwiebus, Klaus; Adams, Christel;  
1829 Sigl, Petra.: The ELSA-Vegetation-Stack: Reconstruction of Landscape  
1830 Evolution Zones (LEZ) from laminated Eifel maar sediments of the last 60,000  
1831 years. *Global and Planetary Change*, 142, 108-135,  
1832 <https://doi.org/10.1016/j.gloplacha.2016.03.005>, 2016.
- 1833 Strahl, J.: Zur Pollenstratigraphie des Weichselspätglazials von Berlin-Brandenburg  
1834 [On the palynostratigraphy of the Late Weichselian in Berlin-Brandenburg],  
1835 Brand. Geowissensch. Beitr., 12, 87–112, 2005.
- 1836 Tarasov, P.E., Müller, S., Zech, M., Andreeva, D., Diekmann, B., Leipe, C.: Last glacial  
1837 vegetation reconstructions in the extreme-continental eastern Asia:  
1838 Potentials of pollen and n-alkane biomarker analyses. *Quat. Int.* 290–291,  
1839 253–263. <https://doi.org/10.1016/j.quaint.2012.04.007>, 2013.
- 1840 Tarasov, P.E., Peyron, O., Guiot, J., Brewer, S., Volkova, V.S., Bezusko, L.G.,  
1841 Dorofeyuk, N.I., Kvavadze, E.V., Osipova, I.M., Panova, N.K.: Last Glacial  
1842 Maximum climate of the former Soviet Union and Mongolia reconstructed  
1843 from pollen and plant macrofossil data. *Clim. Dyn.* 15, 227–240.  
1844 <https://doi.org/10.1007/s003820050278>, 1999.
- 1845 Tarasov, P.E., Volkova, V.S., Iii, T.W., Guiot, J., Andreev, A.A., Bezusko, L.G., Bykova,  
1846 G.V., Dorofeyuk, N.I., Kvavadze, E.V., Osipova, I.M., Panova, N.K.,  
1847 Sevastyanov, D.V.: Black well Science, Ltd Last glacial maximum biomes  
1848 reconstructed from pollen and plant macrofossil data from northern Eurasia.  
1849 *J. Biogeogr.*, 27, 609-620, <https://doi.org/10.1046/j.1365-2699.2000.00429.x>,  
1850 2000.
- 1851 Ter Braak, C.J.F., Juggins, S.: Weighted averaging partial least squares regression (WA-  
1852 PLS): an improved method for reconstructing environmental variables from  
1853 species assemblages. *Hydrobiologia* 485–502, 1993.
- 1854 Tonkov, S., Lazarova, M., Bozilova, E., Ivanov, D., Snowball.I.: A 30,000-year pollen  
1855 record from Mire Kupena, Western Rhodopes Mountains (south Bulgaria).  
1856 *Rev. Palaeobot. Palynol.* 209, 41–51.  
1857 <https://doi.org/10.1016/j.revpalbo.2014.06.002>, 2014.
- 1858 Trasune, L., Väiliranta, M., Stivrins, N., Amon, L., Schenk, F., Salonen, J.S.: A  
1859 comparison of plant macrofossil-based quantitative climate reconstruction  
1860 methods: A case study of the lateglacial Baltic States. *Quat. Sci. Rev.* 338,  
1861 108811. <https://doi.org/10.1016/j.quascirev.2024.108811>, 2024.
- 1862 Tzedakis, P. C., Frogley, M. R., Lawson, I. T., Preece, R. C., Cacho, I., and de Abreu, L.:  
1863 Ecological thresholds and patterns of millennial-scale climate variability: The  
1864 response of vegetation in Greece during the last glacial period, *Geology*, 32,  
1865 109–112, <https://doi.org/10.1130/G20118.1>, 2004.
- 1866 Vegas-Vilarrúbia, T., González-Sampéris, P., Morellón, M., GilRomera, G., Pérez-Sanz,  
1867 A., and Valero-Garcés, B.: Diatom and vegetation responses to late glacial and  
1868 early holocene climate changes at lake estanya (southern pyrenees, NE Spain),  
1869 *Palaeogeogr. Palaeoclim. Palaeoecol.*, 392, 335–349,  
1870 <https://doi.org/10.1016/j.palaeo.2013.09.011>, 2013.



Fénisse et al.,

- 1871 Viau, A.E., Gajewski, K.: Reconstructing Millennial-Scale, Regional Paleoclimates of  
1872 Boreal Canada during the Holocene. *J. Clim.* 22, 316–330.  
1873 <https://doi.org/10.1175/2008JCLI2342.1>, 2009.
- 1874 Watts, W. A., Allen, J. R. M., and Huntley, B.: Vegetation history and palaeoclimate of  
1875 the last glacial period at Lago grande di Monticchio, southern Italy,  
1876 *Quaternary Sci. Rev.*, 15, 133–153, [https://doi.org/10.1016/0277-](https://doi.org/10.1016/0277-3791(95)00093-3)  
1877 [3791\(95\)00093-3](https://doi.org/10.1016/0277-3791(95)00093-3), 1996.
- 1878 Williams, J.W., Shuman, B.: Obtaining accurate and precise environmental  
1879 reconstructions from the modern analog technique and North American  
1880 surface pollen dataset. *Quat. Sci. Rev.* 27, 669–687.  
1881 <https://doi.org/10.1016/j.quascirev.2008.01.004>, 2008
- 1882 Wu, H., Guiot, J., Brewer, S., Guo, Z.: Climatic changes in Eurasia and Africa at the last  
1883 glacial maximum and mid-Holocene: reconstruction from pollen data using  
1884 inverse vegetation modelling. *Clim. Dyn.* 29, 211–229.  
1885 <https://doi.org/10.1007/s00382-007-0231-3>, 2007.
- 1886 Xu, Q., Zhang, S., Gaillard, M., Li, M., Cao, X., Tian, F., Li, F.: Studies of modern pollen  
1887 assemblages for pollen dispersal- deposition- preservation process  
1888 understanding and for pollen-based reconstructions of past vegetation,  
1889 climate, and human impact: A review based on case studies in China. *Quat.*  
1890 *Sci. Rev.* 149, 151–166. <https://doi.org/10.1016/j.quascirev.2016.07.017>,  
1891 2016.